Spring 2-17-2014

Modulating Amyloid Beta Clearance by Altering Cellular and Whole Brain Apolipoprotein E Metabolism

Jacob Martin Basak
Washington University in St. Louis

WASHINGTON UNIVERSITY IN ST. LOUIS

Division of Biology and Biomedical Sciences

Molecular Cell Biology

Dissertation Examination Committee:
David Holtzman, Chair
Randall Bateman
Carl Frieden
Jin-Moo Lee
Daniel Ory
Philip Stahl

Modulating Amyloid β Clearance by Altering Cellular and Whole Brain Apolipoprotein E Metabolism

by

Jacob Martin Basak

A dissertation presented to the
Graduate School of Arts and Sciences
of Washington University in
partial fulfillment of the
requirements for the degree
of Doctor of Philosophy

May 2014

St. Louis, Missouri

Table of Contents

List of Figures Page #

List of Tables Page #

Acknowledgments

The work presented in this thesis would not have been possible without the help and support of many individuals. I would first like to thank my mentor and thesis advisor, Dr. David Holtzman. You have provided me with an abundance of support and guidance over the past several years that have allowed me to be successful. Your encouragement as a mentor was invaluable, and I am grateful for your advice and encouragement.

To all the members of my thesis committee, thanks for your advice and guidance in my projects. Your suggestions kept my projects on track and allowed me to attain my research goals.

To our collaborators, particularly Dr. Randy Bateman and all of the members of his lab, thanks for your help with mass spec analysis and for letting me run my samples on your instruments. In particular, Yuriy Pyatkivskyy and Kristin Wildsmith were of utmost value to my projects, and I am sincerely grateful for their time and effort.

To the Medical Scientist Training Program, for allowing me to come to Washington University and for supporting me both financially and academically during my time here. Also, to the National Institutes of Health (NIH) and the American Health Assistance Foundation (AHAF) for providing financial support for my projects in the lab.

To all of the members of the Holtzman lab, thanks for your help and for providing me with a very enjoyable work environment. You were a great group of individuals to work with, and provided a perfect mix of laughs and serious scientific discussion. I would in particular like to thank Philip Verghese for his help on my projects and his willingness

to always talk about apoE, and Hong Jiang for her help with the dissection of many mice brains.

To Jungsu Kim, your guidance, discussion, and help in my scientific pursuits over the past few years have been invaluable. Thanks for all you have taught me about the scientific world, and for being a great friend. It has been fun to watch your career evolve.

Finally, I would not be where I am today without my family, especially my parents, Bruce and Mary Ann Basak, and sisters, Jaclyn and Jennifer Basak. You have supported me to the fullest in everything I have done throughout my life. I am so grateful for your amazing love and support, and owe so much to you. And most importantly to my wonderful wife, Alison. I would not have made it to this point without you. Thank you so much for being so supportive of me and my work, and for helping me get through the past few years. You are an inspiration to me in all that you do. I love you.

ABSTRACT OF THE DISSERTATION

Modulating Amyloid β Clearance by Altering Cellular and Whole Brain Apolipoprotein E Metabolism

by

Jacob Martin Basak

Doctor of Philosophy in Biology and Biomedical Sciences

Molecular Cell Biology

Washington University in St. Louis, 2014

Professor David Holtzman, Chairperson

The aggregation and accumulation of the amyloid beta (Aβ) peptide in the brain is hypothesized to be an initial necessary event in the pathogenesis of Alzheimer's disease (AD). Since the level of monomeric soluble Aβ as well as Aβ-binding molecules determine the onset and amount of Aβ aggregation, significant attention has been devoted to defining the molecular and systemic pathways that modulate Aβ synthesis and clearance in the brain. Extensive evidence exists that both the isoform and amount of apolipoprotein E (apoE), an Aβ-binding molecule, influence Aβ aggregation and clearance from the brain. Therefore, studying how the molecular mechanisms that modulate apoE levels in the brain affect Aβ clearance will enhance our insight into the disease process. The apoE receptor low-density lipoprotein receptor (LDLR) and ATP-binding cassette transporter A1 (ABCA1), a protein that regulates apoE lipidation, have previously been shown to modulate brain Aβ levels. In the work presented in this

dissertation, we found that increasing LDLR levels enhanced the cellular uptake and degradation of Aβ by primary astrocytes, and increased Aβ transport to lysosomes. The effect of LDLR on Aβ uptake and clearance occurred independently of apoE, and potentially involved a direct interaction between Aβ and LDLR. To measure the clearance of apoE and Aβ in the mouse brain, we developed a technique that couples stable isotope-labeling kinetics (SILK) with mass spectrometry. We validated this technique by demonstrating that apoE clearance is enhanced in the brains of mice overexpressing LDLR. We also applied this technique to measure apoE clearance rates in the brains of human apoE targeted-replacement mice. Finally, we analyzed the effect of ABCA1 on apoE and Aβ clearance from the mouse brain. The fractional clearance rate of apoE was increased in amyloid precursor protein (APP) transgenic mice that either lacked or overexpressed ABCA1, while ABCA1 levels had no effect on Aβ clearance. Therefore, ABCA1 likely influences Aβ aggregation *in vivo* through a process other than modulating Aβ clearance. These data further our understanding of how proteins involved in apoE metabolism influence AD pathogenesis, and have important implications for future therapeutic strategies that target brain apoE levels and function.

Chapter 1

Introduction and Perspective

Alzheimer's disease: Epidemiology and pathology

Alzheimer's disease (AD) is the most common cause of dementia in individuals older than 60 years of age, and currently afflicts an estimated 30 million people worldwide. Increases in the aging population are expected to greatly increase this number, with an estimated 4-fold rise in AD cases over the next forty years (World Alzheimer Report, 2009). The worldwide burden of AD from both an economical and societal viewpoint is alarming, as significant monetary and emotional resources are needed for the care of afflicted individuals. With no current effective treatment available for AD, further understanding of the disease pathogenesis is necessary to promote the development of novel therapeutics.

The main pathological hallmarks of AD, originally described by Alois Alzheimer in 1906, are extracellular amyloid plaques, intracellular neurofibrillary tangles (NFTs), and extensive neuronal loss (Holtzman et al., 2011). The amyloid plaques are primarily composed of the amyloid β (Aβ) peptide (Masters et al., 1985), and are characterized as either diffuse or dense-core depending on the aggregation state of Aβ . Diffuse plaques consist of Aβ present in a non-fibrillar form, while dense-core plaques contain fibrillar Aβ that aggregate into a β-sheet structure. Regions of the brain surrounding dense-core plaques are typically characterized by extensive neuritic degeneration, along with the local activation of astrocytes and microglia (Itagaki et al., 1989). Microglia secrete cytokines and other proteins involved in the immune response that promote inflammation within the neuropil (Wyss-Coray, 2006). Aβ aggregation in the blood vessel walls also occurs in AD brains and is termed cerebral amyloid angiopathy (CAA) (Smith and

Greenberg, 2009). Within neuronal cell bodies and processes, the microtubule-binding protein tau aggregates into paired helical filaments to form NFTs and neuropil threads, respectively (Mandelkow and Mandelkow, 1998). As the disease progresses, significant neuronal and synaptic loss occurs along with gross atrophy of the brain. These changes, along with the loss of neurotransmitters and network connections between different brain regions, ultimately lead to the cognitive symptoms that define the clinical course of AD.

Amyloid β production and accumulation in the brain

One of the main theories explaining the mechanism of AD pathogenesis is the amyloid cascade hypothesis (Hardy and Selkoe, 2002). The central tenet of this hypothesis is that Aβ accumulation in the brain, along with the resulting aggregation of monomeric Aβ into higher order species and amyloid plaques, initiates a cascade of events that leads to synaptic dysfunction and neuronal cell death. In the healthy brain, steady-state Aβ levels are likely determined by the overall rates of Aβ production and clearance. Alterations in either of these processes via increased Aβ production or impaired clearance could increase Aβ levels and initiate the pathogenic cascade leading to AD. Aβ originates primarily from neurons and is produced by the proteolytic processing of the amyloid precursor protein (APP). Sequential cleavage of APP by the enzymes β-secretase and γ-secretase produces several different species of Aβ, including Aβ38, Aβ40, and Aβ42, that vary in length by the number of amino acids at the C-terminus (De Strooper, 2010). Though Aβ40 is the most abundant species of Aβ found in the brain, Aβ42 is more amyloidogenic and thus exhibits a greater propensity to

aggregate (Jarrett et al., 1993). Aβ is produced in endosomes, where the environment is more favorable for enzymatic cleavage of APP, and subsequently secreted into the extracellular space (Cirrito et al., 2008; Koo and Squazzo, 1994).

Genetic and molecular evidence demonstrate that increased Aβ production can cause AD. Autosomal dominant mutations in the genes for either APP or presenilin, a component of the γ-secretase complex, are responsible for the early-onset familial form of AD (FAD) (Tanzi and Bertram, 2005). Most of these mutations increase either the amount of Aβ42 produced relative to Aβ40, or in some instances elevate the level of all Aβ species. Also, individuals with Down syndrome possess an extra copy of the chromosomal region in which APP is found, and the resulting increase in APP levels significantly heightens the likelihood of these patients developing AD later in life (Rovelet-Lecrux et al., 2006). However, the cause of Aβ deposition in the more common late-onset form of AD (LOAD) is less evident. Few current studies suggest that Aβ production is elevated in individuals with LOAD. A more likely cause for the amyloid formation in these cases is either a change in the aggregation properties of Aβ, impaired clearance of Aβ from the brain, or both. A study measuring Aβ kinetics in the human central nervous system (CNS) has provided direct evidence for a role of impaired Aβ clearance in AD pathogenesis, as the clearance rate of Aβ in individuals with AD was decreased compared to controls (Mawuenyega et al., 2010). However, the mechanisms underlying the decreased clearance are unknown. Therefore, greater understanding of the pathways that are responsible for Aβ removal from the brain and the molecular

mechanisms underlying Aβ degradation is necessary to further our knowledge of AD pathogenesis and identify new therapeutic targets.

Aβ homeostasis in the brain

According to studies of Aβ turnover in both humans and mice, Aβ is rapidly produced and metabolized in the central nervous system and the periphery. Studies in humans have shown that Aβ is synthesized and cleared from the cerebral spinal fluid at a rate of roughly 8% per hour (Bateman et al., 2006). In transgenic mice that overexpress human APP, the half-life of Aβ has been determined to be in the range of 30 minutes to 2 hours (Abramowski et al., 2008; Barten et al., 2005; Cirrito et al., 2003; Savage et al., 1998). The clearance rate of Aβ in the plasma is even greater than in the brain. The observed half-life of Aβ in the plasma of mice is in the range of 2.5 to 3 minutes (Ghiso et al., 2004). Efficient clearance of Aβ is likely a primary reason that Aβ levels are maintained at a low level in APP transgenic mice and humans without AD.

In the brain, several different pathways for Aβ clearance have been proposed. Aβ is actively transported across the blood-brain barrier into the blood, where it is then either catabolized by the liver or excreted through the kidney (Ghiso et al., 2004; Zlokovic, 2008). The lipoprotein receptor low-density lipoprotein receptor-related protein 1 (LRP1) has been proposed to be one of the main mediators of this process (Deane et al., 2004; Shibata et al., 2000). Aβ can also be passively transported from the brain interstitial fluid to the cerebral spinal fluid (CSF), where it is then removed into the circulation via bulk flow of the CSF (Weller et al., 2008). Another pathway for Aβ clearance is through direct

enzymatic degradation of Aβ in the brain. Several proteases have been shown to directly degrade Aβ, including neprilysin (Iwata et al., 2001), insulin degrading enzyme (Qiu et al., 1998), matrix metalloproteinases (Yin et al., 2006), and tissue plasminogen activator (Melchor et al., 2003). Finally, Aβ can be directly taken up and degraded by cells within the brain, as discussed in the following section. The relative contribution of each of these pathways to Aβ clearance, along with which pathway predominates in both healthy and pathogenic conditions is unknown. For instance, blood-brain barrier transport may be the primary method of Aβ clearance in young healthy individuals, but as vascular insults (such as hypertension and vascular disease) increase with age the cellular and enzymatic clearance of Aβ may become more important. It is also not known to what extent each of these pathways contributes to the removal of aggregated Aβ species and fibrillar amyloid plaques.

Cellular metabolism of Aβ

Several cell-types in the brain have been shown to be capable of internalizing Aβ both in cell culture and *in vivo*, including neurons, microglia, astrocytes, and endothelial cells. However, the degradative capabilities of these cell types are not equal, and internalization of Aβ may have different consequences depending on its ultimate intracellular fate. Primary neurons endocytose Aβ in culture (Kanekiyo et al., 2011; Saavedra et al., 2007) and intraneuronal Aβ staining has been observed *in vivo (LaFerla et al., 2007)*, but no solid evidence exists that neurons actively degrade Aβ in the brain. In fact, a potential reason for the accumulation of intraneuronal Aβ in individuals with AD

is that the degradative machinery has simply been overwhelmed in these cells due to increased Aβ levels. As suggested by one study, intraneuronal Aβ accumulation could play a role in promoting AD pathogenesis through the seeding of amyloid formation (Hu et al., 2009).

The uptake of Aβ by microglia and astrocytes likely plays a more prominent role in the cellular clearance of Aβ than neuronal uptake because of the greater degradative capabilities of glial cells. Microglia have been postulated to play both a beneficial and detrimental role in the pathogenesis of AD. Microglia may promote the clearance of Aβ via uptake and degradation (Lee and Landreth, 2010), but because of their immuno-modulatory function, they can also promote pro-inflammatory pathways that enhance Aβ deposition and neurotoxicity (Hickman et al., 2008). Microglia have been shown to internalize both soluble and fibrillar Aβ in culture (Chung et al., 1999; Mandrekar et al., 2009; Paresce et al., 1997; Paresce et al., 1996) and in the brain (Bolmont et al., 2008; Pluta et al., 1999; Simard et al., 2006). Different internalization pathways have been shown to facilitate the uptake of soluble and fibrillar Aβ. Soluble Aβ uptake is mediated primarily by fluid phase macropinocytosis (Mandrekar et al., 2009). Fibrillar uptake occurs through the binding of Aβ to scavenger receptors and Toll-like receptors on the surface membrane, followed by the activation of intracellular signaling cascades that turn on the phagocytic machinery (Bamberger et al., 2003; Paresce et al., 1996; Reed-Geaghan et al., 2009). The ability of microglia to degrade Aβ also appears to depend upon the state of Aβ aggregation. Soluble Aβ has been shown to be efficiently degraded by microglia in culture (Jiang et al., 2008; Mandrekar et al., 2009), but internalized

fibrillar Aβ remained intact and was slowly released from the cells over time (Chung et al., 1999; Paresce et al., 1997; Paresce et al., 1996). These latter studies suggested that microglia may not play a major role in clearing amyloid plaques. The role of microglia in plaque homeostasis in the brain was formally tested *in vivo* in APP transgenic mice crossed with mice that have a CD11b-driven thymidine kinase (TK) protein (Grathwohl et al., 2009). Treating these mice with ganciclovir resulted in the ablation of all endogenous microglia. In comparison to CD11b/TK mice with intact endogenous microglia, ganciclovir-treated mice had the same levels of Aβ deposition in the brain. However, the ganciclovir mice also had higher levels of astrocytosis in the mouse brain. Though the authors of this study concluded that microglia play no role in the formation and maintenance of amyloid plaques, it is not possible to rule out the possibility that the resultant increase in astrocyte activity balanced out the lack of microglia. Therefore, the role of microglia in both soluble and fibrillar Aβ clearance *in vivo* remains an issue of debate.

The roles of astrocytes in the degradation of Aβ and the molecular pathways that regulate Aβ uptake in these cells are more poorly defined than for microglia. Astrocytes have been shown to internalize Aβ in the brain via immunohistochemical studies (Funato et al., 1998; Nagele et al., 2003; Thal et al., 2000). Other papers have also described the ability of primary astrocytes grown in culture to endocytose and degrade soluble Aβ (Mandrekar et al., 2009; Nielsen et al., 2009; Shaffer et al., 1995; Wyss-Coray, 2006) and fibrillar Aβ present in the plaques of murine brain slices (Koistinaho et al., 2004; Wyss-Coray et al., 2003). In the latter studies, the ability of astrocytes to degrade fibrillar Aβ

was inhibited in the presence of the receptor-associated protein (RAP), a known antagonist of receptors in the low-density lipoprotein receptor (LDLR) family (Koistinaho et al., 2004). These results suggest that a member of the LDLR family may play an important role in facilitating the uptake of Aβ by astrocytes, though the specific LDLR receptors have yet to be identified. Therefore, further studies are necessary to characterize the specific molecular pathways that mediate astrocytic Aβ endocytosis, and to determine whether astrocytes contribute to the *in vivo* clearance of Aβ.

Apolipoprotein E and Alzheimer's disease

One protein that has been shown to potentially influence amyloid aggregation through the modulation of Aβ clearance is apolipoprotein E (apoE). ApoE is a 34 kDa glycoprotein whose main function outside of the brain is to regulate cholesterol and lipid metabolism (Mahley, 1988). ApoE is expressed at the highest level in the liver, followed by the brain (Elshourbagy et al., 1985). Astrocytes are the main cell-type in the brain that produces apoE, though microglia also express apoE (Fig. 1) (Grehan et al., 2001; Pitas et al., 1987). In the periphery, apoE is one of the protein constituents present on very low-density lipoprotein (VLDL) and high-density lipoprotein (HDL) particles. ApoE functions in the transport and redistribution of cholesterol by binding to receptors of the LDLR family, and consequently facilitating the uptake of VLDL and HDL into hepatic and extra-hepatic cells (Mahley, 1988). In the brain, the normal physiological function of apoE is poorly defined. Unlike in the periphery, where HDL particles contain apolipoprotein A-1 (apoA-1) as the major lipoprotein, apoE is the predominant

apolipoprotein in the brain (Pitas et al., 1987). In the brain, apoE is present on HDL-like lipoprotein particles that are discoidal in shape and possess cholesterol and phospholipids (DeMattos et al., 2001b; Fagan et al., 1999). The role of these particles in normal brain function is unclear, although some evidence suggests that cholesterol released from these particles is used to promote synaptogenesis (Mauch et al., 2001; Pfrieger and Ungerer, 2011).

ApoE has been the focus of considerable attention in AD research because *APOE* genotype is currently the strongest genetic risk factor for LOAD. The human *APOE* gene contains several single-nucleotide polymorphisms (SNPs), with three SNPs resulting in the most common isoforms of apoE: apoE2 (cys112, cys158), apoE3 (cys112, arg158), and apoE4 (arg112, arg158) (Zannis et al., 1982). Prior to its known genetic association with AD, apoE immunoreactivity was observed in amyloid plaques (Namba et al., 1991; Wisniewski and Frangione, 1992). The ε4 allele of the *APOE* gene was subsequently discovered to be a major risk factor for the likelihood of developing AD (Corder et al., 1993; Strittmatter et al., 1993a), with one ε4 allele and two ε4 alleles conferring an approximate 3-fold and 12-fold increased risk, respectively (Bertram et al., 2007). The *APOE* ε4 allele is also associated with an earlier age of AD onset (Corder et al., 1993; Roses, 1996). Conversely, the ε2 allele of *APOE* confers a protective effect and lowers the risk of developing AD (Corder et al., 1994). Currently, one of the main hypotheses for how apoE affects AD pathogenesis is that it regulates the ability of Aβ to deposit in the brain. As described in the next two sections, the mechanism for this effect could occur through the ability of apoE to either influence the aggregation properties of Aβ,

modulate Aβ metabolism, or both (Kim et al., 2009a; Verghese et al., 2011). Therefore, understanding how various aspects of apoE biology influence Aβ metabolism and aggregation are important for further characterizing the role of apoE in AD pathogenesis.

Effect of apoE on Aβ aggregation

In vitro and *in vivo* studies in mice and humans have clearly demonstrated that the apoE isoforms differentially regulate the propensity of Aβ to aggregate. *In vitro* biophysical assays have been used to assess the effect of apoE on the nucleation and fibrillization of synthetic Aβ into filaments. ApoE has been shown to enhance the fibrillization of both Aβ40 and Aβ42, with apoE4 having a greater effect than apoE2 and apoE3 (Castano et al., 1995; Ma et al., 1994; Wisniewski et al., 1994). However, other studies observed that apoE decreases the nucleation of Aβ into fibrils, with no apparent isoform-dependent effects (Evans et al., 1995; Wood et al., 1996). Studies in APP-transgenic mouse models have shown an apoE isoform-dependent effect on amyloid deposition *in vivo*. In PDAPP mice (APP transgenic mice expressing the human *APP* gene via the platelet-derived growth factor promoter) that express the individual human apoE isoforms via transgenic expression, apoE4-expressing mice had increased levels of Aβ deposits and thioflavine-S-positive amyloid deposition than apoE3-expressing mice (Fagan et al., 2002; Holtzman et al., 2000a; Holtzman et al., 1999). Similar results were obtained when APP transgenic mice were crossed to apoE2, apoE3, and apoE4 targeted-replacement mice, which express human apoE under the endogenous mouse promoter. ApoE4 targeted-replacement mice had significantly more Aβ accumulation than apoE2

and apoE3 targeted-replacement mice (Bales et al., 2009; Fryer et al., 2005b). In humans, autopsy studies from AD brains have demonstrated that *APOE* ε4 allele dosage is associated with increased plaque amounts (Rebeck et al., 1993; Schmechel et al., 1993; Tiraboschi et al., 2004). The effect of apoE4 on amyloid deposition has also been measured in living subjects whose brains were imaged with an amyloid imaging agent to detect fibrillar Aβ levels. In cognitively normal individuals, *APOE* ε4 carriers had increased amyloid levels compared to non-carriers in all age groups analyzed (Kantarci et al., 2012; Morris et al., 2010; Reiman et al., 2009). Therefore, apoE4 increases the amount of amyloid deposition in the human brain prior to the onset of clinical AD.

Studies in mice have demonstrated that the level of apoE is also a critical factor in regulating amyloid deposition. Deletion of mouse apoE led to a significant decrease in Aβ deposition and an almost complete lack of amyloid plaques in the PDAPP and Tg2576 APP-transgenic mouse models (Bales et al., 1999; Bales et al., 1997; Holtzman et al., 1999; Holtzman et al., 2000b). Genetically decreasing human apoE levels in APP/PS1 transgenic mice crossed with human apoE3 or apoE4 targeted-replacement mice also decreased Aβ deposition in the brain (Kim et al., 2011). Significantly decreased Aβ and amyloid deposition were detected in the brains of APP/PS1 mice with one copy of the *APOE* ε3 allele or *APOE* ε4 allele compared to mice with two copies of *APOE* ε3 or *APOE* ε4, respectively. Therefore, lower levels of human apoE in the mouse brain decreased Aβ deposition in a manner that was independent of apoE isoform status.

Effect of apoE on Aβ clearance

In addition to exerting an effect on Aβ aggregation, apoE has been shown to alter the transport and metabolism of Aβ in cultured cells and the brain. Several studies using various types of neuronal cells have demonstrated that apoE facilitates the binding and internalization of soluble Aβ, though no overall trend in the effect of the apoE isoforms has emerged (Beffert et al., 1998, 1999a; Cole and Ard, 2000; Nielsen et al., 2009; Yamauchi et al., 2002; Yamauchi et al., 2000; Yang et al., 1999). The ability of both microglia and astrocytes to degrade Aβ *in vitro* was also enhanced in the presence of apoE in several studies (Jiang et al., 2008; Koistinaho et al., 2004; Lee et al., 2012). Though apoE appears to enhance Aβ clearance *in vitro*, *in vivo* studies in mice have shown that apoE impairs Aβ clearance (Bell et al., 2007; Deane et al., 2008; DeMattos et al., 2004). The reason for the difference in the effect of apoE between *in vitro* and *in vivo* studies is currently unknown. In terms of apoE isoforms, the clearance of Aβ from the brain interstitial space is significantly decreased in PDAPP mice that express apoE4 compared to mice that express apoE2 and apoE3 (Castellano et al., 2011). The transport of Aβ across the blood-brain-barrier (BBB) was also significantly impaired when Aβ was complexed with apoE4, in comparison to Aβ complexed with either apoE2 or apoE3 (Deane et al., 2008).

At a molecular level, the mechanism explaining the effect of apoE on Aβ clearance largely depends upon whether apoE interacts with the Aβ peptide directly in the brain (Fig. 1). An abundance of *in vitro* studies have demonstrated an interaction between apoE and Aβ (LaDu et al., 1994; Strittmatter et al., 1994; Tokuda et al., 2000). However,

many of these studies used sub-physiological molar ratios of apoE to Aβ, and often demonstrated that a very small fraction of Aβ is bound to apoE. Therefore, the relevance of the described apoE-Aβ interactions to the *in vivo* environment remains unknown. If an apoE-Aβ complex is present, apoE-containing lipoprotein particles may sequester Aβ in the brain. The apoE-Aβ complex could then be taken up by cells via receptor-mediated endocytosis or transported across the blood-brain-barrier (Fig. 1). In this scenario, the clearance of soluble Aβ would likely depend upon the uptake/transport rates of each individual apoE isoform, which could be faster or slower than the rates for the uptake /transport of unbound Aβ. It is also possible that the amount and/or isoform of apoE could influence Aβ clearance without interacting with Aβ. One possibility is that apoE and Aβ may bind to the same receptors. In this case, apoE could function as a competitive ligand for the receptor-mediated uptake of Aβ into cells or transport across the BBB, effectively blocking Aβ clearance. Further studies are needed to characterize the interaction of Aβ with known apoE receptors to determine the feasibility of this mechanism.

ApoE levels and turnover in the brain

Since the amount of apoE in the brain regulates the extent of Aβ deposition, understanding the mechanisms regulating apoE levels and kinetics in the brain will further elucidate the role of apoE in AD pathogenesis. For instance, the difference in amyloid deposition and clearance between apoE isoforms could be mediated by differences in apoE levels. In humans, multiple studies have analyzed the effect of apoE

isoform status on apoE protein levels in the CSF (Bekris et al., 2008; Castellano et al., 2011; Fukumoto et al., 2003; Lehtimaki et al., 1995; Wahrle et al., 2007) and brain (Beffert et al., 1999b; Bertrand et al., 1995; Harr et al., 1996; Wood et al., 1996). However, results from these studies have not demonstrated any clear trend in apoE levels, likely due to issues with sample stability following collection and heterogeneity in the subject population. Many of the techniques used to measure apoE also rely upon different apoE antibodies which may not recognize the various apoE isoforms with equal affinity. ApoE targeted-replacement mice have become popular tools to measure the effect of the apoE isoforms on Aβ deposition *in vivo*, and attention has been devoted to characterizing the apoE levels in these mice. Since apoE is expressed in these mice under the control of the endogenous mouse *APOE* gene promoter and regulatory elements (Sullivan et al., 1997), protein levels should be a reflection of the natural turnover rates of apoE in the mouse CNS. An initial study characterizing apoE levels in the brains of these mice detected no differences between apoE2, apoE3, and apoE4 (Sullivan et al., 2004). However, subsequent studies have described a genotype-dependent difference in apoE levels (apoE2 > apoE3 > apoE4) in the brain and CSF of these mice (Fryer et al., 2005b; Mann et al., 2004; Ramaswamy et al., 2005; Riddell et al., 2008; Vitek et al., 2009). Further studies are needed to verify these differences and to investigate whether apoE synthesis and degradation rates differ between apoE isoforms.

Mechanistic insight into differences in apoE levels in the brain could be gained by measuring the kinetics of apoE turnover. However, few studies have analyzed apoE turnover in the brain. The clearance of apoE across the BBB has been assessed in mice by

infusing both unlabeled and radiolabeled apoE into the brain and measuring disappearance of the infused proteins over time (Bell et al., 2007; Deane et al., 2008). Clearance of lipid-poor apoE3 occurred at a very slow rate across the BBB and via bulk flow through the ISF (0.03-04 pmol/min g ISF), and the rate was even slower with lipidated apoE3. Using this same technique, the clearance of radiolabeled apoE4 across the BBB was demonstrated to be significantly slower than the clearance of apoE2 and apoE3 (Deane et al., 2008). No studies have analyzed the kinetics of endogenous apoE in the brain, largely because of the lack of techniques to measure protein turnover in the brain. Therefore, the development of methods to measure brain protein dynamics *in vivo* will significantly enhance the mechanistic understanding of apoE dynamics and their relationship to apoE levels.

ApoE receptors and brain apoE metabolism

Given the proposed effect of apoE levels on Aβ clearance, significant attention has been devoted to understanding the cellular pathways for apoE clearance in the brain. Modulating the clearance of apoE via these pathways represents a potential therapeutic strategy for decreasing Aβ deposition in the brain. In the periphery, apoE is internalized by receptor-mediated endocytosis via members of the LDLR family (Mahley, 1988). The LDLR family consists of several different receptors with both endocytic and signaling functions (Herz and Bock, 2002). The low-density lipoprotein receptor (LDLR) is the original member of this family and has been shown to play a central role in the removal

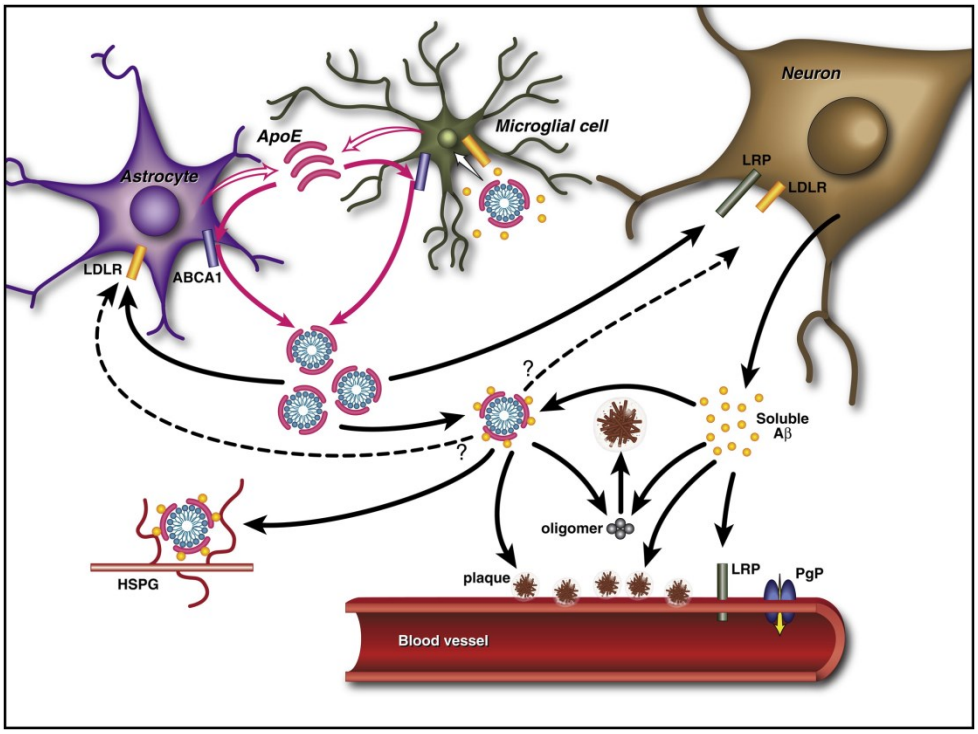

Figure 1.1: Effects of apoE and apoE receptors on Aβ clearance and deposition: ApoE is produced by astrocytes and microglia, and is lipidated by ABCA1 to form lipoprotein particles. ApoE-containing lipoprotein particles are endocytosed into various cell-types via LDLR and LRP. ApoE facilitates the aggregation of soluble Aβ into amyloid plaques in an isoform specific manner (apoE2>apoE3>apoE4). ApoE could bind to Aβ and facilitate its uptake into cells or transport across the blood-brain-barrier. Soluble Aβ could also be cleared by apoE receptors in an apoE-independent process, as has been shown for LRP1. (Reprinted from (Kim et al., 2009a) with permission from Elsevier).

of cholesterol containing low-density lipoprotein particles from the circulation (Brown and Goldstein, 1986). Apolipoprotein B (apoB) or apoE bind to LDLR and facilitate the uptake of lipoprotein particles into cells. In the acidic environment of the endosome, thelipoproteins are released from LDLR and cholesterol is released into the cell, while the receptors are recycled back to the cell surface. Both the lipidation state and isoform status of apoE regulate the binding affinity of apoE with LDLR. ApoE binding to LDLR requires the presence of lipids (Blacklow, 2007), and apoE2 has only 1-2% of binding affinity to LDLR in comparison to apoE3 and apoE4 (Weisgraber et al., 1982).

Several LDLR family members are expressed in various cell-types in the brain, including LDLR, lipoprotein receptor-related protein 1 (LRP1), very low-density lipoprotein receptor (VLDLR), and apolipoprotein E receptor 2 (apoER2) (Herz and Bock, 2002). Current evidence suggests that LDLR and LRP1 are the primary receptors that regulate brain apoE levels. LDLR is more highly expressed on glial cells, while LRP1 is predominately expressed on neurons and to a lesser extent in glia (Rapp et al., 2006). Deletion of the *LDLR* gene in the mouse brain led to a significant increase in the amount of apoE in the brain and CSF (Fryer et al., 2005a), while overexpression of LDLR in the brain decreased apoE levels (Kim et al., 2009b). Alterations of LRP1 showed a similar effect, with conditional deletion of LRP1 leading to increased brain apoE levels (Liu et al., 2007) and overexpression of an LRP1 mini-receptor causing decreased apoE levels (Zerbinatti et al., 2006). Taken together, these studies suggested that LDLR and LRP1 regulate metabolism of apoE in the brain.

Effect of apoE receptors on Aβ metabolism

The effect of LRP1 on Aβ metabolism has been studied both in culture and *in vivo*. LRP1 has been demonstrated to promote the clearance of Aβ via cellular uptake and the BBB (Fig. 1). Increasing LRP1 levels in neuronal cell lines and primary neurons led to increased Aβ uptake, whereas decreasing LRP1 levels had the opposite effect (Fuentealba et al., 2010; Kanekiyo et al., 2011). LRP1 has also been shown to facilitate the binding and internalization of Aβ by mouse brain capillaries (Deane et al., 2004), and inhibition of LRP1 with an antibody impairs the BBB transport of Aβ in the mouse brain (Shibata et al., 2000). The detailed mechanism for how LRP1 facilitates Aβ transport/uptake remains unclear, but may involve a direct physical interaction between LRP1 and Aβ (Deane et al., 2004).

LDLR has been shown to regulate Aβ deposition and clearance in the mouse brain. The effect of deleting the *LDLR* gene on Aβ deposition in APP transgenic mice has produced conflicting results. A study using the Tg2576 mouse (mice that express human APP with the Swedish familial AD mutation) observed a modest increase in amyloid deposition with *LDLR* deletion (Cao et al., 2006), while a second study using PDAPP mice showed no effect (Fryer et al., 2005a). The effect of increasing LDLR on Aβ levels in the brain has also been studied using LDLR transgenic mice. LDLR overexpression in APP/PS1 transgenic mice led to a significant decrease in amyloid load in the brain, and significantly enhanced clearance of Aβ from the interstitial space (Kim et al., 2009b). The mechanism for how LDLR regulates Aβ clearance remains largely unknown. LDLR overexpression in the brain may act indirectly on the clearance of Aβ by decreasing apoE

levels, or LDLR could directly modulate Aβ clearance. In the latter case, it is possible that LDLR may regulate the cellular uptake and degradation of Aβ. This could occur through an apoE-dependent process, such as the uptake of an apoE-Aβ complex. An apoE-independent effect of LDLR on Aβ uptake is also possible, such as a direct interaction with Aβ.

ApoE lipidation in the brain

Along with apoE receptor levels, the amount of lipids and cholesterol associated with apoE in the brain is another factor that regulates the apoE protein level. In the periphery, apoE-containing HDL particles acquire cholesterol and phospholipids from cells through a process known as reverse cholesterol transport (RCT) (Mahley et al., 2006). This process is mediated by the cholesterol transporter ATP-binding cassette A1 (ABCA1), which mediates the efflux of cholesterol to lipid-poor apoA-1 and apoE to form nascent-HDL particles (Krimbou et al., 2004; Wang et al., 2007). Loss-of-function mutations in ABCA1 in humans cause Tangier's disease, which is characterized by extremely low plasma HDL levels and intracellular cholesterol accumulation (Bodzioch et al., 1999; Brooks-Wilson et al., 1999; Rust et al., 1999). Following the ABCA1-mediated formation of nascent HDL particles, further cholesterol efflux to the partially lipidated HDL particles occurs via the protein ATP-binding cassette G1 (ABCG1) (Kennedy et al., 2005). Finally, subsequent maturation of the HDL particles occurs by cholesterol esterification via the enzyme lecithin:cholesterol acyltransferase (LCAT) (Jonas, 1998).

Studies in mice have shown that many of the RCT proteins function in a similar manner in the brain to modulate the lipidation of apoE (Fig. 1). ABCA1, ABCG1, and LCAT are all expressed in the brain (Tachikawa et al., 2005; Warden et al., 1989; Wellington et al., 2002). In culture, ABCA1 was shown to play an important role in the cholesterol efflux capacity of primary astrocytes and microglia (Hirsch-Reinshagen et al., 2004). Deletion of the *ABCA1* gene in the mouse brain led to a significant decrease in apoE levels in the brain, and apoE isolated from the CSF was poorly lipidated (Hirsch-Reinshagen et al., 2004; Wahrle et al., 2004). Interestingly, overexpression of the ABCA1 protein in the brain also decreased apoE levels, although to a lesser extent than ABCA1 deletion (Wahrle et al., 2008). Analysis of the CSF from ABCA-overexpressing mice showed an increase in the size of apoE-containing lipoprotein particles, likely due to increased lipidation. The effect of both ABCG1 and LCAT on apoE levels *in vivo* has also been assessed. Overexpression of ABCG1 had no effect on apoE levels in the mouse brain (Burgess et al., 2008), while deletion of the *LCAT* gene significantly increased mouse brain apoE levels (Hirsch-Reinshagen et al., 2009). These studies suggest that altering the properties of apoE lipidation alters its stability in the brain.

ABCA1 and Aβ deposition

Since lowering apoE levels decreased amyloid deposition in the mouse brain, it was hypothesized that altering ABCA1 levels would also alter amyloid deposition in APP transgenic mice. APP transgenic mice have been generated that have either the *ABCA1* gene deleted or overexpressed. Despite decreased apoE levels with both ABCA1 deletion

and overexpression, only ABCA1 overexpression caused a significant decrease in amyloid load in the mouse brain of APP transgenic animals (Wahrle et al., 2008). The amyloid load in APP transgenic mice lacking ABCA1 remained stable or even increased when ABCA1$^{-/-}$ mice were crossed to various APP transgenic models (Hirsch-Reinshagen et al., 2005; Koldamova et al., 2005a; Wahrle et al., 2005). The opposing effects of ABCA1 deletion and overexpression on Aβ deposition suggests that ABCA1 likely alters Aβ levels and deposition through a mechanism distinct from modulating apoE levels. None of the above studies observed any changes in secreted or cell-associated APP fragments, suggesting ABCA1 does not affect APP processing to form Aβ. Other possible mechanisms may be that the lipidation state of apoE alters the fibrillization or clearance of Aβ from the brain (Hirsch-Reinshagen and Wellington, 2007; Wahrle et al., 2008). ABCA1 could also alter these properties of Aβ in a manner that is independent of apoE. However, none of these possibilities have been thoroughly investigated *in vivo*.

Directions

Provided this background, this thesis work had several aims to further characterize how the pathways that regulate apoE levels modulate Aβ metabolism. The initial aim of this work was to further characterize the role LDLR plays in the metabolism of Aβ by demonstrating an effect of LDLR on the cellular uptake and degradation of Aβ. We further defined the mechanism dictating LDLR-mediated cellular uptake of Aβ by determining whether apoE plays a role in this process and whether LDLR could

physically interact with Aβ. We then designed a new technique for the characterization of apoE turnover in the mouse brain using stable isotope labeling coupled to mass spectrometry. This technique was used to measure the effect of LDLR on apoE clearance in the brain, and to measure the kinetics of the human apoE isoforms in the mouse brain. Finally, to further define the role of ABCA1 in apoE and Aβ clearance, we applied stable isotope labeling kinetics to measure the effect of ABCA1 levels on the clearance of both apoE and Aβ in the mouse brain.

Chapter 2

Low-density Lipoprotein Receptor Represents an Apolipoprotein E-Independent Pathway of Aβ Uptake and Degradation by Astrocytes

(This work was completed with the assistance of several individuals. Dr. Philip Verghese performed the SPR binding experiments. Hyejin Yoon and Dr. Jungsu Kim performed the qPCR experiments. Dr. David Holtzman, Dr. Verghese, and Dr. Kim provided guidance and helpful discussion throughout the study. This work was published in the *The Journal of Biological Chemistry*.)

Summary

Accumulation of the amyloid beta (Aβ) peptide within the brain is hypothesized to be one of the main causes underlying the pathogenic events that occur in Alzheimer's disease (AD). Consequently, identifying pathways by which Aβ is cleared from the brain is crucial for better understanding of the disease pathogenesis and developing novel therapeutics. Cellular uptake and degradation by glial cells is one means by which Aβ may be cleared from the brain. In the experiments described in this chapter, we demonstrate that modulating levels of the low-density lipoprotein receptor (LDLR), a cell surface receptor that regulates the amount of apolipoprotein E (apoE) in the brain, altered both the uptake and degradation of Aβ by astrocytes. Deletion of LDLR caused a decrease in Aβ uptake, while increasing LDLR levels significantly enhanced both the uptake and clearance of Aβ. Increasing LDLR levels also enhanced the cellular degradation of Aβ and facilitated the vesicular transport of Aβ to lysosomes. Despite the fact that LDLR regulated the uptake of apoE by astrocytes, we found that the effect of LDLR on Aβ uptake and clearance occurred in the absence of apoE. Finally, we provide evidence that Aβ can directly bind to LDLR, suggesting an interaction between LDLR and Aβ could be responsible for LDLR-mediated Aβ uptake. Therefore, these results identify LDLR as a receptor that mediates Aβ uptake and clearance by astrocytes, and provide evidence that increasing glial LDLR levels may promote Aβ degradation within the brain.

Introduction

Alzheimer's disease (AD), the most common cause of dementia, is characterized by the appearance of extracellular amyloid plaque deposition in the brain, intraneuronal neurofibrillary tangle formation, and marked neuronal and synaptic loss (Holtzman et al., 2011). Aggregation of the amyloid β (Aβ) peptide into oligomers and fibrils is hypothesized to lead to a pathological cascade resulting in synaptic dysfunction, neuronal loss, and ultimately cognitive decline (Hardy and Selkoe, 2002). Aβ is produced by the proteolytic processing of the amyloid precursor protein (APP) via the proteases β- and γ-secretase, and is subsequently secreted into the extracellular space (De Strooper, 2010). Familial mutations in *APP*, *presenilin 1 (PSEN1)*, and *presenilin 2 (PSEN2)* cause the rare early-onset form of AD primarily through altering the production of Aβ (Hardy, 2006). However, Aβ production does not appear to be altered in the more common late-onset form of AD (Holtzman et al., 2011; Selkoe, 2001). In fact, a recent study suggests that Aβ clearance from the central nervous system, and not production, may be impaired in individuals with late-onset AD (Mawuenyega et al., 2010). Therefore, better characterization of the mechanisms underlying Aβ elimination from the brain may lead to insights into the pathogenesis of the disease and reveal unique therapeutic targets.

Several clearance pathways for Aβ likely exist in the central nervous system, including cellular uptake and lysosomal degradation, transport across the blood-brain barrier, extracellular degradation by proteolytic enzymes, and bulk flow drainage of interstitial fluid and CSF. Aβ clearance via the blood-brain barrier and degradation by extracellular enzymes has been extensively studied (Selkoe, 2001; Tanzi et al., 2004;

Zlokovic, 2008). However, the mechanisms regulating the process of cellular uptake and degradation of Aβ are less characterized. Current evidence suggests that astrocytes are one of the main cell-types in the brain that play a central role in the clearance of Aβ. Astrocytes localize around Aβ plaques in AD brains (Itagaki et al., 1989; Mandybur and Chuirazzi, 1990; Pike et al., 1995), and have been shown to exhibit intracellular Aβ immunoreactivity in histological studies (Funato et al., 1998; Nagele et al., 2003; Thal et al., 1999; Thal et al., 2000). Cell-based assays have shown that cultured astrocytes take up and degrade soluble Aβ and enhance the clearance of fibrillar Aβ from *ex vivo* brain slices (Koistinaho et al., 2004; Nielsen et al., 2009; Shaffer et al., 1995; Wyss-Coray et al., 2003). However, the receptors mediating Aβ uptake into astrocytes are currently unknown.

An isoform of apolipoprotein E (apoE4) is currently the strongest known genetic risk factor for AD. ApoE is a ligand that facilitates the receptor-mediated endocytosis of lipoprotein particles into cells (Mahley, 1988). ApoE is hypothesized to play a central role in AD pathogenesis in large part through the regulation of Aβ deposition and clearance (Kim et al., 2009a; Verghese et al., 2011). Murine studies have shown that the amount of apoE in the brain dramatically affects the extent of Aβ deposition, as deletion of apoE in APP transgenic mouse models significantly decreased brain amyloid levels (Bales et al., 1999; Bales et al., 1997). Therefore, targeting proteins in the brain that modulate apoE levels represents an attractive pathway for decreasing amyloid deposition. The low-density lipoprotein receptor (LDLR) family of receptors is a group of proteins sharing similar structural characteristics that exhibit various important endocytic and

signaling functions. Members of this family include LDLR, lipoprotein receptor related-protein 1 (LRP1), very-low density lipoprotein receptor (VLDLR), apolipoprotein E receptor 2 (ApoER2), and megalin (LRP2) (Herz and Bock, 2002). LDLR plays a key role in cholesterol metabolism in the periphery through facilitating the removal of cholesterol-containing lipoprotein particles from the circulation (Brown and Goldstein, 1986). The uptake of lipoprotein particles occurs through the binding of apolipoprotein B-100 (apoB-100) or apoE to LDLR and subsequent clathrin-mediated endocytosis. In the central nervous system, the function of LDLR is less well-characterized. Recently, we have shown that increasing LDLR levels in the brain significantly decreased apoE levels and markedly inhibited amyloid deposition in the APPswe/PSEN1ΔE9 (APP/PS1) transgenic mouse model (Kim et al., 2009b). Using *in-vivo* microdialysis, we also observed that LDLR overexpression decreased steady-state interstitial fluid Aβ levels and enhanced the clearance of Aβ from the brain extracellular space (Kim et al., 2009b). These findings clearly demonstrated that LDLR is capable of regulating brain Aβ levels. However, the possibility that LDLR-mediated endocytosis represents a pathway for the cellular regulation of Aβ levels has yet to be analyzed.

In the first part of this thesis work, we investigated how altering LDLR levels in primary astrocytes affects Aβ uptake and degradation. We provide evidence that both LDLR overexpression and deletion alters soluble Aβ uptake. We demonstrate that increasing levels of LDLR facilitates Aβ transport to lysosomes and enhances Aβ intracellular degradation. We also show that LDLR can modulate cellular Aβ uptake and clearance through a pathway that does not require the presence of apoE. Finally, we

provide evidence that Aβ directly binds to LDLR. The findings from this study identify a specific receptor-mediated pathway for the uptake and clearance of Aβ by astrocytes, and suggest that enhancing LDLR levels in glial cells represents a potential approach to lowering Aβ levels in the brain.

Experimental Procedures

Reagents - Aβ(1-40), Aβ(1-42), and Aβ(40-1) were purchased from American Peptide Company (Sunnyvale, CA). HiLyte Fluor 488-labeled Aβ42, TAMRA-labeled Aβ42, and Dutch/Iowa Aβ40 were purchased from Anaspec (Fremont, CA). Aβ peptides were reconstituted in dimethylsulfoxide (DMSO) at a concentration of 200 μM and stored at -80°C prior to use. I^{125}-Aβ(1-40) was purchased from PerkinElmer Life Sciences (Waltham, MA), reconstituted at a concentration of 22.7 nM in DMSO, and stored at -20°C prior to use. Recombinant mouse LDLR protein (extracellular domain, amino acids 1-790) was purchased from Sino Biological Inc. (Cat. # 50305-M08H, Beijing, China), reconstituted in water at a concentration of 500 μg/mL, and dialyzed in PBS overnight at 4°C. The dialyzed peptide was then stored at -80°C prior to use. Lysotracker probe and DiI-LDL were purchased from Invitrogen. Recombinant RAP protein was purchased from EMD Biosciences (Cat# 553506). Recombinant mouse PCSK9 protein was purchased from Sino Biological Inc. (Cat. #50251-M08H, Beijing, China), reconstituted in water at a concentration of 500μg/mL, and stored at -80°C prior to use.

Primary cultures - The generation and characterization of the LDLR Tg mice were described previously (Kim et al., 2009b). $LDLR^{-/-}$ mice were purchased from Jackson Laboratory (Catalog # 002207, Bar Harbor, ME). For all experiments, wild type (Wt) littermates were used as controls. All experimental protocols were approved by the Animal Studies Committee at Washington University in St. Louis. Cortical primary murine astrocytes were cultured from postnatal day 2 (P2) mouse pups. Cortices were dissected from the brain and placed in Hanks balanced salt solution (HBSS). The brain tissue was then washed with HBSS and treated with 0.05% trypsin/EDTA for 15 min at 37°C. Following trypsin digestion, the tissue was resuspended and triturated using fire-polished pipets in growth media containing DME/F12, 20% fetal bovine serum (FBS), 10 ng/ml epidermal growth factor, 100 units/ml penicillin/streptomycin, and 1 mM sodium pyruvate. The cell suspension was then passed through a 100-μm nylon filter and plated into T75 flasks coated with poly-D-lysine. The media of the mixed glial cultures was changed after six days, and every three days following the initial change. Once the cells reached confluency, they were shaken at 250 rpm for three hours and the media was aspirated to remove the less adherent microglial cells. The astrocyte-enriched cultures were then washed with PBS, detached from the plate using 0.05% trypsin/EDTA and passaged into 6, 12, or 24 well plates for experiments.

Measurement of apoE levels by ELISA - Primary astrocytes were plated into 12 well plates and grown to confluency. The cell monolayers were then washed twice with serum free media (SFM) (DME/F12, N-2 growth supplement, 100 units/ml

penicillin/streptomycin, and 1 mM sodium pyruvate) and 500 µL of fresh SFM was added. The cells were then incubated at 37°C for 3, 8, or 24 hrs. Following incubation, the media was removed and protease inhibitor was added to the media (Complete protease inhibitor cocktail, Roche, USA). The cells were washed three times in PBS and lysed in 1% Triton X-100 lysis buffer (1% Triton X-100, 150 mM NaCl, 50 mM Tris-HCl, and Complete protease inhibitor cocktail). The lysate was then cleared by centrifugation at 14,000 rpm and total protein content measured by BCA assay. The apoE level in the media was quantified using a sandwich ELISA for apoE. Mouse monoclonal antibody HJ6.2 was used as the capture antibody and mouse monoclonal antibody HJ6.3-biotin was used as the detection antibody (both antibodies were produced in-house with full length astrocyte-derived mouse apoE-containing lipoproteins as the antigen). Pooled C57BL/6J plasma set at a concentration of 329 µg/mL was used as the standard for ELISA. 96 well microtiter plates were coated overnight at 4°C with HJ6.2 antibody (5 µg/mL). All washes were performed 5 times/well using a standard microplate washer. Coated plates were washed and blocked for 1 hr at 37°C in 1% milk in PBS. The plates were then washed again and samples and standards were loaded in 0.5% bovine serum albumin in PBS-0.025% Tween 20 and incubated overnight at 4°C. Then, plates were washed and incubated with HJ6.3-biotin antibody at a concentration of 400 ng/mL in 0.5% bovine serum albumin/PBS-0.025% Tween 20 at 37°C for 90 minutes. Plates were washed and horseradish-peroxidase conjugated streptavidin at a 1:5000 dilution was incubated for 90 min at room temperature. Plates were washed, tetramethylbenzidine

substrate was added, and the absorbance was measured at 650 nm. All apoE values were normalized to total cell protein levels.

Aβ uptake and clearance assays - Primary astrocytes were plated into either 12 or 24 well plates and grown to confluency. To measure Aβ uptake, the cells were first washed twice with SFM, and fresh SFM was added to the cells. Soluble Aβ(1-40) or Aβ(1-42) was then added to the media at a concentration of 2 μg/mL and the cells were incubated at 37°C for 3 hrs. The media was then removed and the cells washed twice with PBS. To remove cell surface-bound Aβ, the cells were incubated with 0.05% trypsin/EDTA for 20 minutes. The cells were then pelleted by centrifugation and the pellet washed twice with PBS. Following centrifugation, 1% Triton X-100 lysis buffer (1% Triton X-100, 150 mM NaCl, 50 mM Tris-HCl, and Complete protease inhibitor cocktail) was added to the cell pellet and the cells were incubated at 4°C for 30 min. The cell lysates were then cleared by centrifugation at 14,000 rpm. For the clearance assays, the cells were first washed twice with SFM and fresh SFM was added to the cells. Soluble Aβ(1-40) or Aβ(1-42) was then added to the media at a concentration of 2 μg/mL and the cells were incubated at 37°C for 24 hrs. A control group was also included in which the Aβ was added directly to fresh SFM in order to calculate how much Aβ was initially added to the cells (0 hr time point). The media was then collected from the cells and Complete protease inhibitor (Roche) was added to the media. The cell monolayer was then washed twice with PBS and 1% Triton X-100 lysis buffer was added to the cells and they were incubated at 4°C for 30 min. The cell lysates were then cleared by centrifugation at 14,000 rpm. Protein

content was measured in all cell lysates using a BCA protein assay (Thermo Scientific). Aβ(x-40) and Aβ(x-42) specific sandwich ELISA's developed in our lab were used to quantify Aβ40 and Aβ42 levels, respectively, in the lysate or media. For the Aβ(x-40) assay, HJ2 (anti-Aβ35-40) was used as the capture antibody and HJ5.1-biotin (anti-Aβ13-28) as the detection antibody. For the Aβ(x-42) assay, HJ7.4 (anti-Aβ37-42) was used as the capture antibody and HJ5.1-biotin (anti-Aβ13-28) as the detection antibody.

I^{125}-Aβ degradation assays - Primary astrocytes were plated into 12 well plates and grown to confluency. The cells were then washed twice with SFM and 0.25 nM of I^{125}-Aβ(1-40) was added to the cells in 500 μL of SFM. The cells were then incubated for 3, 8, or 24 hrs at 37°C. The media was then collected and the cells washed three times in PBS. The cells were then lysed in the plate by the addition of radioimmunoprecipitation assay (RIPA) buffer (1% NP-40, 1% sodium deoxycholate, 0.1% SDS, 25 mM Tris-HCl, 150 mM NaCl) (Cat. # 89901, Thermo Scientific) and the lysate cleared by centrifugation at 14,000 rpm. Total protein content was measured by BCA assay. The media was then subjected to a trichloroacetic acid (TCA) precipitation. 50 mg/mL of BSA and 2% deoxycholate was added to the media and the tubes were vortexed and then incubated on ice for 30 minutes. TCA (20% of final volume) was added to the tubes and following a quick vortex, and the tubes were incubated on ice for 1 hr. All tubes were then spun down at 14,000 rpm for 30 minutes. CPM in both the supernatant and pellet were measured by a gamma counter. To measure Aβ degradation by astrocyte-conditioned media (ACM), primary astrocytes were plated into 12 well plates and grown to confluency. The cells

were then washed twice with SFM and fresh SFM was added to the cells. The cells were then incubated for 3, 8, or 24 hrs at 37°C. The media was then collected, and I^{125}-Aβ(1-40) was added to the ACM for 3, 8, or 24 hrs at 37°C. A TCA acid precipitation was then performed on the media as explained above. The cells from which the media was originally collected were also lysed as above, and total protein content measured with a BCA protein assay.

Fluorescent Aβ uptake and colocalization analysis - Primary astrocytes were plated into 35 mm μ-dish chambers. For DiI-LDL imaging experiments, the cells were washed twice with SFM and HiLyte Fluor 488-labeled Aβ42 (3 μg/mL) was added to the cells in SFM. The cells were then incubated at 37°C for 3 hrs prior to imaging. One hour prior to imaging, DiI-LDL was added to the cells (0.5 μg/mL). The cells were then washed twice with SFM, and fresh SFM medium was added for imaging. For the lysotracker experiments, TAMRA-labeled Aβ42 (2 μg/mL) was added to the cells in SFM and the cells were incubated at 37°C for 3 hrs prior to imaging. Fresh SFM was then added to the cells with 50 nM of the lysotracker probe and the cells were incubated for another 15 min at 37°C. Fresh SFM was then added to the cells prior to imaging. The cells were imaged using a Zeiss LSM5 Pascal system coupled to an Axiovert 200M microscope equipped with an argon 488 and He/Ne 543 laser. For the colocalization studies, the Zeiss AIM software was used. Threshold quadrants were set using cells incubated only with either TAMRA-labeled Aβ42 or lysotracker. Colocalization coefficients were calculated by summing the pixels in the colocalized quadrant and then dividing by the sum of pixels in

the colocalized and non-colocalized quadrant. 2-3 cells were quantified in 5-6 regions of each dish for the statistical analysis.

Construction of LDLR lentivirus and transduction of astrocytes - The LDLR cDNA was subcloned from the pcDNA3.1 vector used to make the LDLR Tg mouse (Kim et al., 2009b) into the FCIV (FM5) lentiviral vector (generous gift of Dr. Jeffrey Milbrandt lab, Washington University). This vector uses the ubiquitin promoter to express the gene of interest and also expresses the Venus protein via an internal ribosome entry site. Using PCR, the LDLR cDNA was amplified from the pcDNA3.1 vector with primers containing the *AgeI* and *AscI* restriction sites (forward primer 5'-ACTGGTACCGGTG CCACCATGAGCACCGCGGATC-3' and reverse primer 5'GTACCAGGCGCGCC TCATGCCACATCGTCCTCCAGG-3'). Following digestion of both the LDLR PCR product and FCIV with *AgeI* and *AscI*, LDLR was ligated into the FCIV vector. The sequence and orientation of the insert was verified by complete sequencing. Lentivirus (FCIV-LDLR and FCIV) was produced and the titer calculated as described previously (Li et al., 2010). Prior to transduction, primary astrocytes were plated in 24 well plates and grown to 60% confluency. Lentivirus was then added to the cells (multiplicity of infection of 1.5) and they were incubated at 37°C for 48 hrs. Fresh medium was then added to the cells and they were cultured for 24 hrs. A second dose of lentivirus was then added to the cells (MOI of 0.75) and they were incubated at 37°C for 24 hrs. Fresh medium was then added and the cells were cultured for 8 to 10 days prior to performing experimental assays, changing the medium every two to three days. Lentivirus

transduction was confirmed by both Venus expression and immunoblot for hemagglutinin (HA) and LDLR (see below).

Immunoblots - Primary astrocytes were lysed in either RIPA buffer (1% NP-40, 1% sodium deoxycholate, 0.1% SDS, 25 mM Tris-HCl, 150 mM NaCl) to measure LDLR, apoE, LRP1, and RAP levels or 1% Triton X-100 lysis buffer to measure Aβ levels. The lysates were spun down at 14,000 rpm for 20 minutes and the supernatant was collected. Protein concentration was determined by bicinchoninic acid (BCA) protein assay. Equal amounts of protein for each sample were run on 4-12% Bis-Tris XT gels for apoE, LDLR, LRP1, and RAP and 16.5% Tris-Tricine gels for Aβ (Bio-Rad), and transferred to polyvinylidene fluoride (PVDF) membranes (0.45 μm pore size) and nitrocellulose membranes (0.2 μm pore size), respectively. Prior to blocking, the Aβ membranes were boiled for 10 minutes in PBS. All membranes were then blocked in 5% milk in TBS-T (tris-buffered saline with 0.125% Tween-20). Blots were probed for LDLR (Novus Cat#NB110-57162 and MBL Cat#JM3839-100), HA (Covance), Aβ (82E1, IBL International), apoE (Calbiochem), LRP1 (generous gift of Dr. Guojun Bu, Mayo Clinic, Jacksonville, FA), RAP (R&D Systems Cat # AF4480), actin (Sigma), and tubulin (Sigma). Protein signal from the membranes was measured using a Lumigen TMA-6 ECL detection kit (Lumigen, USA) and quantified using ImageJ software (NIH).

Coimmunoprecipitation of Aβ and LDLR - His-tag purified recombinant LDLR (5 μg/mL, extracellular domain) was incubated with Aβ40 (400 nM) for 4 hrs at 37°C in

binding buffer (50 mM NaCl, 50 mM Tris-HCl, 2 mM $CaCl_2$, pH = 7.4). For the competition experiments, LDLR was pre-incubated with either RAP, PCSK9 or Aβ(40-1) for 2 hrs at room temperature in binding buffer. For the immunoprecipitation, the LDLR-Aβ samples were diluted 1:1 in binding buffer with 0.1% Triton X-100. 50 µL of anti-His microbeads (Miltenyi Biotec Cat. # 130-091-124, Auburn, CA) were then added to each sample followed by a 30 min incubation with rotation at 4°C. The samples were then applied to µ-columns (Miltenyi Biotec, Cat. # 130-042-701) and the beads were washed 5 times with wash buffer (binding buffer with 1% Triton X-100 and 0.25% sodium deoxycholate) and once with binding buffer. Pre-heated elution buffer was then applied to the columns and the eluate was collected and analyzed by SDS-PAGE (16.5% Tris-tricine). LDLR was detected using an anti-His antibody (Santa Cruz, Cat. # sc-8036HRP) and Aβ was detected using the 82E1 antibody (IBL International).

Surface plasmon resonance (SPR) - Sensor chips were purchased from GE-BIAcore (USA). All SPR experiments were carried out on a BIAcore 2000 instrument at 25°C. Lyophilized Aβ(1-40) and Aβ(1-42) peptides were resuspended in trifluoroacetic acid and incubated at room temperature for 15 minutes. The peptides were then dried under nitrogen gas and resuspended in hexafluoroisopropanol (HFIP). The HFIP was then dried under nitrogen gas, and the peptides were resuspended in HFIP and aliquoted into separate tubes. The HFIP was then dried again under nitrogen gas. The dry Aβ film was then stored at -80°C. Prior to use, the Aβ film was dissolved in DMSO. Aβ(1-40) and Aβ(1-42) were immobilized onto a CM5 sensor chip surface at densities of approximately

4-5 fmol/mm^2 by amine coupling with sodium citrate buffer, pH 4.75 in accordance with the manufacturer's instructions (BIAcore AB). One flow cell was activated and blocked with 1 M ethanolamine without any protein and was used as a control surface to normalize SPR signal from Aβ immobilized on the flow cells. Experiments were conducted in PBS (pH 7.4) and the analyte was injected at a flow rate of 30 μl/min. Dissociation followed using the same buffer for 6 min. After each run, the sensor chip was regenerated using 2 M guanidine-HCl, 10 mM Tris-HC1, pH 8.0 and washed with running buffer for 5-10 min prior to the next injection. Data analysis was performed using Scrubber2 (Center for Bimolecular Interaction, Utah University) and BIAevaluation software (GE-BIAcore), and dissociation constants were calculated using a single-site binding model in GraphPad Prism Software. Data are based on 3 independent measurements using 6 different concentrations for each measurement. K_D values are presented as mean ± S.D.

Quantitative real-time PCR (qPCR) - Total RNAs were extracted from cortical primary astrocytes using TRIzol® Reagent (Invitrogen). RNAs were reverse transcribed with High Capacity cDNA Reverse Transcription kit (Applied Biosystems). qPCR was performed with SYBR® Advantage® qPCR Premix (Clontech) in ABI 7500 instrument (Applied Biosystems) using the default thermal cycling. The forward primer for ApoE was 5'- CTGACAGGATGCCTAGCCG -3', and the reverse primer was 5'- CGCAGGT AATCCCAGAAGC -3'. U6 primer sets included in the mir-X miRNA First-Strand Synthesis kit (Clontech) were used to normalize qPCR signals among samples. To

confirm the specificity of qPCR reactions, dissociation curves were analyzed at the end of qPCR assays. Relative mRNA levels were calculated by comparative Ct method using the Applied Biosystems 7500 software.

Ligand blotting - Purified LDLR extracellular domain (2 μg, Sino Biological) was resolved on nonreducing SDS-PAGE (3-8% Tris-acetate, sample was not boiled and no reducing agent was added) and the protein was then transferred to a PVDF membrane. The LDLR protein was then denatured/renatured in Guan-HCl. The blot was incubated in sequential 30 min washes at room temperature of 6 M, 3 M and 1 M Guan-HCl. The blot was then washed in 0.1 M Guan-HCl for 30 min at 4°C and no Guan overnight at 4°C. For all of the steps the Guan-HCl was diluted into the denaturing/renaturing buffer (10% glycerol, 100 mM NaCl, 20 mM Tris (pH 7.6), 0.5 mM EDTA, 0.1% Tween-20, and 2% milk). The blot was then blocked in 2.5% milk in TBS-T (tris-buffered saline with 0.125% Tween-20). Either Aβ or recombinant apolipoprotein E3 (5 μg/mL, Leinco Technologies, St. Louis, MO) was then incubated with the blot for 3 hr at room temperature in TBS (50 mM Tris-HCl, 150 mM NaCl, pH=7.5), followed by three 10 minute washes in TBS-T. Immunoblotting for either Aβ, apoE, or the His tag was then performed.

Statistics - All data are presented as mean ±standard error of the mean (SEM) unless otherwise noted. Statistical significance (*$p<0.05$, **$p<0.01$, ***$p<0.001$) was determined using GraphPad Prism Software. For the comparison of two means with one

independent variable (genotype), a two-tailed student's t-test was used. For the comparison of multiple means with one independent variable (genotype), a one-way ANOVA followed by a Tukey's post-test was used. For the comparison of multiple means with two independent variables (genotype and time, genotype and lentivirus transduction), a two-way ANOVA followed by a Bonferroni post-test was used.

Results

LDLR overexpression in primary astrocytes increases Aβ uptake and clearance. To determine whether LDLR mediates the uptake and clearance of Aβ by astrocytes, we first cultured primary astrocytes from the cortices of transgenic (Tg) mice that overexpress mouse LDLR under control of the mouse prion promoter (Kim et al., 2009b). The LDLR transgene in these mice contains an HA tag to facilitate detection of LDLR protein levels. Immunoblots were performed to measure the amount of LDLR overexpression in these cells. Consistent with our previous study, LDLR Tg astrocytes expressed about 8-fold higher LDLR levels than wildtype (Wt) cells (Fig. 2.1A). In order to assess the functional effect of increasing LDLR levels in astrocytes, we measured the extra- and intracellular levels of apoE. Astrocytes endogenously secrete lipoprotein particles with discoidal HDL structure and size that contain apoE (Fagan et al., 1999). Since LDLR overexpression dramatically decreased apoE levels in brain tissue (Kim et al., 2009b), we hypothesized that increasing LDLR levels in astrocytes would promote apoE uptake and consequently lead to decreased apoE levels outside of the cells. Wt and LDLR Tg primary astrocytes were cultured in serum-free conditions and the amount of apoE in the media was

measured at several time points. Serum-free conditions were used so that the majority of the lipoproteins present in the media were produced by astrocytes. The medium from LDLR Tg astrocytes had significantly decreased apoE levels at all time points measured, with a maximum 80% decrease observed after 24 hrs (Fig. 2.1B). The amount of intracellular apoE was also measured after 24 hrs by immunoblot, and LDLR Tg cells had increased levels of apoE in comparison to Wt cells (Fig. 2.1C). To confirm that the changes in apoE distribution in the LDLR Tg cells were due to an alteration in uptake rather than apoE production, apoE mRNA levels were measured by quantitative PCR. No differences were observed between Wt and LDLR Tg cells (Fig. 2.2). Therefore, the decrease in extracellular apoE levels and increase in intracellular apoE levels in LDLR-overexpressing astrocytes is likely due to enhanced uptake of apoE-containing lipoprotein particles.

Previous studies have shown that cultured astrocytes are capable of taking up and clearing soluble Aβ from the media (Nielsen et al., 2009; Shaffer et al., 1995; Wyss-Coray et al., 2003). Given the dramatic effect that LDLR overexpression has on lowering Aβ levels in the brain (Kim et al., 2009b), we hypothesized that increasing LDLR levels in astrocytes would enhance Aβ uptake and clearance. Aβ uptake was assessed by the addition of soluble Aβ40 (2 μg/mL) or Aβ42 (2 μg/mL) to the media of Wt and LDLR Tg astrocytes for 3 hrs at 37°C. Trypsin was added to the cells to remove Aβ bound to the extracellular cell surface and the amount of cell-internalized Aβ was measured by ELISA. LDLR overexpression enhanced the amount of intracellular Aβ40 and Aβ42 by 3.1 fold and 2.2 fold, respectively (Fig. 2.3A,B). The differences in intracellular Aβ levels were also confirmed by immunoblot (Fig. 2.3C). These results suggest that

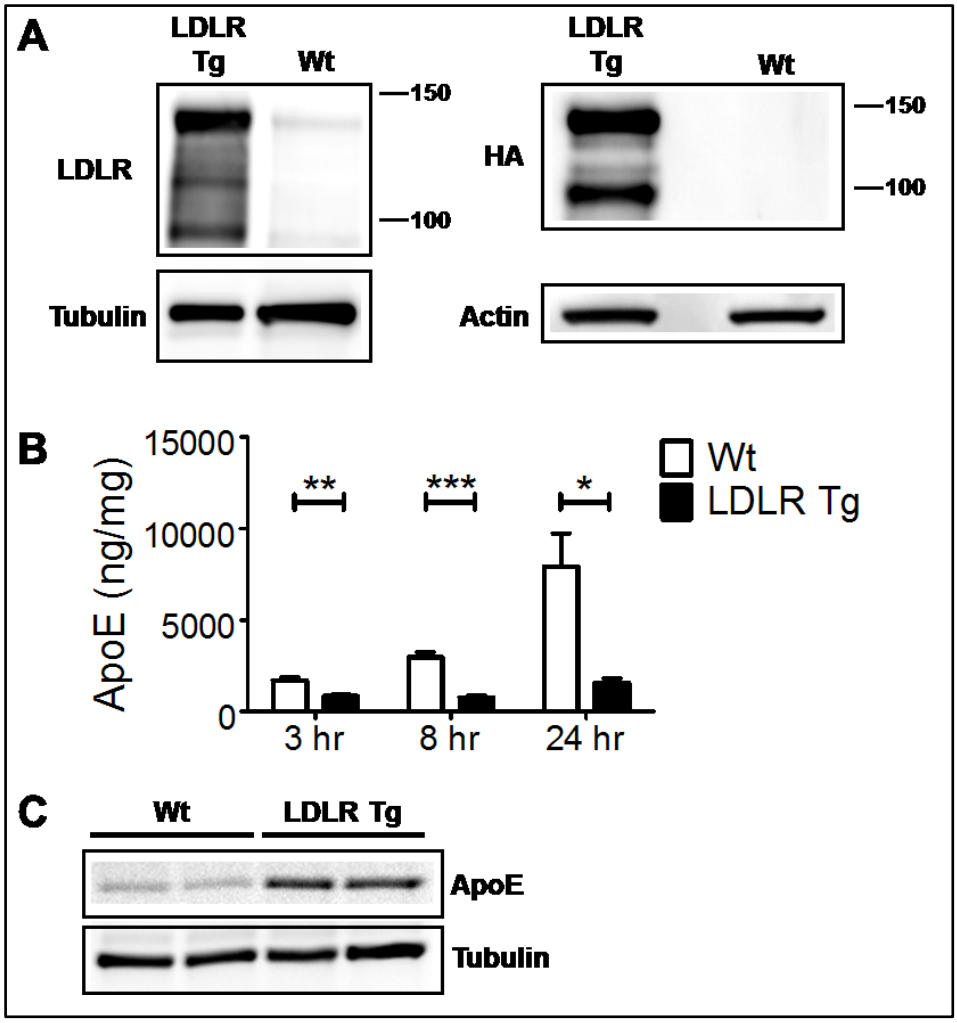
A
LDLR Tg
Wt
LDLR
150
100
Tubulin
LDLR Tg
Wt
HA
150
100
Actin
B
ApoE (ng/mg)
15000
10000
5000
0
**
***
*
3 hr
8 hr
24 hr
Wt
LDLR Tg
C
Wt
LDLR Tg
ApoE
Tubulin

Fig. 2.1. Increased LDLR levels alter the extracellular and intracellular levels of apoE in primary astrocytes. Primary astrocytes were cultured from the cortices of both Wt and LDLR transgenic mice. **(A)** LDLR and HA levels in the cells were measured by immunoblot. Unglycosylated LDLR migrates at 90 kDa and several glycosylated species of the protein migrate between 100 kDa and 150 kDa. Representative images are shown. **(B)** The functional effect of increased LDLR levels on apoE uptake was assessed by measuring the levels of endogenously produced apoE in the culture media. Primary astrocytes were incubated for the indicated time points in serum-free media and the amount of apoE in the media was measured by ELISA. Mean ± SEM (n=4) * denotes $p<0.05$, ** denotes $p<0.01$, *** denotes $p<0.001$. **(C)** The amount of cell-associated apoE was also measured by immunoblot of the cell lysates obtained after a 24 hr incubation. Representative image is shown.

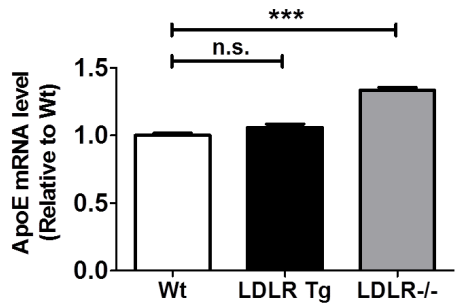

Fig. 2.2. Effect of LDLR levels on apoE mRNA amount in astrocytes. Primary astrocytes were cultured from the cortices of Wt, LDLR$^{-/-}$, and LDLR Tg mice. ApoE mRNA levels were then assessed by qPCR, and the values were normalized to U6 snRNA values. Mean ± SEM (n≥4) *** denotes p<0.001.

increasing LDLR levels enhances Aβ uptake into primary astrocytes. To measure the effect of increasing LDLR levels on Aβ clearance from the media, soluble Aβ40 (2 μg/mL) or Aβ42 (2 μg/mL) was added to the media of Wt and LDLR Tg astrocytes for 24 hrs at 37°C. The amount of Aβ remaining in the medium was then measured by ELISA. After 24 hrs, 71% of Aβ40 remained in the medium of Wt astrocytes while only 30% of Aβ40 remained in the medium of LDLR Tg cells (Fig. 2.3D). For Aβ42, 43% remained in the medium of Wt astrocytes while only 17% remained in the medium of LDLR Tg cells after 24 hrs (Fig. 2.3E). Therefore, the amount of Aβ remaining in the medium after 24 hrs was less for LDLR Tg cells in comparison to Wt cells, with a decrease of 58% for Aβ40 and a decrease of 61% for Aβ42.

LRP1, another member of the LDL receptor family, has also been shown to promote the internalization of Aβ into neuronal cells (Kanekiyo et al., 2011). To

determine whether increasing LDLR levels alters LRP1 levels, the amount of LRP1 in Wt and LDLR Tg astrocytes was analyzed by immunoblot (Fig. 2.4A). LRP1 levels were decreased in LDLR overexpressing astrocytes, suggesting that the increase in Aβ uptake and clearance in these cells is not due to increased LRP1 levels. The levels of receptor-associated protein (RAP), a chaperone for the LDL receptors, were also measured in LDLR Tg and Wt astrocytes (Fig. 2.4B). RAP has been shown to bind to Aβ and regulate its uptake into cells (Kanekiyo and Bu, 2009). LDLR overexpression did not significantly change RAP levels in astrocytes. In summary, these results demonstrate that increasing LDLR levels in primary astrocytes enhanced both the uptake and clearance of soluble Aβ.

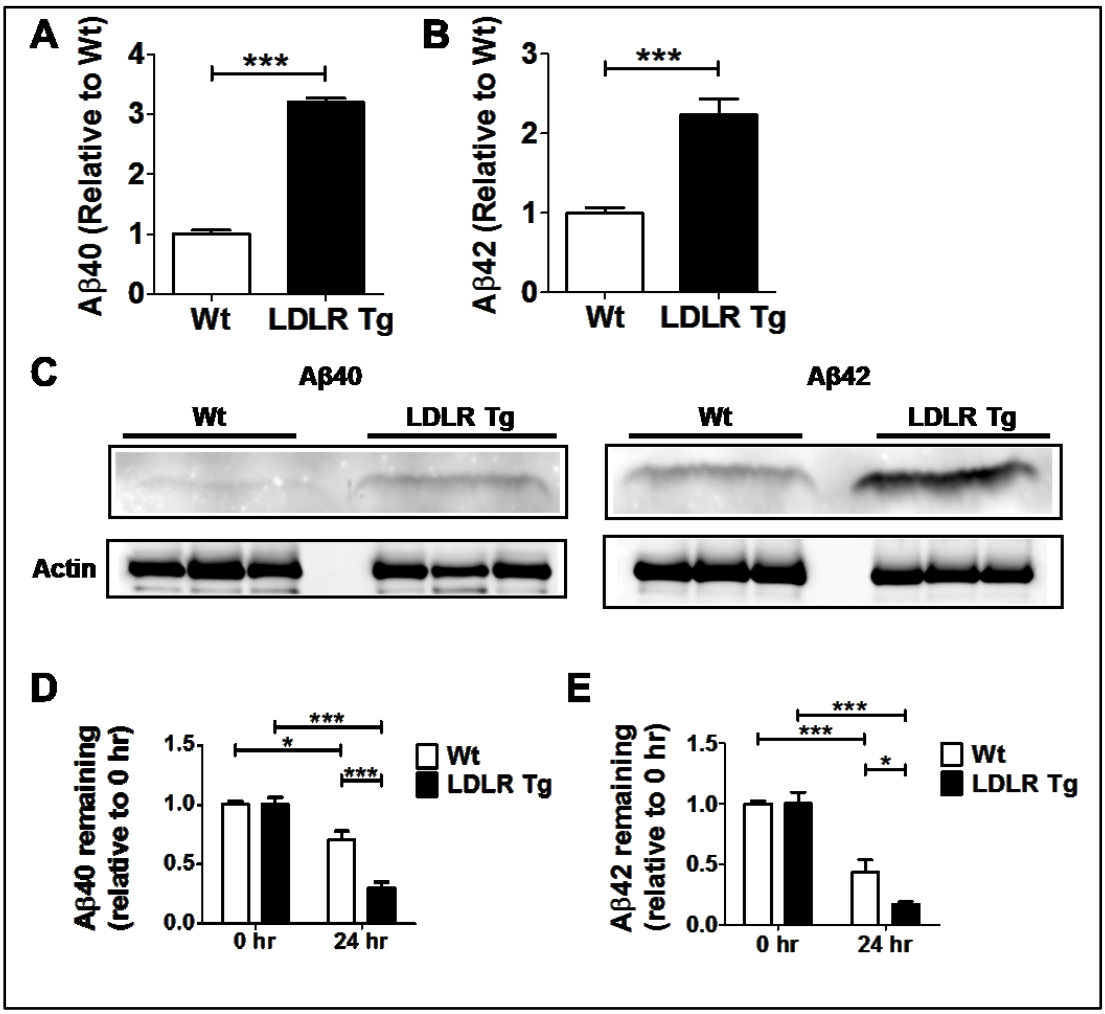
A
Aβ40 (Relative to Wt)
***
Wt
LDLR Tg
B
Aβ42 (Relative to Wt)
***
Wt
LDLR Tg
C
Aβ40
Aβ42
Wt
LDLR Tg
Wt
LDLR Tg
Actin
D
Aβ40 remaining (relative to 0 hr)
***
*
***
Wt
LDLR Tg
0 hr
24 hr
E
Aβ42 remaining (relative to 0 hr)
***
***
*
Wt
LDLR Tg
0 hr
24 hr

Fig. 2.3. LDLR overexpression enhances the uptake and clearance of Aβ by primary astrocytes. Primary astrocytes from either Wt or LDLR transgenic mice were incubated with soluble **(A)** Aβ40 or **(B)** Aβ42 (2 μg/mL) for 3 hrs at 37°C. The cells were then washed with PBS, incubated with trypsin to remove cell-surface bound Aβ, and lysed in Triton X-100 lysis buffer. The cell-internalized Aβ was then assessed by ELISA. Mean ± SEM ($n \geq 4$) *** denotes $p<0.001$. **(C)** Immunoblot analysis for Aβ was also performed on the cell lysates. Representative images are shown. Aβ clearance was assessed by the addition of either **(D)** Aβ40 or **(E)** Aβ42 (2 μg/mL) to the medium of primary astrocytes. After 24 hrs, the levels of Aβ remaining in the medium along with the starting amount of Aβ were measured by ELISA. Mean ± SEM ($n \geq 4$) * denotes $p<0.05$, *** denotes $p<0.001$, n.s. not significant.

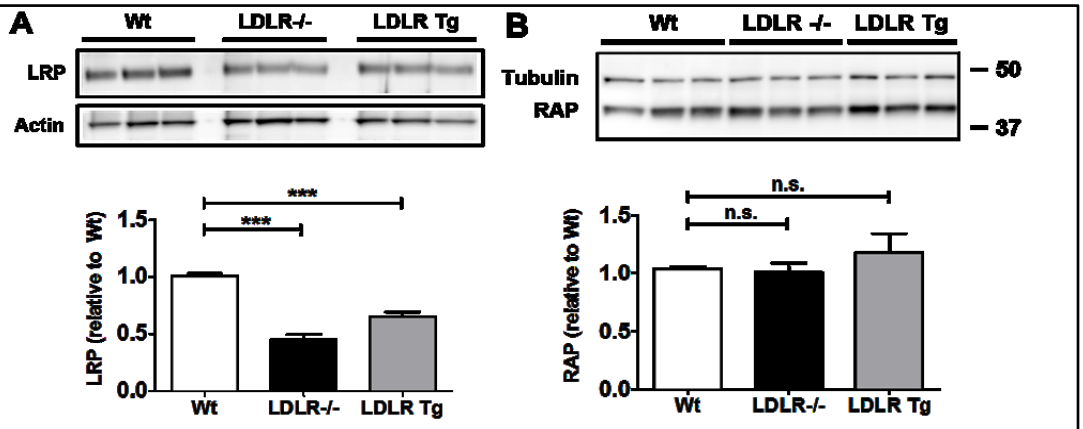

Fig. 2.4. Effect of LDLR levels on the amount of LRP1 and RAP in astrocytes. Primary astrocytes were cultured from the cortices of Wt, LDLR$^{-/-}$, and LDLR Tg mice. **(A)** LRP1 levels and **(B)** RAP levels were measured by immunoblot and normalized to either actin or tubulin levels, respectively. Mean ± SEM (n≥4) *** denotes p<0.001, n.s. not significant.

Increasing LDLR levels in primary astrocytes promotes the cellular degradation of Aβ. In order to verify that the increased Aβ uptake by LDLR-overexpressing astrocytes resulted in enhanced degradation of the peptide, we directly assessed Aβ degradation using I^{125}-Aβ(1-40). I^{125}-Aβ(1-40) was incubated with Wt and LDLR Tg cells at 37°C for several time points and a TCA precipitation was then performed on the cell media. In this assay, degraded Aβ peptide is not precipitated and therefore cannot be efficiently pelleted with centrifugation. The amount of Aβ that has been degraded can be directly quantified by measuring the radioactive counts in the supernatant following centrifugation (Fig. 2.5A). We observed that LDLR Tg cells degraded significantly more Aβ than Wt cells at

all time points analyzed. The amount of intact Aβ measured from the LDLR Tg cells was also lower for all time points (Fig. 2.5B). After 24 hrs of incubation, LDLR Tg cells degraded 80% of the Aβ while Wt cells degraded 53% of the Aβ that was initially added (Fig. 2.5C). These results demonstrate that LDLR overexpression enhances Aβ degradation by primary astrocytes.

Previously it has been shown that astrocytes secrete proteases that are capable of degrading Aβ, including insulin degrading enzyme (IDE) and matrix metalloproteinase (Jiang et al., 2008; Yin et al., 2006). Therefore, to determine whether the effect of LDLR on Aβ degradation is due to intracellular or extracellular degradation we analyzed the ability of astrocyte-conditioned medium from Wt and LDLR Tg astrocytes to degrade Aβ in the absence of cells. Medium from Wt and LDLR Tg primary astrocytes was collected and then incubated with I^{125}-Aβ for the indicated time points. Aβ degradation was then assessed by TCA precipitation. Medium from both Wt and LDLR Tg astrocytes was capable of degrading Aβ, but to a lesser extent than when cells were present (compare Fig. 2.5B and 2.5D). After 8 hrs, medium from the LDLR Tg astrocytes degraded significantly more Aβ than the medium from the Wt cells. After 24 hrs, we observed that medium from LDLR Tg astrocytes degraded significantly less Aβ than the Wt media (Fig. 2.5E). Taken together, the difference in the effect of LDLR on Aβ degradation with and without cells after 24 hrs indicates that LDLR is capable of promoting cellular Aβ degradation.

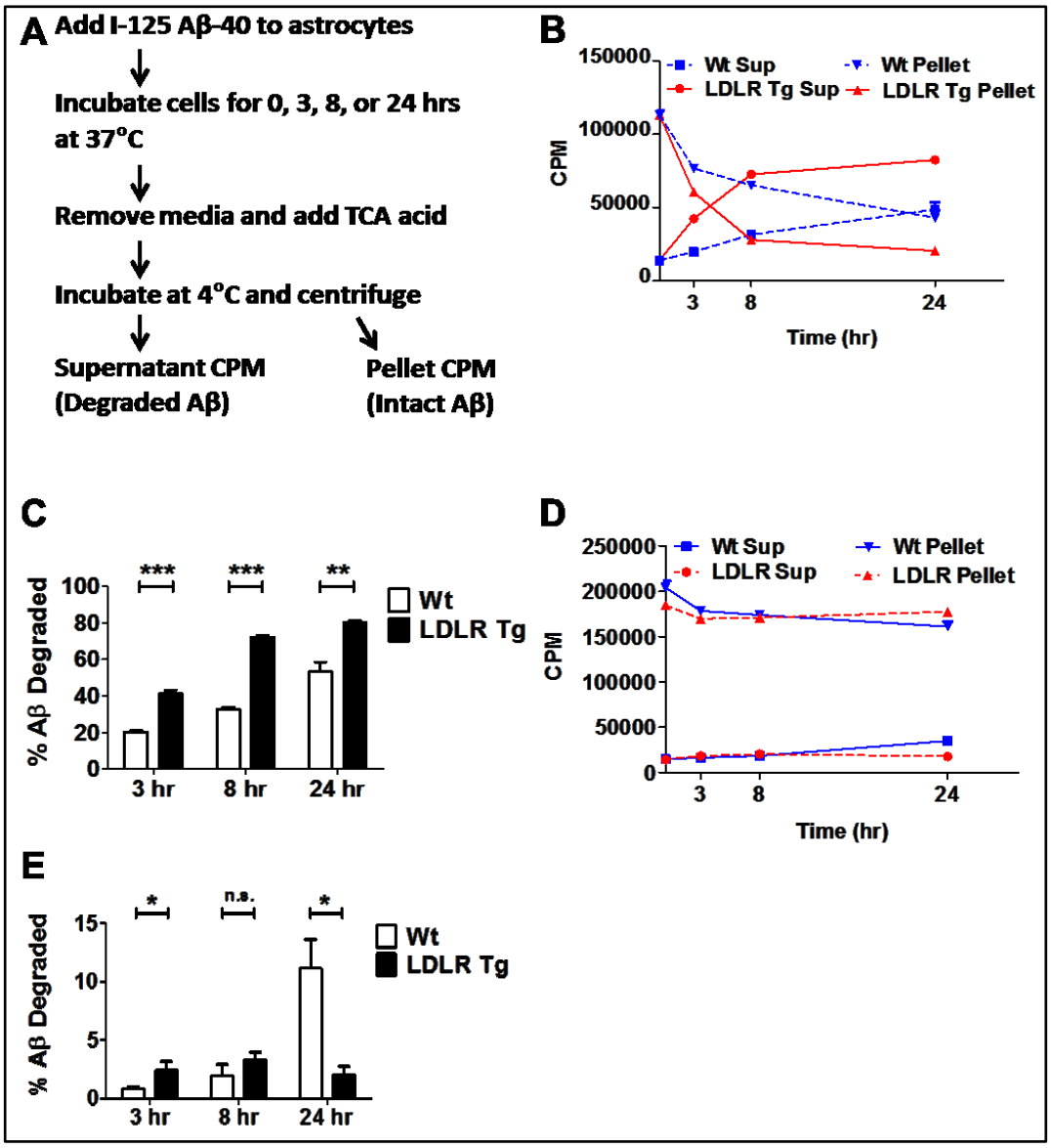
A
Add I-125 Aβ-40 to astrocytes
Incubate cells for 0, 3, 8, or 24 hrs at 37°C
Remove media and add TCA acid
Incubate at 4°C and centrifuge
Supernatant CPM (Degraded Aβ)
Pellet CPM (Intact Aβ)
B
Wt Sup
Wt Pellet
LDLR Tg Sup
LDLR Tg Pellet
CPM
150000
100000
50000
0
3
8
24
Time (hr)
C
% Aβ Degraded
100
80
60
40
20
0
***
***
**
3 hr
8 hr
24 hr
Wt
LDLR Tg
D
Wt Sup
Wt Pellet
LDLR Sup
LDLR Pellet
CPM
250000
200000
150000
100000
50000
0
3
8
24
Time (hr)
E
% Aβ Degraded
15
10
5
0
*
n.s.
*
3 hr
8 hr
24 hr
Wt
LDLR Tg

Fig. 2.5. LDLR overexpression increases the cellular degradation of Aβ by primary astrocytes. (A) Schematic diagram of the experiments used to measure degradation of I^{125}-Aβ by primary astrocytes. I^{125}-Aβ was added to primary astrocytes from either Wt or LDLR Tg mice for the indicated time points. After each time point, the medium was collected and a TCA precipitation was performed to detect degraded Aβ. **(B)** The supernatant (sup) and pellet CPM are plotted as a function of time. Representative data from one experiment is shown. Experiment was repeated three times with similar results. **(C)** Degraded Aβ was quantified by calculating the percent of Aβ degraded as a percent of the total intact Aβ added. Mean ± SEM * denotes $p<0.05$, ** denotes $p<0.01$. **(D)** To measure the ability of astrocyte-conditioned media to degrade Aβ, medium was collected from either Wt or LDLR Tg primary astrocytes. I^{125}-Aβ was then added to the astrocyte-conditioned media for the indicated time points and a TCA acid precipitation was performed. The supernatant (sup) and pellet CPM are plotted as a function of time. Representative data from one experiment is shown. Experiment was repeated two times with similar results. **(E)** Degraded Aβ was quantified by calculating the percent of Aβ degraded as a percent of the total intact Aβ added. Mean ± SEM * denotes $p<0.05$, n.s. not significant.

LDLR facilitates the vesicular trafficking of Aβ to lysosomes. In order to determine whether LDLR promotes the vesicular uptake of Aβ, we incubated primary astrocytes

with fluorescently-labeled Aβ42 (fAβ42) and DiI-LDL. LDL is internalized by receptor-mediated endocytosis through LDLR, and thus serves as an endocytic marker (Dunn and Maxfield, 1992; Goldstein et al., 1985). Wt and LDLR Tg primary astrocytes were incubated with fAβ42 and DiI-LDL for 3 hrs at 37°C. Microscopic visualization demonstrated a punctate pattern for both the DiI-LDL and Aβ42, demonstrating the uptake of both molecules into vesicular compartments. Notably, we observed that there was more DiI-LDL and Aβ42 endocytosed by the LDLR Tg cells (Fig. 2.6A). There was also considerable overlap between the DiI-LDL and Aβ42 signal in the LDLR Tg cells, demonstrating that LDLR overexpression increased the amount of Aβ in endocytic vesicles. To determine the intracellular fate of the internalized Aβ, we incubated primary astrocytes with fAβ42 for 3 hrs at 37°C and then added lysotracker to stain the lysosomes (Fig. 2.6B). LDLR Tg astrocytes displayed significantly increased colocalization of Aβ with the lysosome signal in comparison to Wt cells, with 30% of the Aβ signal colocalized in the LDLR Tg cells and only 12% colocalized in the Wt cells (Fig. 2.6C). Therefore, increasing the LDLR levels in astrocytes enhanced the endocytic transport of Aβ to lysosomes.

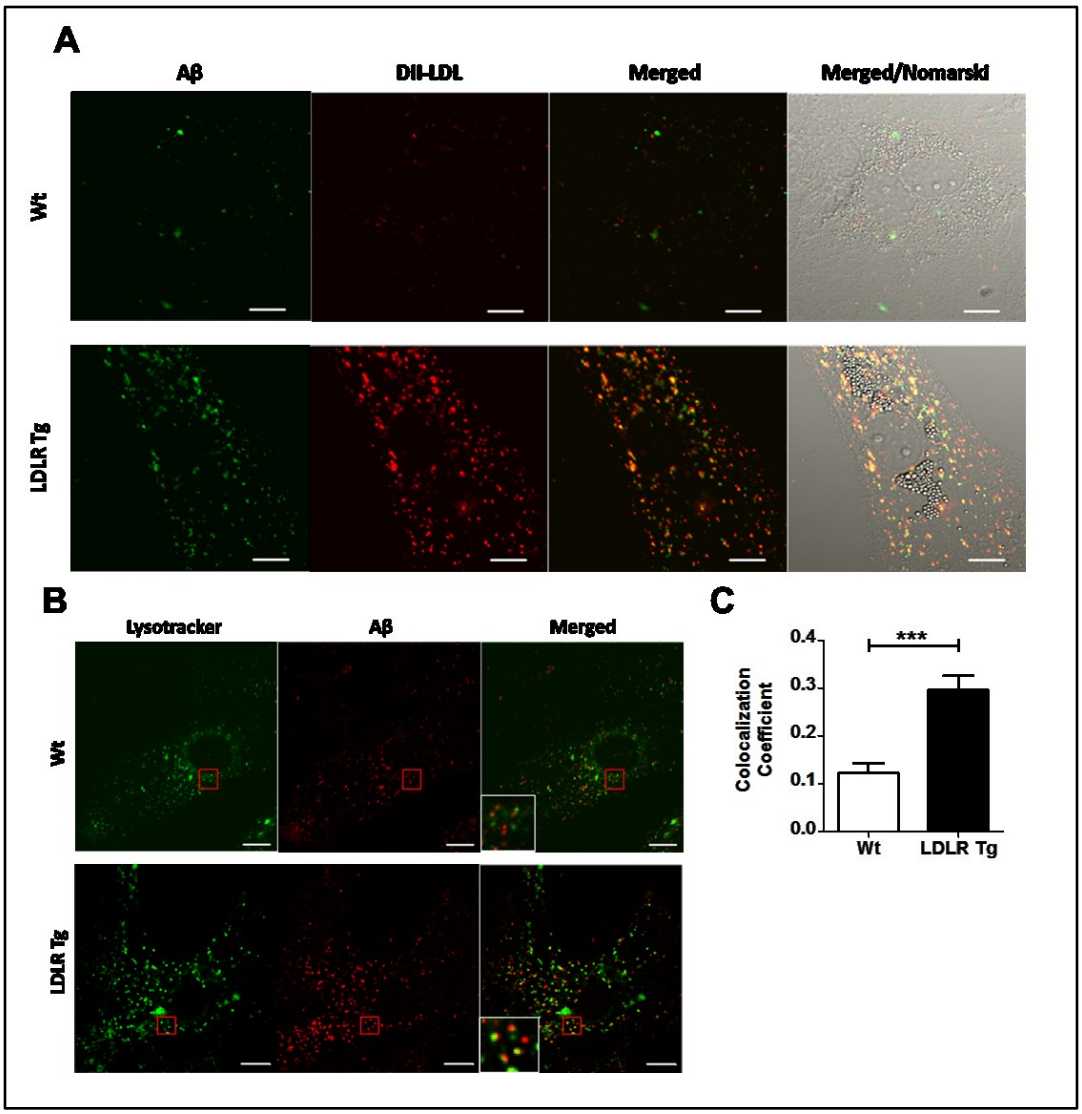
A
Aβ
DiI-LDL
Merged
Merged/Nomarski
Wt
LDLR Tg
B
Lysotracker
Aβ
Merged
Wt
LDLR Tg
C
Colocalization Coefficient
0.4
0.3
0.2
0.1
0.0
***
Wt
LDLR Tg

Fig. 2.6. LDLR facilitates Aβ trafficking to lysosomes through a similar pathway as lipoprotein particles. (A) To demonstrate that increasing LDLR levels promotes the transport of Aβ in similar vesicles as lipoprotein particles, Wt and LDLR Tg primary astrocytes were incubated with fluorescent Aβ42 (3 μg/mL) and DiI-LDL (0.5 ug/mL) for 3 hrs at 37°C. The cells were then washed and imaged using confocal microscopy. Overlap of Aβ and the DiI-LDL signal was observed in the LDLR Tg cells. **(B)** To observe Aβ uptake into lysosomal compartments, Wt and LDLR Tg primary astrocytes were incubated with fluorescent Aβ42 (2 μg/mL) for 3 hrs at 37°C. The cells were then washed and 50 nM of lysotracker was added to the cells for 15 minutes. The cells were then washed again and imaged using confocal microscopy. **(C)** Colocalization of the Aβ and lysotracker signal was analyzed and quantified. Mean ± SEM *** denotes $p<0.001$.

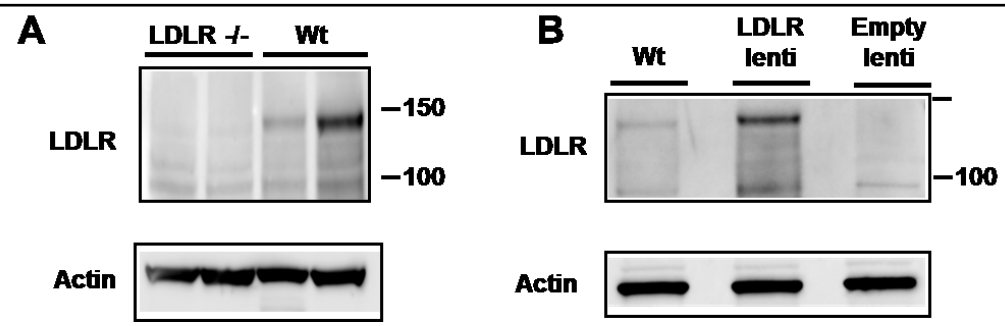

Fig. 2.7. Comparison of LDLR levels in Wt and LDLR$^{-/-}$ primary astrocytes. **(A)** Primary astrocytes were cultured from the cortices of Wt and LDLR$^{-/-}$ mice. After reaching confluency, the cells were lysed in a 1% Triton X-100 lysis buffer. The lysates were then analyzed by SDS-PAGE and probed using an LDLR antibody. **(B)** LDLR was expressed in LDLR$^{-/-}$ astrocytes via lentiviral transduction. LDLR expression was confirmed by immunoblot for HA.

LDLR deletion decreases the uptake and clearance of Aβ by primary astrocytes. To further determine the role of LDLR in the cellular metabolism of Aβ, we analyzed whether endogenous LDLR levels in primary astrocytes participate in Aβ uptake and clearance. Primary astrocytes were cultured from the cortices of Wt and LDLR$^{-/-}$ mice. Immunoblot analysis of the cell lysates confirmed that the LDLR protein was not expressed in LDLR$^{-/-}$ astrocytes (Fig. 2.7). Previous studies have shown that LDLR deletion significantly increased apoE levels in the mouse brain, likely due to impaired uptake and clearance of apoE-containing lipoprotein particles (Cao et al., 2006; Fryer et al., 2005a). To determine whether LDLR deletion affects apoE uptake and clearance by

astrocytes, Wt and LDLR$^{-/-}$ primary astrocytes were cultured in serum-free conditions and the amount of endogenously-produced apoE in the medium was measured after several time points. The cell medium from LDLR$^{-/-}$ cells had significantly increased apoE levels at all time points measured, with a maximum 77% increase observed after 8 hrs and a 62% increase observed after 24 hrs (Fig. 2.8A). The amount of apoE in the cell lysates was also measured by immunoblot after 24 hrs. LDLR$^{-/-}$ astrocytes had decreased apoE levels in comparison to Wt cells (Fig. 2.8B).

Because we could not rule out that the changes in apoE levels in the media and cell lysate were due to changes in protein expression, we measured the amount of apoE mRNA in LDLR$^{-/-}$ and Wt cells. LDLR$^{-/-}$ astrocytes had elevated apoE mRNA amounts in comparison to Wt cells (Fig. 2.2). It is possible that increased apoE production could play a role in the elevation of apoE levels in the LDLR$^{-/-}$ astrocyte media. However, the known role of LDLR in the uptake of lipoproteins combined with the observation that the LDLR$^{-/-}$ astrocytes contained less intracellular apoE than Wt cells suggest the increase in media apoE levels in LDLR$^{-/-}$ cells is primarily due to decreased uptake.

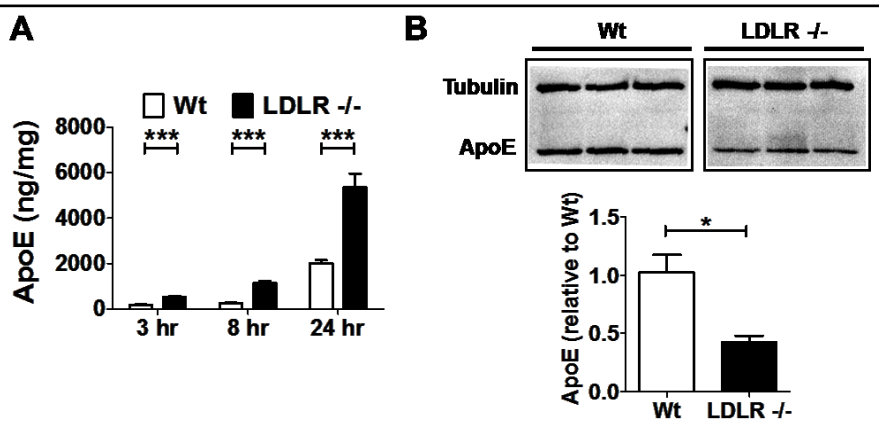

Fig. 2.8. LDLR deletion alters extra- and intra-cellular apoE levels. Primary astrocytes were cultured from the cortices of Wt and LDLR$^{-/-}$ mice. **(A)** ApoE uptake was assessed by measuring the levels of endogenously produced apoE in the culture media. Primary astrocytes were incubated for the indicated time points in serum-free media and the apoE amount in the media was measured by ELISA. Mean ± SEM (n≥4) *** denotes $p<0.001$. **(B)** The amount of cell-associated apoE was also measured by immunoblot of the cell lysates obtained after the 24 hr incubation. Quantification of the apoE band intensity normalized to tubulin intensity is shown below the image.

The effect of LDLR deletion on Aβ uptake was assessed by the addition of soluble Aβ40 (2 μg/mL) to LDLR$^{-/-}$ and Wt primary astrocytes for 3 hrs. Quantification of Aβ ELISA showed that cellular Aβ levels decreased by 43% in LDLR$^{-/-}$ astrocytes compared to Wt cells (Fig. 2.9A). The difference in internalization was qualitatively confirmed by immunoblot analysis of the cell lysates (Fig. 2.9B). To confirm that the

decrease in Aβ uptake in $LDLR^{-/-}$ astrocytes was due to lack of LDLR rather than a non-specific alteration in cellular function, we increased LDLR function by transducing the $LDLR^{-/-}$ astrocytes with an LDLR-expressing lentivirus. Immunoblot analysis confirmed that the lentiviral-transduced astrocytes expressed LDLR (Fig. 2.7B). Cell-internalized Aβ increased by 1.4 fold in the LDLR-lentiviral transduced cells in comparison to cells transduced with an empty-virus control (Fig. 2.9C). Finally, to measure the effect of LDLR deletion on the clearance of Aβ from the medium, soluble Aβ40 (2 μg/mL) was added to the media of Wt and LDLR Tg astrocytes for 24 hrs at 37°C. The amount of Aβ remaining in the media was then measured by ELISA. $LDLR^{-/-}$ astrocytes cleared less Aβ in comparison to Wt cells, however the difference was not significant (Fig. 2.9D).

As measured with the astrocytes that overexpress LDLR, the effect of LDLR deletion on LRP1 and RAP levels was assessed by immunoblot (Fig. 2.4A,B). Deletion of LDLR resulted in a significant decrease in LRP1 levels, but did not affect RAP levels. As a result, we cannot rule out the possibility that a decrease in LRP1 plays a role in the effect of LDLR deletion on Aβ uptake. However, the LDLR overexpression data convincingly demonstrates that LDLR has an effect on Aβ uptake and clearance that is independent of LRP1. In summary, this data demonstrates that endogenous LDLR may represent a pathway of Aβ uptake in primary astrocytes, though this effect may also be mediated by compensatory decreases in LRP1 levels.

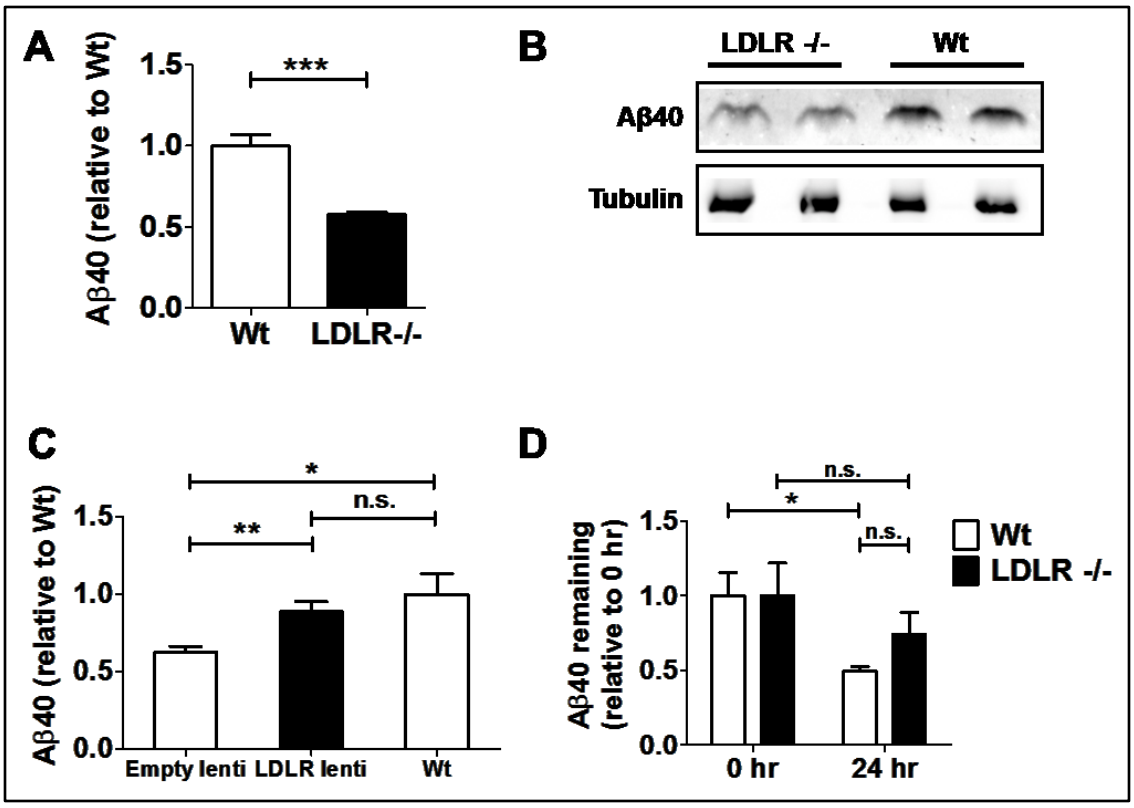
A
Aβ40 (relative to Wt)
1.5
1.0
0.5
0.0
***
Wt
LDLR-/-
B
LDLR -/-
Wt
Aβ40
Tubulin
C
Aβ40 (relative to Wt)
1.5
1.0
0.5
0.0
*
n.s.
**
Empty lenti
LDLR lenti
Wt
D
Aβ40 remaining (relative to 0 hr)
1.5
1.0
0.5
0.0
n.s.
*
n.s.
0 hr
24 hr
Wt
LDLR -/-

Fig. 2.9. Lack of LDLR impairs Aβ uptake in astrocytes. To assess the effect of LDLR deletion on Aβ uptake, Wt and $LDLR^{-/-}$ astrocytes were incubated with Aβ40 (2 μg/mL) for 3 hrs. The cells were then washed with PBS, incubated with trypsin to remove cell surface bound Aβ, and lysed in Triton X-100 lysis buffer. The amount of Aβ in the cell lysate was then assessed by **(A)** ELISA and **(B)** immunoblot. For the immunoblot, a representative image is shown. Mean ± SEM ($n \geq 4$) *** denotes $p<0.001$. **(C)** To verify the effect of LDLR deletion on Aβ uptake, LDLR function was restored in the $LDLR^{-/-}$ astrocytes by transduction with an LDLR lentivirus. Aβ uptake was then assessed as in **(A)** and compared to the level of uptake by $LDLR^{-/-}$ cells transduced with control lentivirus and Wt cells. Mean ± SEM ($n \geq 4$) ** denotes $p<0.01$. **(D)** The effect of LDLR deletion on Aβ clearance was assessed by the addition of Aβ40 (2 μg/mL) to the media of Wt and $LDLR^{-/-}$ astrocytes. After 24 hrs, the amount of Aβ remaining in the media was measured by ELISA and compared to the starting amount. Mean ± SEM ($n \geq 4$) * denotes $p<0.05$, n.s. not significant.

LDLR effect on Aβ uptake and clearance does not require apoE. ApoE has previously been shown to bind to Aβ (LaDu et al., 1994; Strittmatter et al., 1993b; Tokuda et al., 2000), and is capable of enhancing the cellular degradation of Aβ byprimary astrocytes and microglia (Jiang et al., 2008; Koistinaho et al., 2004). The effect of LDLR on Aβ uptake and clearance may therefore depend upon LDLR modulation of astrocyte apoE levels, or may occur due to direct binding of an apoE-Aβ

complex to LDLR. To determine if the effect of LDLR on Aβ uptake is dependent upon the presence of apoE, we overexpressed HA tagged-LDLR in apoE$^{-/-}$ primary astrocytes through lentiviral transduction. Immunoblot detection of the HA tag showed that the amount of LDLR overexpressed in Wt and apoE$^{-/-}$ astrocytes was comparable (Fig. 2.10A). To determine if the LDLR expressed by the lentivirus had a functional effect in the cells, extracellular apoE levels were measured in LDLR lentiviral-transduced Wt astrocytes. Overexpression decreased apoE levels by 92% after 24 hrs, confirming that the LDLR expressed via the lentivirus was functional (Fig. 2.10B). Aβ uptake was assessed by the addition of soluble Aβ40 (2 μg/mL) to Wt and apoE$^{-/-}$ primary astrocytes transduced with LDLR lentivirus. LDLR overexpression increased Aβ uptake in Wt cells and apoE$^{-/-}$ astrocytes to a similar extent, with a 2.1 fold increase in Wt cells and a 2.4 fold increase in apoE$^{-/-}$ cells (Fig. 2.10C). The effect of LDLR overexpression on Aβ clearance in the absence of apoE was also measured by determining the amount of Aβ remaining in the media of Wt and apoE$^{-/-}$ astrocytes transduced with LDLR after a 24 hr incubation. LDLR overexpression decreased the amount of Aβ remaining in Wt cells by 40% and in apoE$^{-/-}$ cells by 43% (Fig. 2.10D). Therefore, the presence of apoE is not necessary for LDLR to modulate both Aβ uptake and clearance by primary astrocytes.

LDLR binds directly to Aβ in an *in vitro* setting. Since apoE was not required for the effect of LDLR on Aβ internalization, we investigated whether LDLR may directly interact with the Aβ peptide. Coimmunoprecipitation experiments were carried out using

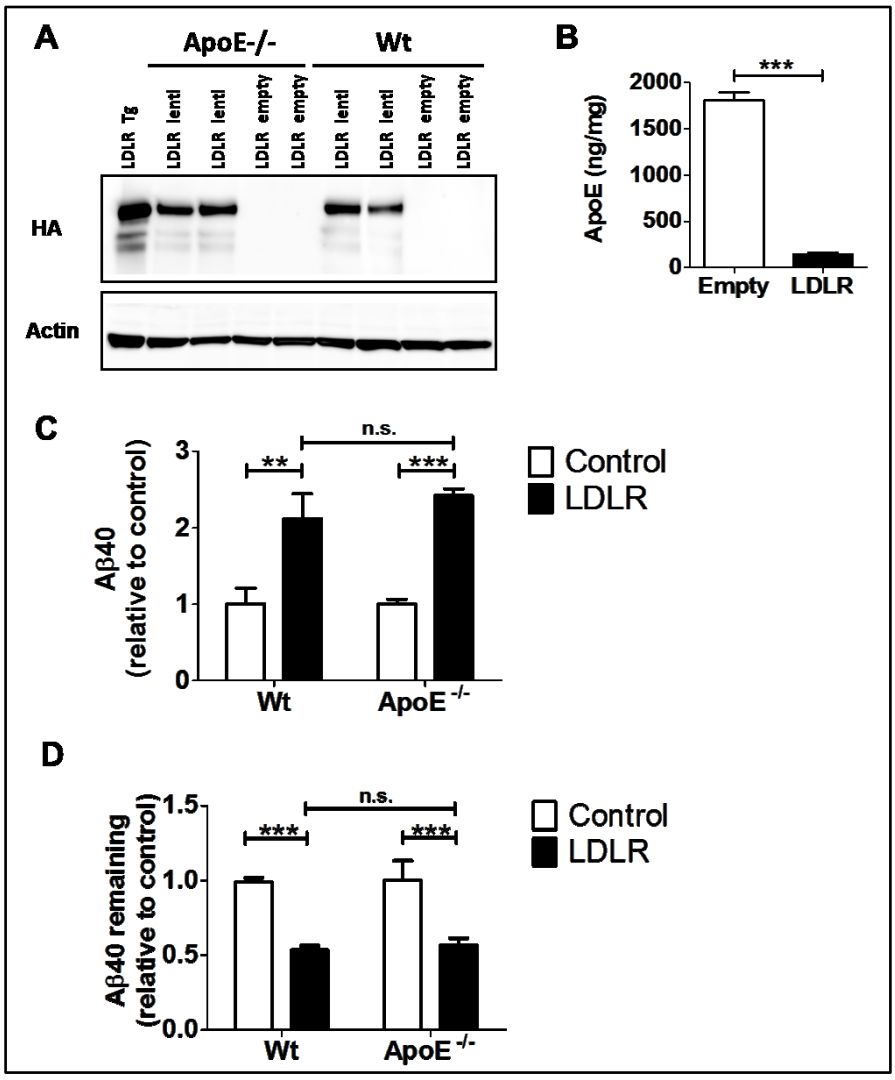
A
ApoE-/-
Wt
LDLR Tg
LDLR lentI
LDLR lentI
LDLR empty
LDLR empty
LDLR lentI
LDLR lentI
LDLR empty
LDLR empty
HA
Actin
B
ApoE (ng/mg)
2000
1500
1000
500
0
***
Empty
LDLR
C
Aβ40 (relative to control)
3
2
1
0
**
n.s.
***
Wt
ApoE -/-
Control
LDLR
D
Aβ40 remaining (relative to control)
1.5
1.0
0.5
0.0
***
n.s.
***
Wt
ApoE -/-
Control
LDLR

Fig. 2.10. The effect of LDLR on Aβ uptake and clearance is not dependent on apoE. (A) LDLR was expressed in apoE$^{-/-}$ and Wt primary astrocytes via lentiviral transduction. LDLR expression was confirmed by immunoblot for HA. LDLR Tg astrocyte lysate is shown for comparison. **(B)** To confirm that the LDLR protein expressed after lentiviral transduction was functional, Wt cells were transduced and the amount of endogenously produced apoE was measured by ELISA in the cell media after a 24 hr incubation. Mean ± SEM (n≥4) ** denotes $p<0.01$. **(C)** Aβ uptake was measured in Wt and apoE$^{-/-}$ primary astrocytes transduced with LDLR lentivirus. Aβ40 (2 μg/mL) was incubated with the cells for 3 hrs. The cells were then washed with PBS, treated with trypsin to remove cell surface-bound Aβ, and lysed in Triton X-100 lysis buffer. The cell-internalized Aβ was then measured by ELISA. Mean ± SEM (n≥4) ** denotes $p<0.01$, *** denotes $p<0.001$, n.s. not significant **(D)** Aβ clearance was assessed by the addition of Aβ40 (2 μg/mL) to the media of Wt and ApoE$^{-/-}$ astrocytes transduced with the LDLR lentivirus. After 24 hrs, the amount of Aβ remaining in the media was measured by ELISA and compared to cells transduced with empty lentivirus. Mean ± SEM (n≥4) *** denotes $p<0.001$, n.s. not significant.

Aβ and the extracellular domain of LDLR. Both Aβ40 and LDLR were incubated together for 4 hrs at 37°C, and LDLR was immunoprecipitated using anti-His beads. LDLR was efficiently pulled down by the anti-His antibody, as shown in Fig. 2.11A (lane 1 and 3). A significant amount of Aβ40 was also pulled down with LDLR (lane 1), which was not due to nonspecific binding of Aβ40 to the anti-His beads (compare lanes 1 and 2). Ligand blotting also verified the direct interaction between LDLR and Aβ40 (Fig. 2.12). To demonstrate the specificity of the interaction between Aβ40 and LDLR, the immunoprecipitation experiment was repeated with the addition of increasing concentrations of either RAP or proprotein convertase subtlisin/kexin type 9 (PCSK9), two established ligands for LDLR. Both RAP and PCSK9 decreased the amount of Aβ bound to LDLR in a dose-dependent manner (Fig. 2.11). Addition of Aβ(40-1) did not impair binding between Aβ40 and LDLR, and interestingly led to an apparent increased binding (Fig. 2.11). Taken together these results demonstrate that Aβ directly binds to LDLR through an interaction that can be blocked using known ligands to LDLR.

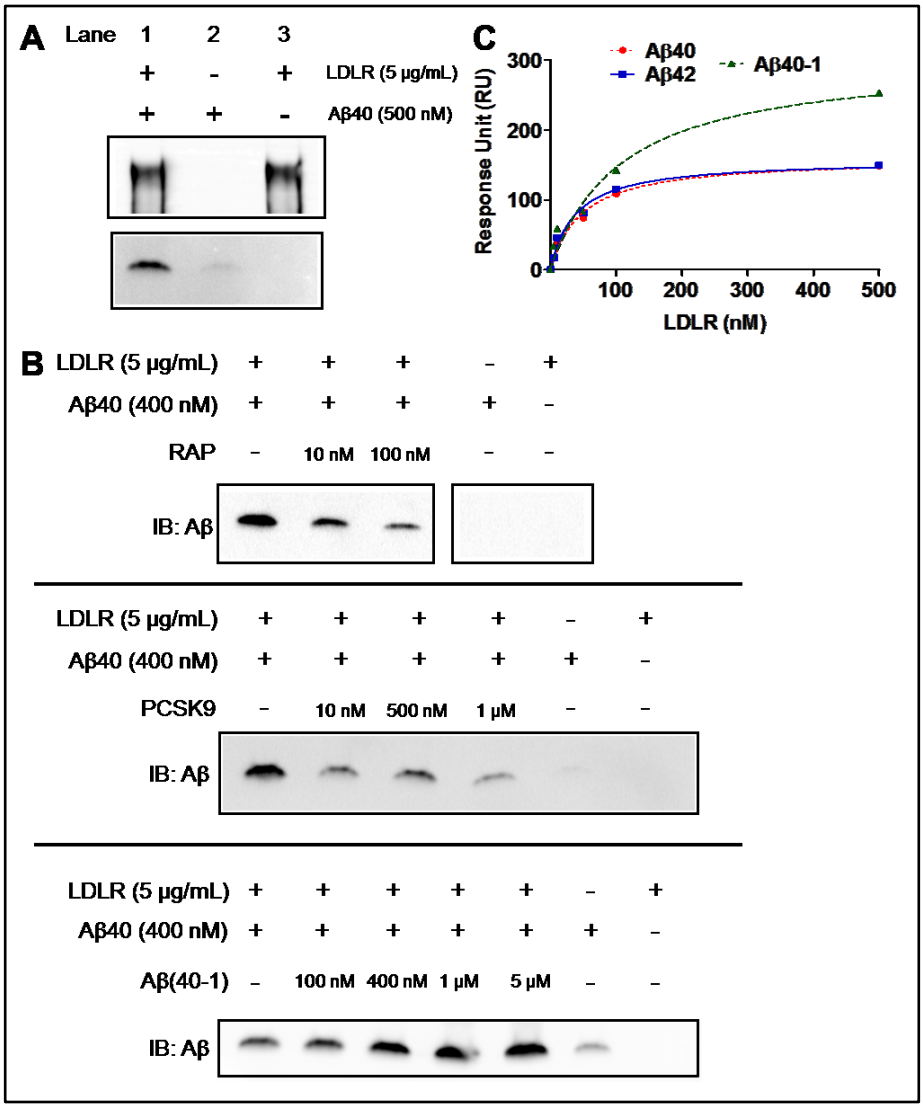
A
Lane 1 2 3
+ - + LDLR (5 μg/mL)
+ + - Aβ40 (500 nM)
C
Aβ40
Aβ42
Aβ40-1
Response Unit (RU)
300
200
100
0
100 200 300 400 500
LDLR (nM)
B
LDLR (5 μg/mL) + + + - +
Aβ40 (400 nM) + + + + -
RAP - 10 nM 100 nM - -
IB: Aβ
LDLR (5 μg/mL) + + + + - +
Aβ40 (400 nM) + + + + + -
PCSK9 - 10 nM 500 nM 1 μM - -
IB: Aβ
LDLR (5 μg/mL) + + + + + - +
Aβ40 (400 nM) + + + + + + -
Aβ(40-1) - 100 nM 400 nM 1 μM 5 μM - -
IB: Aβ

Fig. 2.11. Direct interaction between Aβ and LDLR. (A) Aβ40 (500 nM) and recombinant extracellular LDLR (5 μg/mL) were incubated together and immunoprecipitated using anti-His beads to pull down LDLR. The isolated proteins were then eluted from the beads and subjected to SDS-PAGE and immunoblot analysis for LDLR (His) and Aβ. **(B)** The specificity of the binding of Aβ to LDLR was determined by performing competition experiments with known LDLR ligands. Increasing amounts of either RAP or PCSK9 were pre-incubated with recombinant extracellular LDLR for 2 hrs, and Aβ40 was then added to the protein mixture and incubated at 37°C for 4 hrs. LDLR was then immunoprecipitated using anti-His beads, and the eluted samples subjected to SDS-PAGE and immunoblot analysis for Aβ. The experiment was also repeated using Aβ(40-1) as a competing peptide. **(C)** Surface plasmon resonance was used to measure the interaction between the extracellular domain of LDLR and Aβ. Aβ40, Aβ42, or Aβ(40-1) were immobilized on the SPR chip and various concentrations of LDLR were flown over the surface. In order to calculate the dissociation constant for the interaction (K_D), we plotted the resonance units as a function of LDLR concentration.

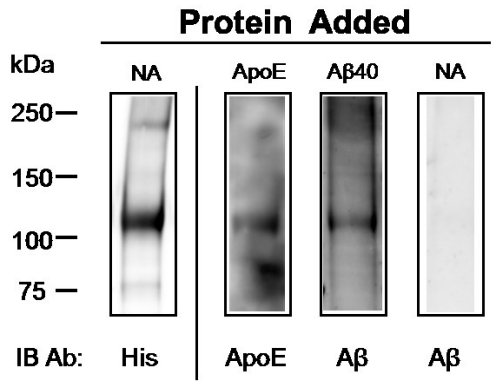

Fig. 2.12. Ligand blotting to detect Aβ-LDLR interaction. The extracellular domain of LDLR (2μg) was resolved by non-reducing SDS-PAGE and transferred to a PVDF membrane. The LDLR protein was then denatured and renatured on the membrane using sequential treatment with decreasing concentrations of guanidine-HCl. To detect the binding of proteins with LDLR in the membrane, either apoE or Aβ40 (5 ug/mL for each) was incubated with the membrane. NA represents no addition. Bound protein was then detected by immunoblot with the respective antibody. To analyze the size of nonreduced LDLR in the membrane, a His tag antibody was used.

We used surface plasmon resonance (SPR) to quantify the affinity of the interaction between LDLR and Aβ. Soluble Aβ40 and Aβ42 were immobilized on the sensor chip, and binding to LDLR was measured by flow of the extracellular LDLR domain over the immobilized Aβ peptides. A dose-dependent interaction between LDLR and both Aβ40 and Aβ42 was detected (representative sensorgrams are shown in Fig.

2.13). We then plotted the SPR response units for each concentration of LDLR tested in order to calculate the thermodynamic dissociation constants (K_D) of the interactions (Fig. 2.11C). The K_D values were 47.4 ± 9.9 nM for Aβ40 and 37.4 ± 8.0 nM for Aβ42. The interaction between LDLR and the reverse Aβ peptide (Aβ40-1) was also measured (Fig. 2.11C). Though Aβ40-1 still associated with LDLR, the interaction was weaker than that of Aβ40 and Aβ42, with a K_D value of 106.7 ± 36.1 nM. Finally, the binding of a mutant form of Aβ (Dutch/Iowa Aβ40, DIAβ40) to LDLR was assessed. Interestingly, the binding of mutant Aβ was stronger than that of Aβ40 and Aβ42, with a K_D of 4.54 ± 0.7 nM (Fig. 2.13A).

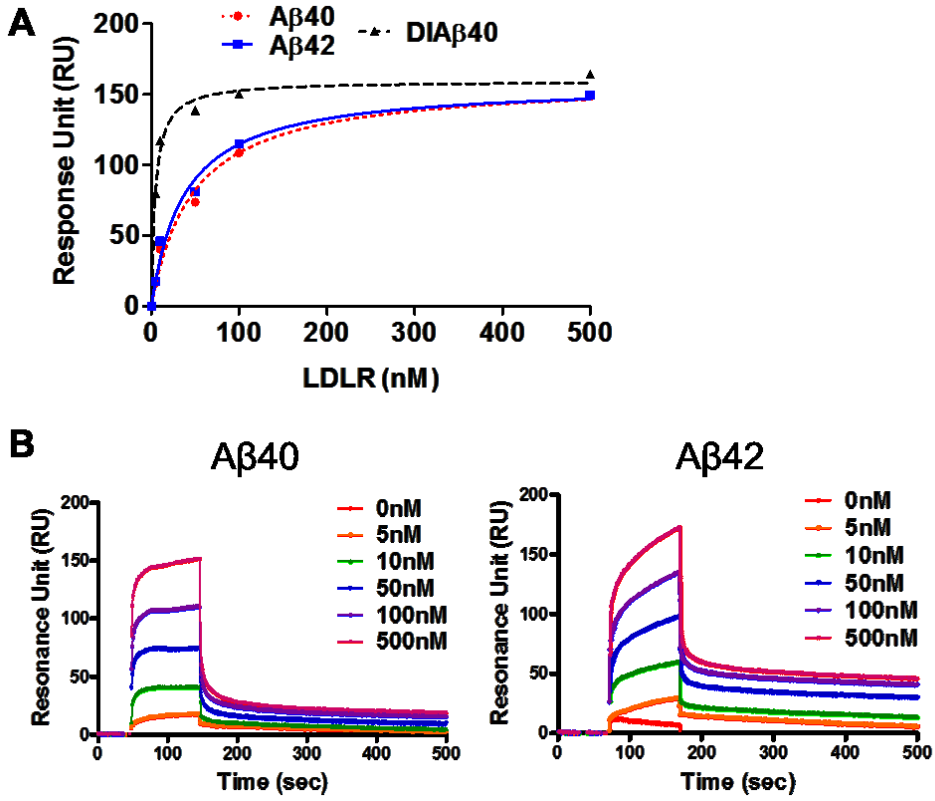

Fig. 2.13. Assessment of Aβ-LDLR interaction via surface plasmon resonance. (A) The interaction between the extracellular domain of LDLR and Aβ was measured by SPR. Aβ40, Aβ42, or DIAβ40 were immobilized on the SPR chip and various concentrations of LDLR were flown over the surface. In order to calculate the dissociation constant for the interaction (K_D), we plotted the resonance units as a function of LDLR concentration. **(B)** Representative sensorgrams show the response over time in resonance units (RU) for the binding of both Aβ40 and Aβ42 at a pH of 7.4 to LDLR.

Discussion

Previously we have shown that LDLR overexpression in the mouse brain markedly decreased the levels of Aβ and extent of plaque deposition in the APP/PS1 transgenic mouse model brain (Kim et al., 2009b). In the experiments performed in this chapter, we analyzed how LDLR regulates the cellular uptake and metabolism of Aβ by astrocytes. Overexpression of LDLR significantly increased the uptake and clearance of both Aβ40 and Aβ42 by astrocytes, while deletion of LDLR had the opposite effect. Increasing LDLR levels also enhanced the cellular degradation of Aβ through facilitating intracellular trafficking of Aβ to the lysosome. Despite the observation that increasing LDLR levels in astrocytes led to a decrease in extracellular apoE levels and increase in intracellular apoE levels, the effect of LDLR on Aβ uptake and clearance did not require apoE. Finally, we show that Aβ is capable of directly binding to LDLR. Overall, these results identify LDLR as a novel pathway for Aβ uptake into astrocytes and suggest that increasing glial levels of LDLR may be a feasible therapeutic strategy for promoting Aβ clearance from the extracellular space.

Several cell-types in the brain are capable of internalizing both fibrillar and soluble Aβ, including astrocytes (Koistinaho et al., 2004; Mandrekar et al., 2009; Nielsen et al., 2009; Wyss-Coray et al., 2003), microglia (Jiang et al., 2008; Mandrekar et al., 2009), neurons (Saavedra et al., 2007), and endothelial cells (Deane et al., 2004; Yamada et al., 2008). The ability of microglia and astrocytes to degrade soluble Aβ suggests that both of these cell types play a role in Aβ clearance from the brain. Several pathways and receptors regulate Aβ clearance by microglia, including scavenger receptors, Toll-like

receptors, and fluid phase macropinocytosis (for a review, see (Lee and Landreth, 2010)). However, the cellular pathways that facilitate Aβ uptake and clearance by astrocytes have not been extensively characterized. Previously it has been shown that primary astrocytes grown in culture were capable of degrading soluble Aβ and fibrillar Aβ present in the plaques of murine brain sections (Koistinaho et al., 2004; Wyss-Coray et al., 2003). ApoE appears to play an important role in this process, as astrocytes cultured from apoE$^{-/-}$ mice were not capable of degrading Aβ in tissue sections. Furthermore, co-incubation of primary astrocytes with receptor-associated protein (RAP), a protein that antagonizes ligand binding to receptors of the LDLR family, inhibited the ability of astrocytes to degrade Aβ (Koistinaho et al., 2004). These results suggest that both apoE and a receptor from the LDLR family function in regulating the clearance of Aβ by astrocytes. In our current study, we extend these previous findings by highlighting the importance of LDLR in regulating both the uptake and clearance of soluble Aβ by astrocytes.

The ε4 allele of the *APOE* gene is currently the strongest genetic risk factor for late-onset AD (Kim et al., 2009a). Data from human studies and animal models suggest that apoE primarily influences AD pathogenesis through altering the aggregation of Aβ and its clearance from the brain (Castellano et al., 2011; Deane et al., 2008; Kim et al., 2009a; Verghese et al., 2011). Altering the amount of apoE in the brain influences amyloid deposition and clearance (Bales et al., 1999; Bales et al., 1997; DeMattos et al., 2004). For this reason, recent attention has been devoted to identifying receptors in the brain that regulate apoE levels. In mouse studies, modulation of LDLR protein levels in the brain altered apoE amounts. LDLR$^{-/-}$ mice had significantly elevated amounts of apoE

in the brain and the CSF (Cao et al., 2006; Elder et al., 2007; Fryer et al., 2005a; Katsouri and Georgopoulos, 2011), whereas mice overexpressing LDLR in the brain had lower levels of apoE (Kim et al., 2009b). In the current study, we demonstrate that modulation of LDLR levels in astrocytes similarly alters apoE levels. Astrocytes that overexpress LDLR have decreased apoE levels in the medium and increased levels within the cell, while $LDLR^{-/-}$ astrocytes have elevated apoE levels in the media and decreased intracellular levels of apoE. Notably, we observed a statistically significant increase in apoE mRNA levels in $LDLR^{-/-}$ astrocytes. The reason for this increase is unclear, but it may be a compensatory response of the cells to the decrease in intracellular apoE and cholesterol. Despite the increase in apoE mRNA, total intracellular apoE levels in the $LDLR^{-/-}$ cells were lower than Wt cells. Therefore, this data strongly suggests that LDLR regulates the uptake of apoE-lipoprotein particles from the media. Though several cell-types in the brain likely mediate the effect of LDLR on apoE levels *in vivo*, these *in vitro* results provide evidence that astrocytes may contribute to the differences in apoE amount observed in the mouse brain following LDLR deletion or overexpression.

The effect of LDLR on the amount of Aβ in the brain has been studied through genetic modulation of LDLR levels in transgenic mouse models of human Aβ deposition. Although several groups have analyzed the effect of LDLR deletion on Aβ deposition, the results have been inconsistent. In Tg 2576 APP transgenic mice and 5XFAD APP/PS1 transgenic mice, LDLR deletion caused an increase in human amyloid deposition (Cao et al., 2006; Katsouri and Georgopoulos, 2011). However, in PDAPP mice crossed to $LDLR^{-/-}$ mice there was no significant change in human Aβ levels,

though there was a trend toward increased Aβ deposition in mice lacking LDLR (Fryer et al., 2005a). A different group looking at the effect of LDLR deletion on mouse Aβ levels found no changes in comparison to Wt mice (Elder et al., 2007). Our studies have found that LDLR overexpression in the mouse brain dramatically decreased Aβ deposition in APP/PS1 transgenic mice. Furthermore, we observed that the clearance of Aβ from the interstitial fluid was significantly increased in LDLR transgenic mice (Kim et al., 2009b). Several mechanisms could be responsible for this effect, including increased cellular catabolism of Aβ or increased transport of Aβ across the BBB into the plasma where it is rapidly degraded. In these mice, one of the primary cell-types expressing the transgene was astrocytes. In the current study, we provide a potential cellular mechanism for the effect of LDLR overexpression on Aβ levels in the brain. LDLR overexpression in primary astrocytes by expression of an LDLR transgene or through LDLR lentiviral transduction significantly increased Aβ uptake and enhanced Aβ clearance from the medium. $LDLR^{-/-}$ astrocytes internalized less Aβ in comparison to Wt cells and exhibited less Aβ clearance from the medium, though the effect on clearance was not statistically significant. Taken together, these results suggest that LDLR is an important mediator of Aβ uptake and clearance in astrocytes, and differences in astrocyte-mediated clearance of Aβ may explain the decrease in extracellular Aβ levels observed in the LDLR Tg mouse brain. However, LDLR could also influence other pathways of Aβ clearance from the brain, including transport across the blood-brain barrier or clearance by other cell-types. Also, we observed that altering LDLR levels changes LRP1 levels in primary astrocytes, another LDL receptor that has been shown to regulate Aβ levels. However, LDLR

overexpression actually led to a decrease in LRP1 levels, suggesting the increase in Aβ uptake and clearance is due to LDLR rather than LRP1 in these cells. In future studies, it will be important to determine whether LDLR alters other modes of Aβ clearance and to better characterize the interaction between LDLR and LRP1-mediated Aβ uptake.

We also provide evidence in this study that LDLR overexpression in astrocytes directly promotes the cellular degradation of Aβ. Quantification of I^{125}-Aβ degradation via TCA precipitation showed that LDLR-overexpressing astrocytes degraded significantly more Aβ than Wt cells. Secreted extracellular proteases were not responsible for the effect of LDLR on Aβ degradation. The medium from LDLR-overexpressing astrocytes degraded even less Aβ than Wt cells after a 24 hr incubation. Regardless of genotype, we observed that the extent of Aβ degradation by astrocyte-conditioned media was minor in comparison to the Aβ degradation that occurred in the presence of primary astrocytes. Previous groups have demonstrated significant Aβ clearance in the presence of astrocyte-conditioned media due to the presence of extracellular proteases such as metalloproteinases and insulin degrading enzyme (IDE) (Jiang et al., 2008; Yin et al., 2006). The reason for the difference between our findings and these previous studies is not clear, but may be due to methodological differences in how Aβ degradation was measured. Previous studies described the degradation of Aβ by measuring the disappearance of full-length Aβ as detected by ELISA or immunoblot, or the appearance of large proteolytic fragments (Jiang et al., 2008; Yin et al., 2006). However, our study quantified Aβ degradation products that were too small to be precipitated by TCA acid, and likely represent complete digestion of the Aβ peptide. Despite the lack of significant

extracellular Aβ degradation by astrocyte-conditioned media, our results show that increasing the levels of LDLR in astrocytes enhances intracellular Aβ degradation. The increased degradation likely occurs though the lysosomal pathway, as LDLR promoted the intracellular trafficking of Aβ to the lysosome. It is important to point out that Aβ in the brain exists in several different aggregation states, including oligomers and fibrils (Holtzman et al., 2011). Since our study focused on the degradation of soluble Aβ, it will be important in the future to determine whether LDLR enhances the ability of astrocytes to degrade higher-order species of Aβ associated with amyloid plaques.

The effect of LDLR on Aβ uptake and clearance does not appear to be dependent upon apoE. Several studies have shown that apoE is capable of binding to Aβ (LaDu et al., 1994; Strittmatter et al., 1993b; Tokuda et al., 2000). Therefore, we hypothesized that apoE may facilitate the uptake of Aβ via LDLR through binding of an apoE-Aβ complex to LDLR. However, we found that LDLR was capable of promoting the uptake of Aβ into primary astrocytes even in $apoE^{-/-}$ cells. Therefore, it is likely LDLR regulates the internalization of apoE and Aβ through independent processes, though we cannot rule out that a small amount of Aβ is taken up as a complex with apoE. ApoE also can enhance the ability of both astrocytes and microglia to degrade Aβ (Jiang et al., 2008; Koistinaho et al., 2004). Despite the increased intracellular apoE levels in LDLR-overexpressing astrocytes that could promote intracellular Aβ degradation, apoE was not required for the effect of LDLR on Aβ clearance. Support also exists *in vivo* that LDLR can regulate Aβ levels independently of apoE. A recent study demonstrated that deletion of LDLR increases the level of amyloid and Aβ deposition in the brains of 5XFAD APP/PS1

transgenic mice even in the brains of mice lacking apoE (Katsouri and Georgopoulos, 2011). 5XFAD/LDLR$^{-/-}$ mice had decreased astrocytosis regardless of whether apoE was present, suggesting LDLR may function in the astrocytic response to Aβ deposition *in vivo* (Katsouri and Georgopoulos, 2011) Therefore, although apoE may regulate Aβ uptake and clearance by astrocytes, the effect of LDLR and apoE on these processes appears to be independent. In the future, it will be of interest to determine if LDLR overexpression can decrease plaque deposition in the brain in the absence of apoE.

Since apoE did not appear to regulate the uptake of Aβ via LDLR, we analyzed whether Aβ could directly bind to LDLR *in vitro*. We showed via immunoprecipitation and surface plasmon resonance that both Aβ40 and Aβ42 can bind to the extracellular domain of LDLR with K_D values of 47.4 nM and 37.4 nM, respectively. Competition experiments using both PCSK9 and RAP demonstrated that these LDLR ligands impaired Aβ binding to LDLR. These results suggest that Aβ may interact with the domains of LDLR that bind PCSK9 and RAP. Future studies will be necessary to define the exact Aβ-binding site on LDLR. Another member of the LDLR receptor family, LRP1, has also been shown to bind directly to Aβ with K_D values in the low nanomolar range (Deane et al., 2004). Despite the fact that the binding we observe between LDLR and Aβ is slightly weaker than the binding of Aβ to LRP1, a direct interaction with LDLR may still be relevant for Aβ internalization. Furthermore, we cannot rule out the possibility that Aβ binds to the cell surface through another protein that potentially functions as a co-receptor with LDLR, and LDLR then subsequently facilitates Aβ uptake after it binds to

the cell surface. Such a cooperative process has recently been proposed for Aβ uptake into neuronal cells via LRP1 and heparan sulfate proteoglycan (Kanekiyo et al., 2011).

Conclusions

In summary, we identified LDLR as a novel pathway of Aβ uptake and degradation in primary astrocytes. We also show that the ability of LDLR to facilitate Aβ uptake and clearance is not dependent upon apoE. Finally, we have identified a potential interaction between Aβ and LDLR that may play a role in the ability of LDLR to regulate Aβ internalization into cells. Regulating glial levels of LDLR appears to be a potential approach toward lowering brain Aβ levels. Therefore, it will be important in the future to better characterize how brain LDLR levels can be regulated from both a molecular and pharmaceutical perspective in order to identify unique therapeutic targets to treat AD.

Chapter 3

Measurement of Protein Kinetics in the Mouse Brain Using Bolus Stable Isotope Labeling

(This work involved the collaboration of several labs, and could not have been completed without the contribution of several individuals. Dr. Jungsu Kim and Dr. David Holtzman originally conceived the ideas for these experiments; Dr. Kim also aided with the method development and optimization. Hong Jiang and Maia Parsadanian aided with mouse tissue sample collection. All of the mass spectrometry data collection and analysis was performed in the lab of Dr. Randall Bateman. In particular, Dr. Yuriy Pyatkivskyy and Dr. Kristin Wildsmith aided in the mass spectrometry method development. Finally, Dr. Bruce Patterson provided expertise and helpful discussion for interpreting the data. Work from this chapter is included in manuscripts published in the journals *Molecular Neurodegeneration* and *PLoS ONE.*)

Summary

Abnormal proteostasis due to alterations in protein synthesis and clearance has been postulated to play a central role in several neurodegenerative diseases, including Alzheimer's disease. In chapter 2, our experiments were focused on characterizing a molecular pathway for the cellular clearance of apoE and Aβ. However, it is of interest ultimately to study pathways and processes that regulate whole brain apoE and Aβ clearance *in vivo*. Therefore, the development of techniques to quantify protein turnover in the brain is critical for understanding the pathogenic mechanisms of these diseases. We have developed a bolus stable isotope-labeling kinetics (SILK) technique coupled with multiple reaction monitoring mass spectrometry to measure the clearance of proteins in the mouse brain. In this technique, cohorts of mice are pulse labeled with $^{13}C_6$-leucine and the brains are isolated after pre-determined time points. Following lysis of the brain tissue, the extent of $^{13}C_6$-leucine incorporation in the cohort of mice is measured over time using mass spectrometry to measure the ratio of labeled to unlabeled protein. The fractional clearance rate is then calculated by analyzing the time course of disappearance for the labeled protein species. In this chapter, we provide a description of this technique and its application to measuring the kinetics of apoE turnover in both LDLR overexpressing mice and human apoE targeted-replacement mice.

Introduction

In the proteomics era, significant effort has been devoted to developing techniques that accurately and efficiently determine differences in protein amounts under normal physiological conditions and disease states (Ong and Mann, 2005). However, quantifying protein turnover rates at both a cellular and systemic level is also necessary for a complete understanding of the mechanisms dictating changes in protein levels (Doherty and Beynon, 2006). Several neurodegenerative diseases are characterized by the accumulation of protein aggregates in the brain, including Alzheimer's disease (AD) (Holtzman et al., 2011), Parkinson's disease (Goedert, 2001), Huntington's disease (DiFiglia et al., 1997), and frontotemporal dementia (Trojanowski and Dickson, 2001). Although the underlying cause of protein aggregation in these diseases remains unclear, it is likely due to abnormal proteostasis caused by alterations in protein production or clearance (Balch et al., 2008; Mawuenyega et al., 2010). Therefore, the development of techniques that can assess protein dynamics in the brain are fundamental for advancing our understanding of these disease processes and aiding the conception of innovative therapeutics.

Stable isotope tracers have been in use for many years to facilitate the analysis of protein turnover in cells and whole organisms (Wolfe and Chinkes, 2005). Mass spectrometry (MS) has proven an effective tool for the analysis of stable isotope incorporation into individual proteins (Aebersold and Mann, 2003). Liquid chromatography-mass spectrometry (LC-MS) analysis allows for the comparison of the relative abundance of labeled to unlabeled peptides due to their mass separation.

Coupling stable isotope amino acid labeling with LC-MS has been applied to quantify protein synthesis and degradation in yeast (Pratt et al., 2002), mammalian cell lines (Doherty et al., 2009; Schwanhausser et al., 2009), and small animals (Doherty et al., 2005; Price et al., 2010). However, protein turnover studies in animals have been limited due to issues with MS detection sensitivity and accurate label quantification, along with difficulties in achieving cost-effective and practical methods for tracer administration. Recently, Bateman *et al.* have developed a method using stable isotope labeling kinetics (SILK) to measure the dynamics of low abundance proteins in the cerebral spinal fluid (CSF) of humans (Bateman et al., 2006). In this technique, $^{13}C_6$-leucine is injected intravenously into research participants and samples of the lumbar CSF are serially collected for a predetermined time period. The synthesis and clearance rates of proteins are then measured by quantifying the appearance and disappearance of the $^{13}C_6$-leucine in proteins over time via LC-MS (Bateman et al., 2007; Bateman et al., 2006). The value of this technique has specifically been highlighted for the amyloid β (Aβ) peptide, which accumulates in the brains of AD patients and has been implicated in the disease pathogenesis (Holtzman et al., 2011). Application of stable isotope labeling to studies of Aβ dynamics have demonstrated impaired Aβ clearance in individuals with AD and the ability of a gamma secretase inhibitor to decrease Aβ synthesis in the CNS (Bateman et al., 2006; Bateman et al., 2009; Mawuenyega et al., 2010).

Apolipoprotein E (apoE) plays a central role in the transport of cholesterol by functioning as a ligand for the receptor-mediated endocytosis of lipoprotein particles into cells (Mahley, 1988). In humans, three common apoE isoforms exist (apoE2, apoE3, and

apoE4) that differ by amino acids at positions 112 and 158. ApoE4 is currently the strongest known genetic risk factor for late-onset AD, and as a result significant effort has been devoted to understanding apoE's physiological function in the brain along with its role in AD pathogenesis (Kim et al., 2009a). A major hypothesis for how apoE4 affects the onset of AD contends that apoE promotes the aggregation of Aβ into amyloid plaques in the brain, either through impairing Aβ clearance (Castellano et al., 2011; Deane et al., 2008), directly regulating the propensity of Aβ to form amyloid fibrils (Evans et al., 1995; Ma et al., 1994), or both mechanisms. The amount of apoE in the brain also appears to be critical for determining the extent of amyloid deposition (Bales et al., 1997; Kim et al., 2011). Therefore, understanding how apoE levels in the brain are regulated has been the focus of significant attention in AD research. ApoE receptors, including LDLR and LRP1, have been shown to regulate the amount of apoE in the mouse brain. Increasing both LDLR and LRP1 levels in the mouse brain significantly decreased apoE levels (Kim et al., 2009b; Zerbinatti et al., 2006). It has also been hypothesized that the isoform-specific effects of apoE on Aβ deposition may be due to differences in the apoE amount between isoforms (Bales et al., 2009). Several studies have shown that in the human apoE targeted-replacement mice, mice with apoE4 have less total apoE than mice with apoE2 or apoE3 (Bales et al., 2009; Castellano et al., 2011; Fryer et al., 2005b; Ramaswamy et al., 2005; Riddell et al., 2008). However, other studies have found no differences in the amount of apoE between isoforms (Korwek et al., 2009; Sullivan et al., 2004). The reason for the discrepancy in these results is unknown, but may be due to different tissue lysis conditions or the use of antibodies that recognize the

apoE isoforms with different affinities. Since the apoE protein levels are intrinsically related to the turnover of apoE, studying the kinetics of apoE in these mice will provide a mechanistic explanation for the differences, or lack thereof, in apoE protein levels in the mouse brain.

In this chapter, we describe an adaptation of the SILK analysis technique to study protein clearance in the mouse brain. We show that following a bolus injection of $^{13}C_6$-leucine into mice, LC-MS analysis of brain tissue can be used to measure the fractional clearance rate (FCR) of individual proteins. We validate our technique by analyzing changes in the clearance of apolipoprotein E (apoE) in mice that have been genetically engineered to overexpress LDLR. Finally, we apply this technique to study the clearance of the human apoE isoforms in the brains of human apoE targeted-replacement mice.

Experimental Procedures

Materials - $^{13}C_6$-leucine was obtained from Cambridge Isotope Laboratories (Andover, MA, USA). HJ6.3 (mouse ApoE) and WUE4 (human apoE) antibodies were made in-house. Protein G Sepharose 4 Fast Flow beads were obtained from GE Healthcare (Piscataway, NJ, USA). Formic acid (Optima LC-MS) was obtained from Fisher Scientific and triethylammonium bicarbonate was obtained from Sigma-Aldrich (St. Louis, MO, USA). Trypsin Gold (mass spec grade) was purchased from Promega (Madison, WI, USA).

Animal labeling and tissue collection - The production and characterization of the LDLR transgenic mice were described previously (Kim et al., 2009b). LDLR $Tg^{+/-}$ mice (B line, roughly 8 fold overexpression of LDLR) were bred to Wt mice to generate mice that were LDLR $Tg^{+/-}$ and LDLR $Tg^{-/-}$. Homozygous PDAPP mice containing the human *APP* V717F mutation were generated on a mixed background of DBA/2J, C57BL/6J, and Swiss Webster (gift from Eli Lilly and Co.). To generate APP transgenic mouse models with human apoE, PDAPP mice were crossed with human *APOE* targeted-replacement mouse models in which the endogenous murine *APOE* gene is replaced with the *APOE2*, *APOE3*, or *APOE4* gene (gift from Dr. Patrick Sullivan, Duke University) (Sullivan et al., 1997). 3.5 month old mice were used for all experiments. Mice were maintained under constant light/dark conditions and had free access to food and water. All experimental protocols were approved by the Animal Studies Committee at Washington University in St. Louis.

Prior to injection, the $^{13}C_6$-leucine was dissolved in medical-grade normal saline to a concentration of 7.5 mg/mL. The mice were weighed and then intraperitoneally injected with $^{13}C_6$-leucine (200 mg/kg of body weight). After predetermined time points, the animals were anesthetized and the blood was collected by cardiac puncture. The mice were then perfused with PBS-heparin and regional brain dissection was performed. All brain samples were subsequently frozen on dry ice.

Primary astrocyte cell culture and *in vitro* labeling - Primary astrocytes were cultured from postnatal day 1 (P1) C57/BL/6J mouse pups as described previously (Kim et al.,

2009b). Cells were cultured in serum-containing growth medium (DME/F12, 15% fetal bovine serum, 10 ng/mL epidermal growth factor, 100 units/mL penicillin/streptomycin, and 1 mM sodium pyruvate) until they reached 70 percent confluency. The cell medium was then changed to serum free medium that did not contain any leucine (DME/F12 without leucine prepared by the Washington University Tissue Culture Support Center, N2 growth supplement, 100 units/mL penicillin/streptomycin, and 1 mM sodium pyruvate) and cultured for 12 hr. $^{13}C_6$-leucine was then diluted into unlabeled leucine to make labeled/unlabeled percentages that were either 0, 1.25, 2.5, 5, 10, or 20%. These different percent-labeled leucine solutions were then added to separate flasks of primary astrocytes, and the cells were cultured for an additional 48 hrs. The media was then collected from the cells, spun down at 1500 rpm to clear cellular debris, and stored at -80°C.

ApoE immunoprecipitation - Mouse and human apoE were immunoprecipitated from the brain tissue using the antibodies HJ6.3 and WUE4, respectively. HJ6.3 antibody was produced by immunizing apoE$^{-/-}$ mice with mouse apoE immunopurified from the media of primary astrocyte cultures. Four different mouse apoE antibodies were produced (HJ6.1, HJ6.2, HJ6.3, and HJ6.4), however only HJ6.3 antibody was capable of immunoprecipitating mouse apoE from brain tissue lysate (Fig. 3.1). Antibody beads were prepared by covalently binding either HJ6.3 (mouse apoE) or WUE4 (human apoE) to Protein G Sepharose 4 Fast Flow beads. The beads initially were washed 3 times with ice-cold PBS and then resuspended in ice-cold PBS to make a 50% slurry of beads.

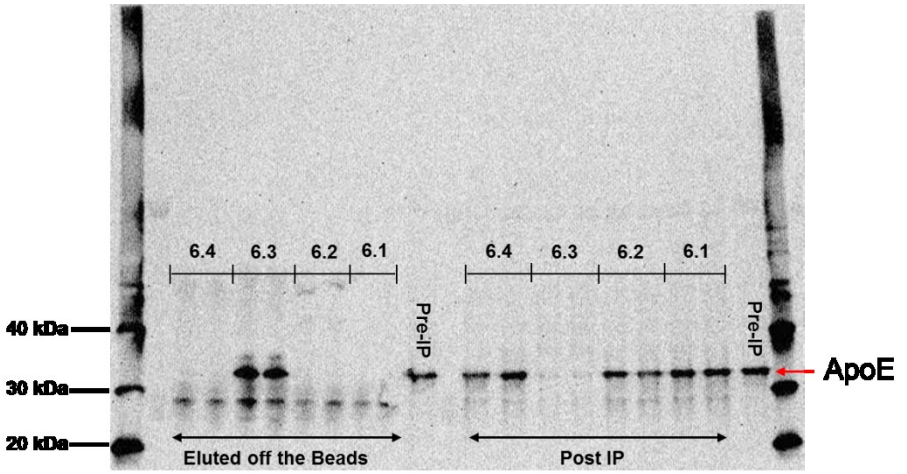

Fig. 3.1. Immunoprecipitation of mouse apoE with HJ6 antibodies. The ability of the HJ6 antibodies to immunoprecipitate mouse apoE from the brain cortex lysate was evaluated. Only beads conjugated with the HJ6.3 antibody pulled down apoE protein, as shown via immunoblot analysis of the pre-IP, post-IP and eluted samples. No eluted protein was observed with HJ6.1, HJ6.2, and HJ6.4.

300 µL of the washed 50% beads were then mixed with antibody (0.4 µg/µL of 50% bead mixture), 10 µL of 1% Triton X-100 and ice-cold PBS to make a final volume of 1000 µL. This mixture was then tumble incubated overnight at 4°C. The beads were then washed 3 times with 1% Triton X-100 lysis buffer (Triton X-100, 150 mM NaCl, 50 mM Tris-HCl) and 2 times with 0.2 M triethanolamine (pH = 8.2). Freshly prepared dimethyl pimelimidate in 0.2 M triethanolamine (pH = 8.2) was then added to the beads, followed by a 30 minute (min) incubation with tumbling at room temperature to allow for

crosslinking. The beads were then washed once with 50 mM Tris (pH = 7.5) to stop the crosslinking reaction, and twice with 0.1% Triton X-100 in PBS. The washing solution was removed by vacuum aspiration, and the beads were resuspended in PBS to make a 50% bead slurry.

Brain cortex samples were weighed and one cortical hemisphere was lysed using a 1% Triton X-100 lysis buffer (Triton X-100, 150 mM NaCl, 50 mM Tris-HCl, 1 X Roche Complete Protease Tablet) and the other cortical hemisphere was lysed using a PBS lysate buffer (with 1 X Roche Complete Protease Tablet). The lysis buffers were added at a concentration of 150 mg brain tissue/mL of lysis buffer. The triton samples were then sonicated (2 rounds of 20 1-sec pulses) and centrifuged at 14,000 rpm for 30 min. The PBS samples were homogenized with a manual grinder and centrifuged at 14,000 rpm for 30 min. The supernatant was collected and used for subsequent immunoprecipitation steps. Brain lysates and cell media were pre-cleared with 50 µL of the 50% bead slurry (no antibody coupled) for 4 hrs at 4°C. The pre-cleared lysate and media samples were then tumble incubated with antibody-conjugated beads overnight at 4°C. The beads were then washed 3 times with PBS and 3 times with 25 mM triethylammonium bicarbonate (TEABC). Following the last TEABC wash, the TEABC was removed via vacuum aspiration with a pipette tip. Formic acid was then added to the beads to elute the bound proteins, and the mixture was vortexed for 20 minutes. The beads were then centrifuged at 14,000 rpm for 5 min and the supernatant was collected from the beads. The formic acid supernatant was transferred to a new microcentrifuge tube and evaporated in a Savant SpeedVac for 60 min (37°C). The dried proteins were

then resuspended in 20% acetonitrile/80% 25 mM TEABC and vortexed for 30 minutes. The samples were then digested with 500 ng of mass spectrometry-grade trypsin (Promega) and incubated at 37°C for 16 hrs. The digested samples were dried again by vacuum evaporation, resuspended in 10% acetonitrile and 0.1% formic acid in water, and transferred to mass spectrometry vials.

Liquid Chromatography/Mass Spectrometry - LC-MS/MS measurements were performed on a Waters Xevo TQ-S triple quadrupole mass spectrometer (Waters Inc., Milford, MA) coupled to a Waters nano-ACQUITY ultra performance liquid chromatography (UPLC) system, equipped with a Waters nano-ESI ionization source. To identify multiple reaction monitoring (MRM) transitions, the synthetic mouse ApoE peptide LQAEIFQAR and synthetic human apoE peptide SWFEPLVEDMQR were purchased from AnaSpec, Inc. (Fremont, CA), and directly infused into the LC-MS for automatic tuning of optimized MRM transitions produced by the peptide. For both the mouse and human apoE peptide, optimal conditions were identified as a capillary voltage of 3.3 kV, source temperature of 80°C, cone voltage of 52 V, purge gas flow rate set at 100 L/hr, and cone gas at 50 L/hr. Obtained MRM transitions (Table 3.1) were then validated by the analysis of apoE cell culture media standards. For the actual experiments, all digested peptide samples were kept at 4°C and 1 μL aliquots were injected onto a Waters BEH130 nanoAcquity UPLC column (C18 particle, 1.7 μm, 100 μm x 100 mm). The peptide mixtures were separated on a reverse-phase nanoUPLC operated at a flow rate of 500 nL/min with a gradient mixture of solvents A (0.1% formic

acid in water) and B (0.1% formic acid in acetonitrile). The column was initially kept at 99% solvent A for 1.5 min, followed by a separation gradient of 1% to 97% solvent B from 1.5 to 18 min. The column was then kept at 97% solvent B for another 5 min followed by 1% solvent B to re-equilibrate for 10 min to prepare for the next injection. All raw data were acquired and quantified using Waters MassLynx 4.1 software suite. The labeled/unlabeled ratio was obtained by dividing the area under the curve (AUC) of the MRM total ion for the labeled peptide by the AUC for the unlabeled peptide, and converted to tracer-to-tracee ratios (TTRs) by reference to the standard curve.

Table 3.1. MRM Transitions for Mouse and Human ApoE

Protein	Peptide sequence	Precursor m/z	Product m/z	Collision Energy (V)
Mouse ApoE	LQAEIFQAR	538.2852	634.2609	14
Mouse ApoE	LQAEIFQAR	538.2852	763.2590	12
Mouse ApoE	LQAEIFQAR	538.2852	834.2775	14
Mouse ApoE	[$^{13}C_6$]LQAEIFQAR	541.2852	634.2609	14
Mouse ApoE	[$^{13}C_6$]LQAEIFQAR	541.2852	763.2590	12
Mouse ApoE	[$^{13}C_6$]LQAEIFQAR	541.2852	834.2775	14
Human ApoE	SWFEPLVEDMQR	769.177	987.660	28
Human ApoE	SWFEPLVEDMQR	769.177	1116.727	30
Human ApoE	SWFEP[$^{13}C_6$]LVEDMQR	772.177	993.660	28
Human ApoE	SWFEP[$^{13}C_6$]LVEDMQR	772.177	1122.727	30

Gas chromatography/mass spectrometry - The free leucine tracer-to-tracee ratio was measured from the mouse plasma using GC/MS. Plasma proteins were precipitated with ice-cold acetone, and lipids were extracted using hexane solvent. The resulting aqueous fraction was then dried with a vacuum (Savant Instruments, Farmingdale, NY) and converted to t-butyldimethylsilyl derivatives. The free leucine TTR was then measured by monitoring ions with m/z ratios of 200 (unlabeled) and 203 (labeled) (Patterson et al., 1993).

Kinetic analysis - The mice were in steady-state conditions, since the amount of apoE did not significantly change over the time period of the kinetic analysis. This was determined by measuring the protein level (via ELISA as described below) for the cohorts of mice at each time point following the stable isotope injection, and comparing across groups (see Fig. 3.2 for human apoE data). At metabolic steady state, the fraction of the pool that is synthesized per unit time equals the fraction of the pool catabolized per unit time (FCR), which can be calculated as the negative of the slope of the natural log of TTR plotted over time (Patterson et al., 2002). Production rates (PRs) were determined as: PR (protein amount/mg/hr) = [FCR (pools/hr) x protein concentration (protein amount/mL) x lysate volume (mL)]/brain weight (mg). The half-lives ($t_{½}$) were calculated using the equation $t_{½}$ = ln 2/FCR. Protein concentrations of apoE in the lysates were determined by protein-specific sandwich ELISAs using in-house antibodies. For mouse apoE, HJ6.2 was used as the coating antibody and biotinylated HJ6.3 as the detection

antibody. Pooled C57/BL/6J mouse plasma was used as a standard. For human apoE, HJ6.2 and biotinylated HJ6.1 were used as the coating and detection antibody, respectively. Human apoE isolated from human plasma samples was used as a standard (Calbiochem).

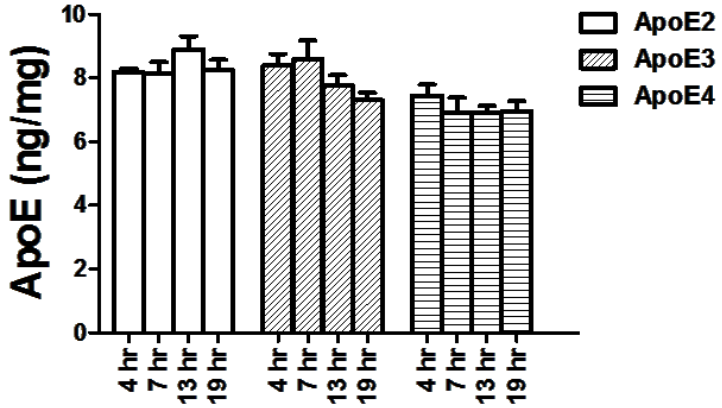

Fig. 3.2. ApoE levels during time course of injection. Human apoE levels were measured by ELISA for each group of mice at each time point following the injection. No differences in apoE levels were observed during the time course of injection for any of the isoforms (one-way ANOVA).

Statistical Analysis - Data were analyzed using GraphPad Prism Software and presented as mean ± standard error of the mean (SEM, *$p<0.05$, **$p<0.01$, ***$p<0.001$). For analyzing differences in protein levels and production rates, a two-tailed student's t-test

was used for the LDLR Tg study and a one-way analysis of covariance (ANOVA) followed by a Tukey's post-test was used for the human apoE studies. Differences in the FCR values were compared using analysis of covariance (ANCOVA) of the slope of the natural log of TTR plotted over time, which was determined using linear regression analysis.

Results

Stable isotope labeling of mice and protein isolation. The outline of our experimental design for the labeling of mice and tissue processing for SILK analysis is shown in Fig. 3.3A. Mice were intraperitoneally (IP) injected with a bolus of $^{13}C_6$-leucine, a non-radioactive stable isotope form of the amino acid leucine. We chose $^{13}C_6$-labeled leucine because it is one of the essential amino acids that rapidly cross the blood brain barrier via facilitative neutral amino acid transport (Smith et al., 1987). IP administration of the label was chosen because it is straightforward and quick, and it allows for high bioavailability upon absorption into the bloodstream. Following the injection, we observed a rapid increase in the amount of $^{13}C_6$-leucine in the plasma of the mice over the first hour, as measured by the ratio of labeled to unlabeled free leucine quantified by GC-MS (Fig. 3.3B). After a predetermined time point, the mice were euthanized and the brains were quickly removed and frozen. Upon collection of all of the brain samples for each time course, the tissue was then lysed in a 1% Triton X-100 lysis buffer and the protein of interest (apoE for this study) was immunoprecipitated with protein-specific antibodies

covalently coupled to protein G sepharose beads. Only the cortex of the brain was used in this study; however this technique could easily be applied to measure protein turnover rates in other regions of the brain. The isolated proteins were eluted off the beads using formic acid, and the concentrated samples were digested with trypsin to generate protein-specific peptides for each protein. These peptide mixtures were then subjected to LC-MS analysis for identification and characterization as described below.

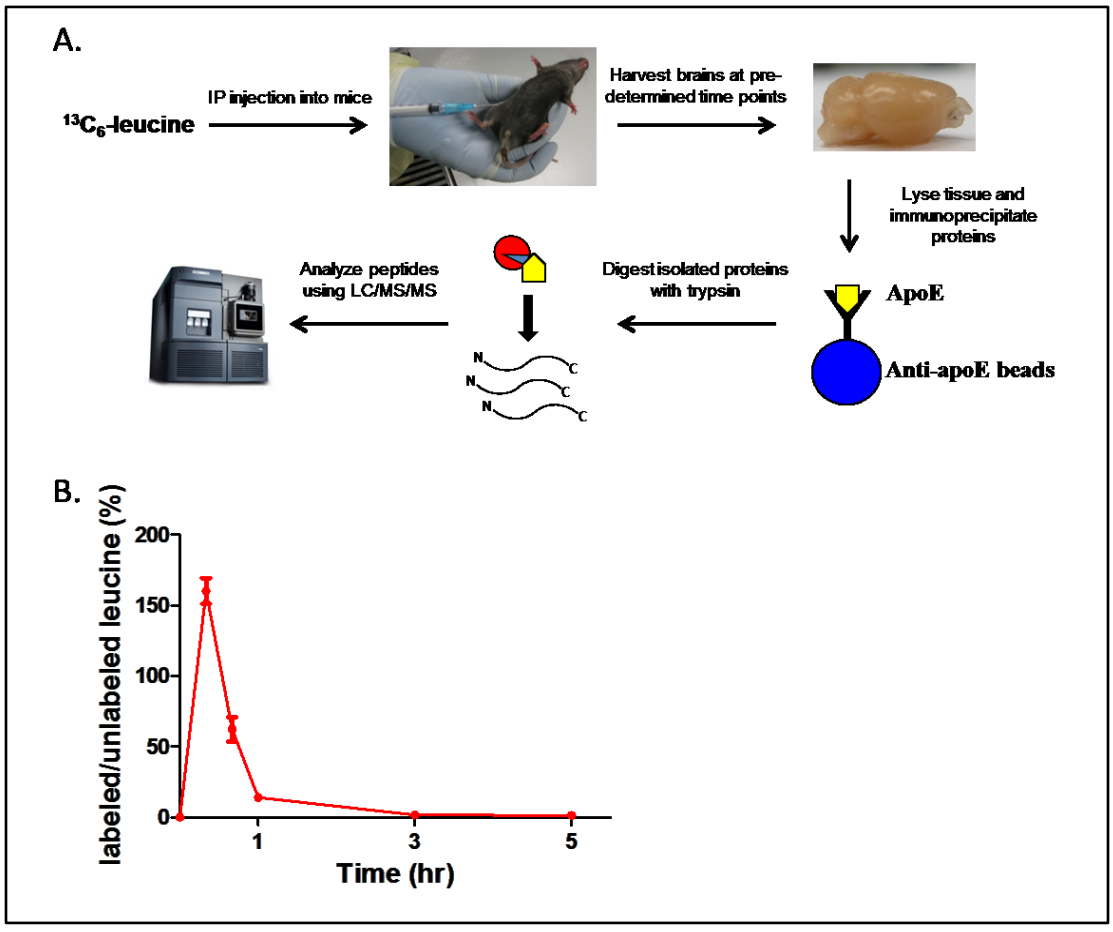

Fig. 3.3. Experimental schematic for stable isotope labeling and isolation of mouse brain proteins. (A) Cohorts of mice were pulse-labeled with $^{13}C_6$-leucine via a bolus intraperitoneal injection. After a pre-determined time following the $^{13}C_6$-leucine administration, the mice were euthanized and the brains were removed. The brain tissue was then lysed, and the protein of interest was immunoprecipitated from the brain lysate (apoE is shown as an example). The precipitated proteins were then eluted from the antibody beads and subjected to trypsin digestion. The resulting peptide mixture was separated and analyzed via ultra performance liquid chromatography tandem mass spectrometry (UPLC/MS/MS) (yellow = apoE, blue = sepharose bead, red = trypsin). **(B)** To observe the bioavailability of the $^{13}C_6$-leucine, plasma samples were collected at sequential time points following the bolus injection and subjected to GC-MS analysis. The tracer-to-tracee ratio (TTR, shown as labeled/unlabeled leucine) was then measured by quantifying the relative amounts of $^{13}C_6$-leucine and dividing by the amount of unlabeled leucine in each sample. Each time point in the graph represents the average value from 5-6 individual mice.

Mass spectrometry analysis to calculate the ratio of labeled to unlabeled peptide. We used a targeted LC-MS approach to accurately and precisely quantify the amount of labeled apoE in the brain. Multiple reaction monitoring (MRM) assays were developed for mouse and human apoE protein by first selecting a peptide that shows high MS signal intensity, contains only one leucine residue, and is specific for each protein (LQAEIFQAR for mouse apoE, SWFEPLVEDMQR for human apoE). Synthetic peptides were then directly injected into the MS to select and optimize the MRM product transitions for each parent ion (Fig 3.4A, Table 3.1). These parent/precursor ion groupings were then used for the relative quantitation of the labeled and unlabeled peptides from the brain sample. The area under the curve (AUC) of the MRM ion count during the course of the parent ion elution was calculated for the labeled and unlabeled peptide peaks (Fig. 3.4B). The AUC for the labeled peak was then divided by the AUC for the unlabeled peak to calculate the TTR for each sample.

In order to accurately compare the TTR values between individual brain samples and across cohorts of animals, we developed standard curves for apoE using the stable isotope labeling of amino acids in cell culture (SILAC) method (Ong et al., 2002). Since astrocytes are the main cell type in the brain that produce apoE (Kim et al., 2009a), we used primary astrocyte cultures to produce a labeled apoE standard curve. For the human apoE, we used a stable astrocyte cell line derived from primary astrocytes cultured from the brains of the targeted-replacement mice (Morikawa et al., 2005). To label newly synthesized apoE, the astrocytes were cultured in leucine-free media supplemented with different ratios of $^{13}C_6$-leucine to unlabeled leucine. Under these conditions, all apoE that

was synthesized and secreted into the cell media are labeled with the percentage of $^{13}C_6$-leucine provided to the cells. After a 48 hr incubation, the cell media was collected and apoE was immunoprecipitated. Following trypsin digestion, the apoE peptides were subjected to LC-MS as described above. The measured amount of percent labeled apoE gave values that were very close to the expected values (Fig. 3.5A). The linear fit for mouse apoE had a slope of 0.976 and an R^2 value of 0.9954. The apoE media standards were used in all subsequent experiments to calibrate the quantitation of the mouse brain samples.

In order to calculate the fractional clearance rates (FCRs) of apoE from the brain for each cohort of mice, mice were injected with $^{13}C_6$-leucine and the brains were removed at predetermined time points following the label administration. To determine the optimal time course for analyzing apoE clearance, a preliminary experiment was performed with 1 to 2 mice at each time point. For the actual experiments, several mice (n=5 to 6) were labeled for each time point and the TTR values were averaged. The averaged TTR values were then plotted over time for the whole cohort of mice to obtain the kinetic time course of label disappearance (Fig. 3.5B). The slope of the monoexponential curve of the downslope was then calculated in order to determine the fractional clearance rate for each protein from the brain.

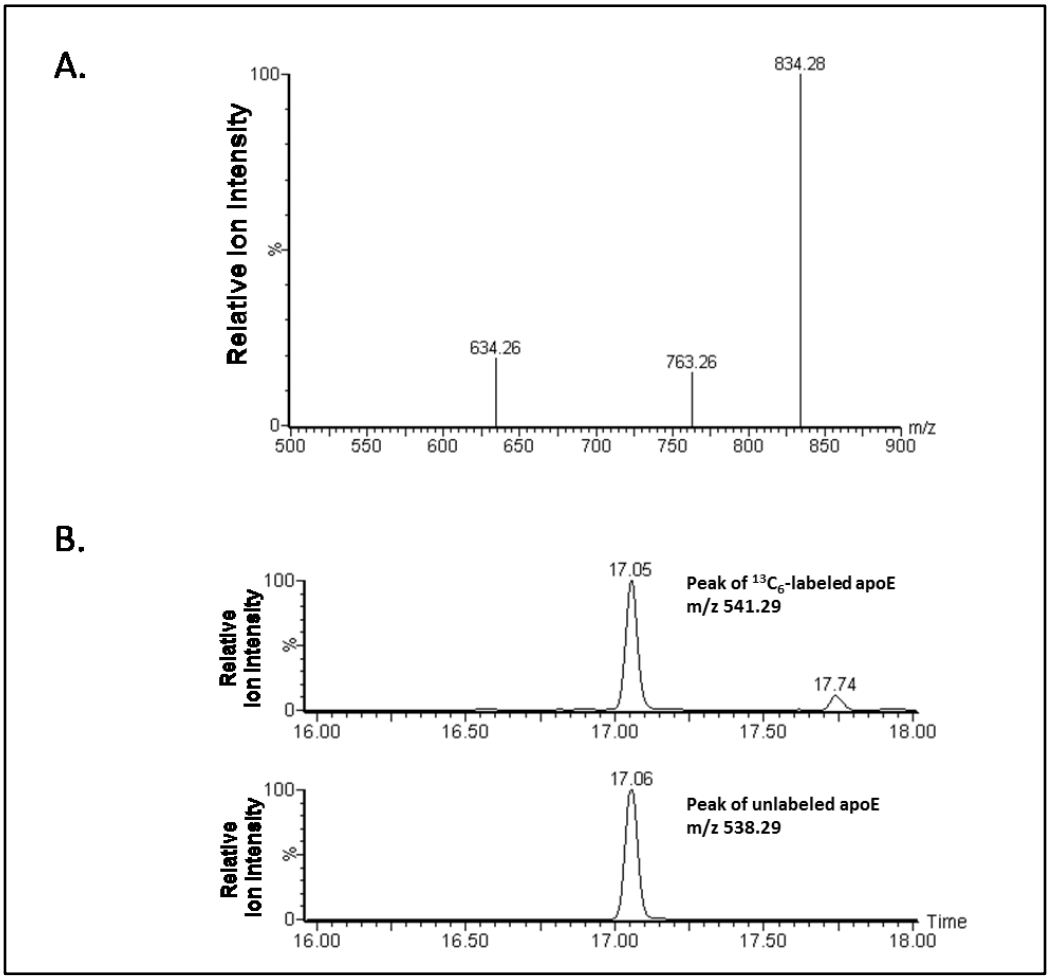
A.
Relative Ion Intensity
100
%
0
834.28
634.26
763.26
500
550
600
650
700
750
800
850
900
m/z
B.
Relative Ion Intensity
100
%
0
17.05
Peak of $^{13}C_6$-labeled apoE
m/z 541.29
17.74
16.00
16.50
17.00
17.50
18.00
Relative Ion Intensity
100
%
0
17.06
Peak of unlabeled apoE
m/z 538.29
16.00
16.50
17.00
17.50
18.00
Time

Figure 3.4. Tandem mass spectrometry (MS/MS) analysis of mouse apoE. (A) Tryptic peptides from immunoprecipitated apoE were separated by liquid chromatography and detected using a Xevo TQ-S triple quadrupole mass spectrometer. To facilitate the accurate and specific quantitation of labeled apoE, MRM transitions and conditions were optimized for the parent ion LQAEIFQAR. MS/MS spectrum for the product MRM transitions is shown. A similar analysis was performed for the human apoE specific peptide. **(B)** Representative relative ion count peaks from multiple reaction monitoring (MRM) analysis of the labeled and unlabeled apoE parent peptide LQAEIFQAR are shown [mass charge ratio (m/z) = 541.29 for labeled peptide and 538.29 for unlabeled peptide]. The area under the curve of the MRM ion counts were used for quantitation of the labeled and unlabeled peptide.

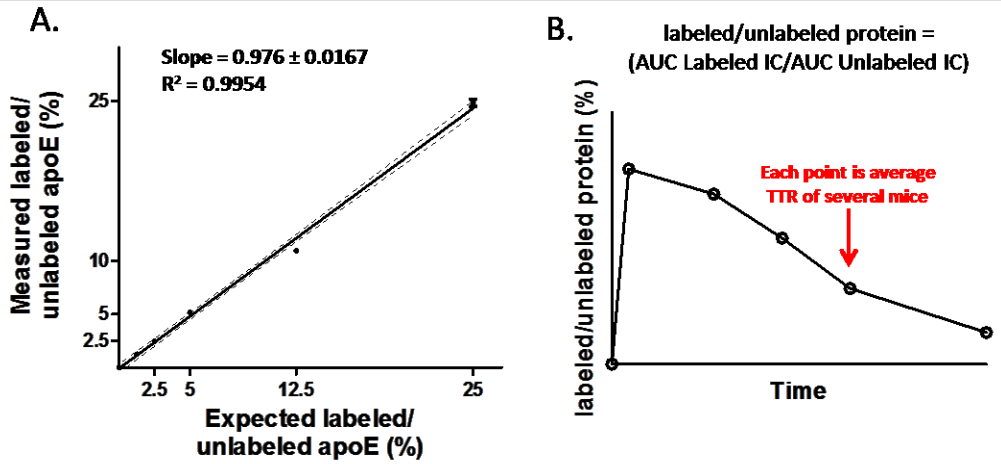

Fig. 3.5. Quantitation and analysis of stable isotope labeled mouse apoE. (A) Standard curve of labeled mouse apoE. To generate a standard curve for the MS quantitation, primary mouse astrocytes were incubated in culture medium with different percentages of labeled leucine. The medium of the astrocytes was then collected and the secreted apoE was immunoprecipitated, digested with trypsin, and analyzed using LC-MS. The measured labeled/unlabeled ratios along with the predicted labeled/unlabeled values are shown with a linear regression line (n = 3, dotted lines represent 95% confidence bands). **(B)** Representative diagram of time course of labeled proteins used for kinetic analyses. The labeled/unlabeled ratio was calculated for individual protein samples by dividing the area under the curve of the labeled ion count by the area under the curve of the unlabeled ion count. The labeled/unlabeled ratios were averaged for all of the mouse brain samples collected at each time point. The averaged labeled/unlabeled ratios were then plotted versus time to obtain the kinetic curve for each mouse genotype.

LDLR overexpression enhances the apoE clearance rate. To verify that our labeling technique could measure differences in the clearance rates of proteins, we measured the effect of overexpressing LDLR on the apoE clearance rate from the brain. LDLR is a receptor that binds to apoB and apoE in the plasma to facilitate the uptake of cholesterol-laden lipoproteins by cells (Brown and Goldstein, 1986). Previously we had shown that LDLR transgenic mice that overexpress LDLR in the brain had significantly decreased levels of brain apoE (Kim et al., 2009b). We therefore hypothesized that the apoE clearance rate in the brain would be increased in mice that have elevated LDLR levels. Wildtype (Wt) and LDLR Tg mice were labeled with $^{13}C_6$-leucine and the apoE TTR values were measured after pre-determined time points. Plots of the TTR values (presented as labeled/unlabeled apoE) over time along with the monoexponential slopes of these curves are shown in Figures 3.6A and 3.6B, respectively. Table 3.2 shows the pool sizes (PS), fractional clearance rates (FCRs), production rates (PR), and half-lives of apoE from each genotype. The FCR of apoE was 2.7-fold faster in the LDLR Tg mice in comparison to the Wt mice, while the apoE pool size was 2.8-fold higher for the Wt mice in comparison to the LDLR Tg mice. These values were used to estimate the PR values for both genotypes (see Experimental Procedures section for explanation of PR calculation), and no statistical difference in the PR was observed between Wt and LDLR Tg mice. These results convincingly demonstrate that apoE clearance is enhanced in the brains of the LDLR Tg mice, providing the likely explanation for the decreased total apoE protein levels. We therefore concluded that the pulsed $^{13}C_6$-leucine injection

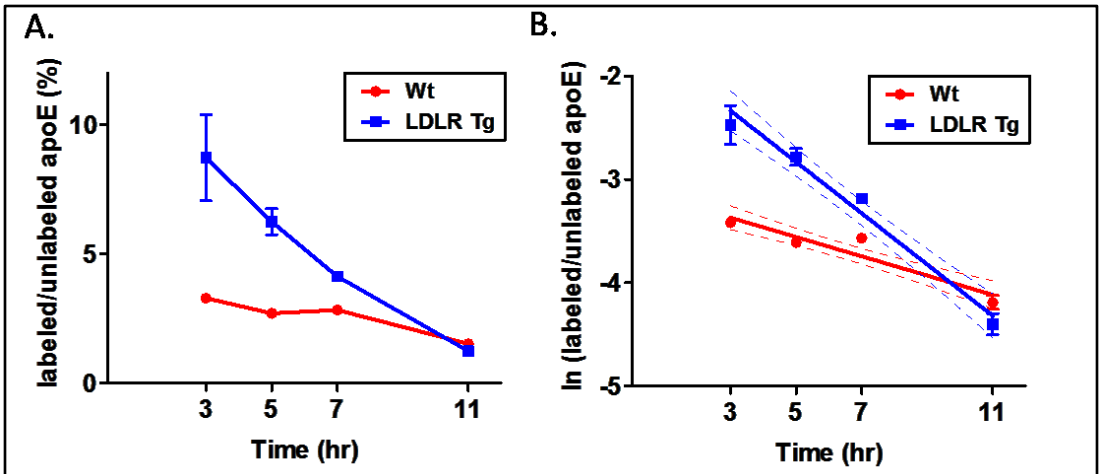

Fig. 3.6. $^{13}C_6$-leucine brain apoE labeling in the presence of increased LDLR levels. (A) Wildtype and LDLR transgenic mice (3.5 months old) were labeled with $^{13}C_6$-leucine and the brains isolated after predetermined time points. ApoE was then immunoprecipitated from the cortex and the labeled/unlabeled ratios calculated via LC-MS. The labeled/unlabeled ratios were then plotted versus time for each genotype. **(B)** To calculate the FCR, the natural log of the labeled/unlabeled ratios were plotted over time and the monoexponential slopes were calculated (n=5 mice per time point, error bars represent SEM, dotted lines represent 95% confidence band).

labeling technique is effective for measuring the clearance of proteins from the brain, and could be used to detect differences in FCRs between genetically modified mouse models.

Table 3.2. Pool Sizes (PS), Fractional Clearance Rates (FCR), Production Rates (PR), and Half-lives for ApoE in Wt and LDLR Tg mice

Genotype	PS (ng/mg)	FCR (pools/hr)	PR (ng/mg/hr)	Half-life ($t_{1/2}$, hrs)
Wt	125.4±9.1	0.093±0.011	11.69±1.64	7.5
LDLR Tg	44.7±1.9	0.25±0.019	11.07±0.96	2.8
P	<0.0001	<0.0001	0.75	

Measurement of human apoE kinetics in the mouse brain. To analyze the clearance of the human apoE isoforms in the mouse brain, human *APOE* targeted-replacement mice that are homozygous for either *APOE2*, *APOE3*, or *APOE4* were pulse labeled with $^{13}C_6$-leucine and the apoE TTR values were measured after pre-determined time points. Plots of the TTR values (presented as labeled/unlabeled apoE) over time along with the monoexponential slopes of these curves are shown in Figures 3.7A and 3.7B. Table 3.3 shows the pool sizes (PS), fractional clearance rates (FCRs), and production rates (PR) for apoE from each genotype. Though we observed a trend of apoE2 having the fastest FCR, followed by apoE3 and apoE4, the differences were not statistically different (Table 3.3 and 3.4). The apoE4 pool size was 16% lower than apoE2 and 12% lower than apoE3, while the apoE4 PR was 48% slower than apoE2 and 32% slower than apoE3 (Table 3.3

and 3.4). We also measured apoE mRNA levels from these mice and observed that apoE4 mice have significantly decreased levels compared to apoE2 and apoE3 mice (Table 3.3 and 3.4). Therefore, these results suggest that the small but significant difference observed in the PS in these mice is likely due to changes in the production of apoE between the isoforms, rather than the clearance of apoE.

Table 3.3. PS, FCR, PR, Half-life, and mRNA Values for ApoE in Human ApoE Targeted-Replacement Mice

Genotype	PS (ng/mg)	FCR (pools/hr)	PR (ng/mg/hr)	Half-life ($t_{1/2}$, hrs)	mRNA (relative to apoE2)
ApoE2	8.38±0.16	0.078±0.0088	0.65±0.074	8.9	1.0±0.016
ApoE3	8.04±0.22	0.062±0.0048	0.50±0.041	11.2	1.09±0.022
ApoE4	7.07±0.16	0.048±0.011	0.34±0.080	14.4	0.84±0.056
P	<0.0001	0.0832	0.009		0.0002

Table 3.4. Statistical Analysis for Values in Table 3.3

Genotype	PS (ng/mg)	FCR (pools/hr)	PR (ng/mg/hr)	mRNA (relative to apoE2)
E2 vs. E3	N.S.	N.S.	N.S.	N.S.
E2 vs. E4	***	N.S.	***	*
E3 vs. E4	**	N.S.	*	***

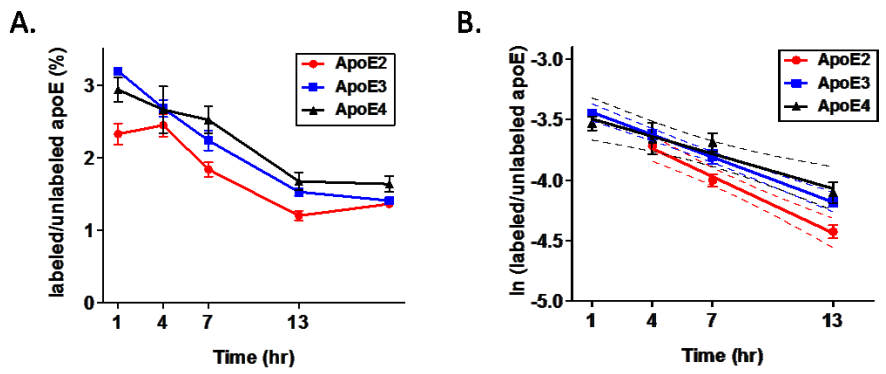

Fig. 3.7. $^{13}C_6$-leucine brain apoE labeling in the human apoE targeted-replacement mice. (A) *APOE2*, *APOE3*, and *APOE4* mice (3.5 months old) were labeled with $^{13}C_6$-leucine and the brains isolated after predetermined time points. Human apoE was then immunoprecipitated from the cortex and the labeled/unlabeled ratios calculated via LC-MS. The labeled/unlabeled ratios were then plotted versus time for each genotype. **(B)** To calculate the FCR, the natural log of the labeled/unlabeled ratios were plotted over time and the monoexponential slopes were calculated (n=3-5 mice per time point, error bars represent SEM, dotted lines represent 95% confidence band).

Measurement of pool-dependent kinetics of human apoE. Since we did not observe any significant differences between the FCRs of the different human apoE isoforms, we decided to analyze whether we could detect a difference in the clearance of the apoE isoforms if we enriched the lysates with the extracellular fraction of apoE. The brain samples analyzed in Figure 3.7 were lysed with a Triton X-100 lysis buffer, which extracts both the intracellular and extracellular proteins from the brain tissue. To enrich

for extracellular apoE, we lysed the tissue from the other cortical hemisphere using a detergent-free PBS lysis buffer. Plots of the TTR values (presented as labeled/unlabeled apoE) over time along with the monoexponential slopes of these curves are shown in Figures 3.8A and 3.8B. For comparison, the labeled/unlabeled ratios for the triton-extracted apoE are also shown in Figure 3.8A. We observed that the peak labeled value is of lower intensity and occurs at a later time point for the PBS samples in comparison to the Triton samples (Fig. 3.8A). This difference is consistent with the Triton and PBS fractions representing a precursor/product relationship. The FCR values for the PBS fraction of apoE were slightly faster than for the apoE in the Triton fraction (Table 3.5). There was also a similar trend in the FCR values between the apoE isoforms in the PBS fraction as for the Triton fraction, with apoE2 having a faster FCR than apoE3 and apoE4. However, the differences between the values were not statistically significant. Therefore, though the PBS and Triton pools of apoE have different labeling kinetics, there does not appear to be a statistically significant difference in the clearance rates between the human apoE isoforms in either pool of proteins analyzed.

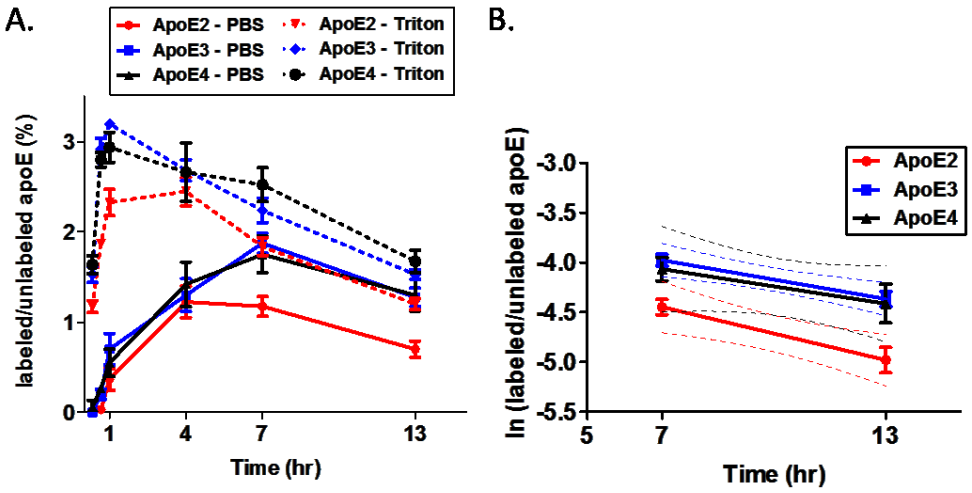

Fig. 3.8. Comparison of pool-dependent $^{13}C_6$-leucine brain apoE labeling kinetics. (A) *APOE2*, *APOE3*, and *APOE4* mice (3.5 months old) were labeled with $^{13}C_6$-leucine and the brains isolated after predetermined time points. Human apoE was then immunoprecipitated from cortex samples lysed in either a Triton lysis buffer or a PBS lysis buffer, and the labeled/unlabeled ratios calculated via LC-MS. The labeled/unlabeled ratios were then plotted versus time for each genotype. **(B)** To calculate the FCR for apoE extracted from the PBS lysis buffer, the natural log of the labeled/unlabeled ratios were plotted over time and the monoexponential slopes were calculated (n=3-5 mice per time point, error bars represent SEM, dotted lines represent 95% confidence band).

Table 3.5. Human ApoE FCR Values from Triton and PBS Extracts

Genotype	Triton FCR (pools/hr)	PBS FCR (pools/hr)
ApoE2	0.0778±0.00876	0.089±0.0249
ApoE3	0.0619±0.00482	0.065±0.00161
ApoE4	0.048±0.0112	0.058±0.047
P	0.0832	0.7489

Discussion

Several different approaches have been described to study protein turnover in animals using stable isotope labeling. Stable isotope tracers are preferred over the use of radioactive tracers because they are safer and can be used to label endogenous proteins. Traditionally, stable isotope incorporation was measured by gas chromatography mass spectrometry (GC-MS) quantitation of labeled amino acids obtained following protein derivatization (Wolfe and Chinkes, 2005). However, this technique is limited to measuring large quantities of proteins, and consequently has only been used to analyze total tissue protein turnover or the kinetics of highly abundant proteins (Garlick et al., 1994; Imoberdorf et al., 2001; Zhang et al., 2002). Recently the more sensitive analytical technique of LC-MS has been applied to quantify the turnover of specific proteins following administration of a stable amino acid in the diet of animals (Doherty et al., 2005; Price et al., 2010). LC-MS allows for the quantitation of protein-specific peptides, and thus does not require breaking proteins down to their amino acid components.

Though these techniques have provided useful information on the turnover of abundant proteins in various organs, the requirement of labeled amino acid delivery via the diet has been a technical issue. Creating a diet enriched with an isotopic label is costly, and inability to control feeding patterns in animals such as mice and rats requires long term exposure (several hours to days) to the labeled diet to achieve reliable and consistent isotope levels in tissues. This is especially problematic in studying proteins with rapid turnover rates, as the difficulty in accurately measuring label incorporation over short time periods (minutes to hours) limits the sensitivity of kinetic analysis. To create a more practical and efficient method of labeling proteins, we have tested whether pulse labeling of mice could be used to measure protein turnover rates in the mouse brain.

Bateman *et al.* previously described a stable isotope labeling kinetics (SILK) technique that can be used to measure the kinetics of proteins in the CSF of humans following the infusion of $^{13}C_6$-leucine into the peripheral bloodstream (Bateman et al., 2007; Bateman et al., 2006). In the method described in this chapter, we adapted this technique to an animal model by injecting mice with a bolus of $^{13}C_6$-leucine. The incorporation of $^{13}C_6$-leucine is then measured in the brains of several cohorts of mice at different time points following injection. Several aspects of the bolus SILK technique outlined in this chapter demonstrate its usefulness for studying protein dynamics in the mouse brain. First, delivery of the stable isotope through a bolus injection provides considerable advantages over administration of the stable isotope label through the diet. Unlike feeding, where it is hard to control when and how much food the mice consume, bolus injection provides a consistent and easily controllable amount of stable isotope.

Since the stable isotope quickly appears in both plasma and brain within minutes of the injection, this technique is particularly suitable for measuring the kinetics of proteins that turn over rapidly. Second, the use of cell-derived labeled protein standards for the MS quantitation insured that our SILK analysis yielded highly reproducible results. The labeling of three different cohorts of Wt control mice resulted in very similar FCR values for apoE (Table 3.1 and Table 4.1; 0.093, 0.10, and 0.09 pools/hr, mean = 0.094 pools/hr ± 0.003). Finally, this labeling technique is particularly useful for comparing the kinetics of proteins in mice with different genetic manipulations, as we have shown in this chapter for mouse and human apoE.

To demonstrate that the SILK technique could detect differences in the clearance rate of a protein, we measured the clearance of apoE from the brains of Wt mice and mice that overexpress the LDLR protein. We observed that the FCR of apoE in the LDLR-overexpressing mice was 2.8-fold faster than in Wt mice. The reason for this effect is likely increased LDLR-mediated cellular uptake and catabolism of apoE within the brain. We also demonstrated that the SILK technique can measure the clearance rates of different pools of a protein by using different tissue lysis conditions. We measured the turnover of human apoE extracted from the brains of human apoE targeted-replacement mice using either a detergent-based lysis buffer (Triton X-100) or a lysis buffer without detergent (PBS). The Triton-containing lysis buffer extracts both intracellular and extracellular proteins due to disruption of the cellular membrane, while extraction using the PBS buffer yields predominantly extracellular proteins. For the SILK analysis, we observed that it took longer for $^{13}C_6$-leucine-labeled apoE to appear in the PBS lysate

compared to the Triton lysate. This difference is likely due to the fact that apoE in the PBS fraction must be synthesized and secreted into the extracellular environment. While labeled apoE will appear in the Triton lysate immediately following synthesis, there will be a delay in the appearance of labeled apoE in the PBS fraction that accounts for the time it takes for the protein to be secreted. The two different pools therefore exist in a precursor/product relationship, as intracellular apoE (Triton lysate) is ultimately secreted and detected in the extracellular space (PBS lysate). Because of different pathways of protein degradation and removal in the intracellular and extracellular environment, the fractional clearance rates of apoE from the Triton and PBS pools may be different. For instance, we observed that the FCR of human apoE in the PBS pool was consistently faster than the FCR of apoE in the Triton pool, suggesting decreased stability of extracellular apoE. Therefore, it is important to take into account the pool from which the proteins are obtained when interpreting results from the SILK analysis.

Studies in mice have shown that both the amount of apoE protein in the brain and the isoform of apoE present play an important role in regulating the extent of Aβ deposition in the brain (Kim et al., 2009a). Whether more or less apoE is beneficial remains unclear. Genetic studies using mice that have one or two copies of either mouse or human apoE demonstrate that more apoE promotes amyloid deposition (Bales et al., 1999; Bales et al., 1997; Kim et al., 2011), while pharmacologic up regulation of apoE in the mouse brain decreases Aβ deposition (Cramer et al., 2012). In terms of the apoE isoforms, human apoE targeted-replacement mice that express human apoE4 exhibit a higher level of Aβ deposition and amyloid plaque load in comparison to mice that express

either apoE2 or apoE3 (Bales et al., 2009; Castellano et al., 2011; Fryer et al., 2005b). It has been hypothesized that a potential reason for the differential effects of the apoE isoforms on Aβ deposition is the total amount of apoE in the brain varies between the isoforms. Several studies have detected a difference in total apoE levels between the human apoE targeted-replacement mice, with the general trend being apoE2>apoE3>apoE4. However, other studies have shown no differences between the levels of apoE in the brains of these mice (Korwek et al., 2009; Sullivan et al., 2004). The reason for the inconsistent results is unknown, but one possibility may be due to the use of multiple antibodies that recognize the isoforms with different affinities. Since these mice have become an important tool for the AD research field, it is important to clarify this issue.

Studying the kinetics of apoE in the brains of the human apoE targeted-replacement mice provides further information on apoE protein stability and a potential mechanistic explanation for differences in protein levels. In the experiments described in this chapter, we measured apoE protein levels in these mice and observed a significant decrease in the amount of apoE4 compared to apoE2 and apoE3. We also applied our SILK technique to measure the FCR of apoE in these mice. No significant differences in FCR were measured between the isoforms, though there was a trend for apoE4's FCR to being slower than that of apoE2 and apoE3. A decreased clearance does not explain the lower total protein levels measured in the brains of the apoE4 mice. However, the apoE4 mice did have a decreased production rate and lower mRNA levels in comparison to the apoE2 and apoE3 mice. Therefore, our results suggest that the differences in apoE levels

in the brains of the targeted-replacement mice are likely due to changes in protein synthesis rather than clearance. Consequently, further studies are warranted to determine the molecular mechanisms dictating different transcription and translation rates between the apoE isoforms.

Conclusions

In summary, we developed a novel method to measure protein kinetics in the mouse brain that uses stable isotope labeling-kinetics (SILK) coupled to multiple reaction monitoring mass spectrometry. We validated the technique by demonstrating that the clearance rate of apoE is increased in the brain in the setting of elevated LDLR levels. We also used this technique to measure the kinetics of human apoE in the brains of the human apoE targeted-replacement mice. We propose that our SILK methodology, and its applicability to studying the clearance of proteins in genetically modified mouse models, will also be useful in studying the kinetics of proteins implicated in other neurodegenerative diseases, such as synuclein, tau, and huntingtin. We also hope that this technique will aid the development and characterization of therapeutics that target protein metabolism in neurodegeneration.

Chapter 4

Effect of ABCA1 Levels on ApoE and Aβ Turnover in the Brain

(This work involved the collaboration of several labs and individuals. Hong Jiang aided with mouse tissue sample collection. All of the mass spectrometry data collection and analysis was done in the lab of Dr. Randall Bateman and performed by Dr. Yuriy Pyatkivskyy. Finally, Dr. Bruce Patterson provided expertise and helpful discussion for interpreting the data. The work from this chapter was published in the journal *Molecular Neurodegeneration*)

Summary

The lipidation status of apoE has been shown to play an important role in regulating both the amount of apoE and the extent of Aβ deposition in the mouse brain. One of the main proteins that function in the lipidation of apoE in the brain is the cholesterol transporter ATP-binding cassette A1 (ABCA1). Deletion and overexpression of ABCA1 in the brains of APP transgenic mice led to an increase and decrease of Aβ deposition, respectively. As a result, it has been hypothesized that regulating ABCA1 levels alters either the clearance of Aβ or its propensity to aggregate into amyloid fibrils. In this chapter, we apply the SILK technique described in chapter 3 to determine the clearance rates of apoE and Aβ in the brains of APP transgenic mice that either lack or overexpress ABCA1. Both overexpression and deletion of ABCA1 increased the fractional clearance rate (FCR) of apoE and decreased the total amount of apoE in the brain. However, at an age prior to Aβ deposition, the level of ABCA1 had no effect on the Aβ FCR or levels of Aβ in the brains of APP transgenic mice. These results therefore suggest that ABCA1 does not regulate Aβ metabolism in the brain, but rather exerts its effect on Aβ deposition via another mechanism.

Introduction

ABCA1 is a transmembrane protein that plays an important role in the elimination of excess cellular cholesterol during the process of reverse cholesterol transport (RCT) (Lawn et al., 1999). In the periphery, ABCA1 functions in the rate-limiting step of high-density lipoprotein (HDL) formation by facilitating the transport of cholesterol and phospholipids to lipid-poor apolipoprotein A-I (apoA-1) to form discoidal pre-HDL particles (Brewer et al., 2004; Wang et al., 2007). Further lipidation of the pre-HDL particles via the ATP-binding cassette transporters G1 and G4 (ABCG1 and ABCG4) and esterification of the cholesterol via the enzyme lecithin: cholesterol acyltransferase (LCAT) leads to the formation of mature HDL particles, which are ultimately transported to the liver (Jonas, 1998; Vaughan and Oram, 2006). Mutations in the *ABCA1* gene that lead to a deficiency in the ABCA1 protein cause Tangier's disease in humans, which is characterized by a dramatic decrease in plasma HDL and apoA-I, accumulation of tissue cholesteryl esters, and increased risk for cardiovascular disease (Bodzioch et al., 1999; Brooks-Wilson et al., 1999; Lawn et al., 1999; Rust et al., 1999). The decrease in apoA-I in these individuals has been shown to be due to increased metabolism of the lipid-poor apoA-I containing lipoprotein particles (Schaefer et al., 1981; Schaefer et al., 1978).

ApoE appears to be the primary lipoprotein receptor for ABCA1 in the brain, as apoA-I is present at levels that are only 0.5% of the amount found in plasma (Demeester et al., 2000). The level of ABCA1 in the brain has been shown to modulate the extent of apoE lipidation and apoE levels. Surprisingly, both deletion and overexpression of ABCA1 in the mouse brain led to a decrease in apoE levels (Hirsch-Reinshagen et al.,

2004; Wahrle et al., 2008; Wahrle et al., 2004). However, the decrease was greater in mice lacking ABCA1. ABCA1 overexpression and deletion had different effects on apoE lipidation. The apoE-containing lipoprotein particles isolated from the cerebral spinal fluid (CSF) of ABCA1$^{-/-}$ mice were poorly lipidated, while those from the CSF of mice overexpressing ABCA1 had higher levels of lipidation compared to wild type animals (Wahrle et al., 2008; Wahrle et al., 2004).

Since lowering apoE levels decreased amyloid deposition in the mouse brain (Bales et al., 1999; Bales et al., 1997), it was hypothesized that altering ABCA1 levels would also alter amyloid deposition in APP transgenic mice. Despite decreased apoE levels with both ABCA1 deletion and overexpression, only ABCA1 overexpression caused a significant decrease in amyloid load in the mouse brain of APP transgenic animals (Wahrle et al., 2008). The amyloid load in APP transgenic mice deficient in ABCA1 did not change, or even increased, when ABCA1$^{-/-}$ mice were crossed to various APP transgenic models (Hirsch-Reinshagen et al., 2005; Koldamova et al., 2005a; Wahrle et al., 2005). Because of the opposing effects of ABCA1 deletion and overexpression on Aβ accumulation, ABCA1 likely alters Aβ levels through a mechanism distinct from solely modulating apoE levels. One proposed mechanism is ABCA1 levels could alter Aβ clearance from the brain (Hirsch-Reinshagen and Wellington, 2007; Wahrle et al., 2008); however this hypothesis has yet to be tested *in vivo*.

In this chapter, we used stable isotope labeling kinetics (SILK) to study the effect of ABCA1 levels on both apoE and Aβ clearance rates in the mouse brain. APP

transgenic mice were generated that either overexpressed or lacked ABCA1, and they were subsequently injected with a bolus of $^{13}C_6$-leucine. Both overexpression and deletion of ABCA1 resulted in an increased fractional clearance rate of apoE. However, ABCA1 levels did not alter the clearance rate of Aβ in the mouse brain, suggesting ABCA1 acts via another pathway, such as directly influencing Aβ aggregation, to regulate amyloid deposition.

Experimental Procedures

Materials - $^{13}C_6$-leucine was obtained from Cambridge Isotope Laboratories (Andover, MA, USA). HJ5.2 (Aβ) and HJ6.3 (ApoE) antibodies were made in-house. Protein G Sepharose 4 Fast Flow beads were obtained from GE Healthcare (Piscataway, NJ, USA). Formic acid (Optima LC-MS) was obtained from Fisher Scientific and triethylammonium bicarbonate was obtained from Sigma-Aldrich (St. Louis, MO, USA). Trypsin Gold (mass spec grade) was purchased from Promega (Madison, WI, USA).

Animal labeling and tissue collection - ABCA1$^{+/-}$ mice on a DBA background were obtained from the Jackson Laboratory (Bar Harbor, ME, USA). PDAPP mice on a C57/BL/6J background were a generous gift from Eli Lilly (Indianapolis, IN, USA). ABCA1 Tg mice were backcrossed to C57/BL/6J mice for 8 generations, and then crossed to DBA mice. PDAPP mice were also crossed to DBA mice and ABCA1$^{+/-}$ mice were crossed to C57/BL/6J mice to create strains that were on a 50% C57/BL/6J /50%DBA background. The ABCA1 Tg$^{+/-}$ and PDAPP$^{+/-}$ mice were then bred to each

other to generate ABCA1 $Tg^{+/-}$/$PDAPP^{+/-}$ and ABCA1 $Tg^{-/-}$/$PDAPP^{+/-}$ mice that were used for the experiments. $ABCA1^{+/-}$ mice were crossed to $PDAPP^{+/-}$ mice to generate mice that were $PDAPP^{+/-}$/$ABCA1^{+/-}$. These mice were then bred to $ABCA1^{+/-}$ mice to generate mice that were $PDAPP^{+/-}$/$ABCA1^{+/+}$, $PDAPP^{+/-}$/$ABCA1^{+/-}$, and $PDAPP^{+/-}$/$ABCA1^{-/-}$. The $PDAPP^{+/-}$/$ABCA1^{+/+}$ and $PDAPP^{+/-}$/$ABCA1^{-/-}$ mice were used for all experiments. Mice were maintained under constant light/dark conditions and had free access to food and water. All experimental protocols were approved by the Animal Studies Committee at Washington University in St. Louis.

Prior to injection, the $^{13}C_6$-leucine was dissolved in medical-grade normal saline to a concentration of 7.5 mg/mL. The mice were weighed and then intraperitoneally injected with the $^{13}C_6$-leucine (200 mg/kg of body weight). After predetermined time points, the animals were anesthetized and the blood was collected by cardiac puncture. The mice were then perfused with PBS-heparin and regional brain dissection was performed. All brain samples were subsequently frozen on dry ice.

Primary astrocyte cell culture and *in vitro* labeling - Primary astrocytes were cultured from postnatal day 1 (P1) C57/BL/6J mouse pups as described previously (Kim et al., 2009b). Cells were cultured in serum-containing growth media (DME/F12, 15% fetal bovine serum, 10 ng/mL epidermal growth factor, 100 units/mL penicillin/streptomycin, and 1 mM sodium pyruvate) until they reached 70 percent confluency. The cell medium was then changed to serum free medium that did not contain any leucine (DME/F12 without leucine prepared by the Washington University Tissue Culture Support Center,

N2 growth supplement, 100 units/mL penicillin/streptomycin, and 1 mM sodium pyruvate) and cultured for 12 hr. $^{13}C_6$-leucine was then diluted into unlabeled leucine to make labeled/unlabeled percentages that were either 0, 1.25, 2.5, 5, 10, or 20%. These different percent-labeled leucine solutions were then added to separate flasks of primary astrocytes, and the cells were cultured for an additional 48 hrs. The medium was then collected from the cells, spun down at 1500 rpm to clear cellular debris, and stored at -80°C.

ApoE and Aβ immunoprecipitation - Antibody beads were prepared by covalently binding either HJ6.3 (apoE) or HJ5.2 (Aβ) to Protein G Sepharose 4 Fast Flow beads. The beads initially were washed 3 times with ice-cold PBS and then resuspended in ice-cold PBS to make a 50% slurry of beads. 300 µL of the washed 50% beads were then mixed with antibody (0.4 µg/µL of 50% bead mixture), 10 µL of 1% Triton X-100 and ice-cold PBS to make a final volume of 1000 µL. This mixture was then tumble incubated overnight at 4°C. The beads were then washed 3 times with 1% Triton X-100 lysis buffer (Triton X-100, 150 mM NaCl, 50 mM Tris-HCl) and 2 times with 0.2 M triethanolamine (pH = 8.2). Freshly prepared dimethyl pimelimidate in 0.2 M triethanolamine (pH = 8.2) was then added to the beads, followed by a 30 min incubation with tumbling at room temperature to allow for crosslinking. The beads were then washed once with 50 mM Tris (pH = 7.5) to stop the crosslinking reaction, and twice with 0.1% Triton X-100 in PBS. The washing solution was removed by vacuum aspiration, and the beads were resuspended in PBS to make a 50% bead slurry.

Brain cortex samples were weighed and 1% Triton X-100 lysis buffer (Triton X-100, 150 mM NaCl, 50 mM Tris-HCl, 1 X Roche Complete Protease Tablet) was added at a concentration of 150 mg brain tissue/mL of lysis buffer. The samples were then sonicated (2 rounds of 20 1-sec pulses) and centrifuged at 14,000 rpm for 30 min. The supernatant was collected and used for subsequent immunoprecipitation steps. Brain lysates and cell media were pre-cleared with beads not conjugated to antibody by tumble incubating the samples with 50 μL of the 50% bead slurry for 4 hrs at 4°C. The pre-cleared lysate and media samples were then tumble incubated with antibody-conjugated beads overnight at 4°C. The beads were then washed 3 times with PBS and 3 times with 25 mM triethylammonium bicarbonate (TEABC). Following the last TEABC wash, the washing solution was removed via vacuum aspiration with a pipette tip. Formic acid was then added to the beads to elute the bound proteins, and the mixture was vortexed for 20 minutes. The beads were then centrifuged at 14,000 rpm for 5 minutes and the supernatant was collected from the beads. The formic acid supernatant was transferred to a new microcentrifuge tube and evaporated in a Savant SpeedVac for 60 min (37°C). The dried proteins were then resuspended in 20% acetonitrile/80% 25 mM TEABC and vortexed for 30 minutes. The samples were then digested with 500 ng of mass spectrometry-grade trypsin (Promega) and incubated at 37°C for 16 hrs. The digested samples were dried again by vacuum evaporation, resuspended in 10% acetonitrile and 0.1% formic acid in water, and transferred to mass spec vials.

Liquid Chromatography/Mass Spectrometry - LC-MS/MS measurements were performed on a Waters Xevo TQ-S triple quadrupole mass spectrometer (Waters Inc., Milford, MA) coupled to a Waters nano-ACQUITY ultra performance liquid chromatography (UPLC) system, equipped with a Waters nano-ESI ionization source. To identify multiple reaction monitoring (MRM) transitions, the synthetic ApoE peptide LQAEIFQAR and synthetic Aβ peptide LVFFAEDVGSNK were purchased from AnaSpec, Inc. (Fremont, CA), and directly infused into the LC-MS for automatic tuning of optimized MRM transitions produced by the peptide. For both the apoE and Aβ peptide, optimal conditions were identified as a capillary voltage of 3.3 kV, source temperature of 80°C, cone voltage of 52 V, purge gas flow rate set at 100 L/hr, and cone gas at 50 L/hr. Obtained MRM transitions (Table 4.1) were then validated by the analysis of apoE and Aβ cell culture media standards. For the actual experiments, all digested peptide samples were kept at 4°C and 1 μL aliquots were injected onto a Waters BEH130 nanoAcquity UPLC column (C18 particle, 1.7 μm, 100 μm x 100 mm). The peptide mixtures were separated on a reverse-phase nanoUPLC operated at a flow rate of 500 nL/min with a gradient mixture of solvents A (0.1% formic acid in water) and B (0.1% formic acid in acetonitrile). For apoE, the column was initially kept at 99% solvent A for 1.5 min, followed by a separation gradient of 1% to 97% solvent B from 1.5 to 18 min. The column was then kept at 97% solvent B for another 5 min followed by 1% solvent B to re-equilibrate for 10 min to prepare for the next injection. For Aβ, the column was initially kept at 90% solvent A for 7.0 min, followed by a separation gradient of 10% to 45% solvent B from 7 to 12 min. The column was then kept at 45% to 95% solvent B

from 12 to 14 min, and at 95% solvent B for another 3 min followed by 10% solvent B to re-equilibrate for 15 min to prepare for the next injection. All raw data were acquired and quantified using Waters MassLynx 4.1 software suite. The labeled/unlabeled ratio was obtained by dividing the area under the curve (AUC) of the MRM total ion for the labeled peptide by the AUC for the unlabeled peptide, and converted to tracer-to-tracee ratios (TTRs) by reference to the standard curve.

Table 4.1. MRM Transitions for ApoE and Aβ Analysis

Protein	Peptide sequence	Precursor m/z	Product m/z	Collision Energy (V)
ApoE	LQAEIFQAR	538.2852	634.2609	14
ApoE	LQAEIFQAR	538.2852	763.2590	12
ApoE	LQAEIFQAR	538.2852	834.2775	14
ApoE	[$^{13}C_6$]LQAEIFQAR	541.2852	634.2609	14
ApoE	[$^{13}C_6$]LQAEIFQAR	541.2852	763.2590	12
ApoE	[$^{13}C_6$]LQAEIFQAR	541.2852	834.2775	14
Aβ	LVFFAEDVGSNK	663.3405	819.3840	24
Aβ	LVFFAEDVGSNK	663.3405	966.4520	24
Aβ	LVFFAEDVGSNK	663.3405	1113.5210	24
Aβ	[$^{13}C_6$]LVFFAEDVGSNK	666.3500	819.3840	24
Aβ	[$^{13}C_6$]LVFFAEDVGSNK	666.3500	966.4520	24
Aβ	[$^{13}C_6$]LVFFAEDVGSNK	666.3500	1113.5210	24

Kinetic analysis - The mice were in steady-state conditions, since the amount of apoE and Aβ did not significantly change over the time period of the kinetic analysis. This was determined by measuring the protein level (via ELISA as described below) for the cohorts of mice at each time point following the stable isotope injection, and comparing

across groups. At metabolic steady state, the fraction of the pool that is synthesized per unit time equals the fraction of the pool catabolized per unit time (FCR), which can be calculated as the negative of the slope of the natural log of TTR plotted over time (Patterson et al., 2002). Production rates (PRs) were determined as: PR (protein amount/mg/hr) = [FCR (pools/hr) x protein concentration (protein amount/mL) x lysate volume (mL)]/brain weight (mg). The half-lives ($t_{½}$) were calculated using the equation $t_{½}$ = ln 2/FCR. Protein concentrations of apoE and Aβ in the lysates were determined by protein-specific sandwich ELISAs using in-house antibodies. For apoE, HJ6.2 was used as the coating antibody and biotinylated HJ6.3 as the detection antibody. Pooled C57/BL/6J mouse plasma was used as a standard. For Aβ, HJ2 (anti-Aβ35-40) and biotinylated HJ5.1 (anti-Aβ13-28) were used as the coating and detection antibody, respectively.

Statistical Analysis - Data were analyzed using GraphPad Prism Software and presented as mean ± standard error of the mean (SEM). For analyzing differences in protein levels and production rates, a two-tailed student's t-test was used. Differences in the FCR values were compared using analysis of covariance (ANCOVA) of the slope of the natural log of TTR plotted over time, which was determined using linear regression analysis.

Results

Effect of ABCA1 levels on apoE clearance rate

Both the overexpression and deletion of ABCA1 from the mouse brain led to a decrease in the amount of apoE in the brain (Hirsch-Reinshagen et al., 2005; Wahrle et al., 2005; Wahrle et al., 2008). To determine whether this decrease in apoE is due to increased clearance of apoE, we used SILK analysis to measure the fractional clearance rate (FCR) of apoE in the brains of APP transgenic mice crossed to $ABCA1^{-/-}$ and ABCA1 Tg mice. To generate APP transgenic mice that either overexpressed or were deficient in ABCA1 levels, we crossed PDAPP mice with ABCA1 Tg and $ABCA1^{-/-}$ mice. These animals were then injected with $^{13}C_6$-leucine and the brain tissue was collected and lysed. The same tissue lysates were used to immunoprecipitate both apoE and Aβ (see following section for discussion on Aβ analysis). Following immunoprecipitation of apoE from the lysates, the FCRs of apoE were measured using liquid chromatography mass spectrometry (LC-MS). Plots of the labeled/unlabeled apoE values over time along with the monoexponential slopes of these curves for the ABCA1 Tg and $ABCA1^{-/-}$ mice are shown in Figures 4.1A,B and 4.2A,B, respectively. Different groups of wildtype (Wt) control mice were used for the ABCA1 Tg and $ABCA1^{-/-}$ mice. The PS, FCR, PR, and half-life values are given in Table 4.2. The apoE FCR was 1.5 fold faster in ABCA1 Tg mice and 1.9 fold faster in $ABCA1^{-/-}$ mice compared to Wt mice; however the difference was only statistically significant for the $ABCA1^{-/-}$ mice. The apoE PS decreased by 20% in ABCA1 Tg mice and by 51% in $ABCA1^{-/-}$ mice compared to Wt mice. No statistical differences existed between the calculated values for the PR.

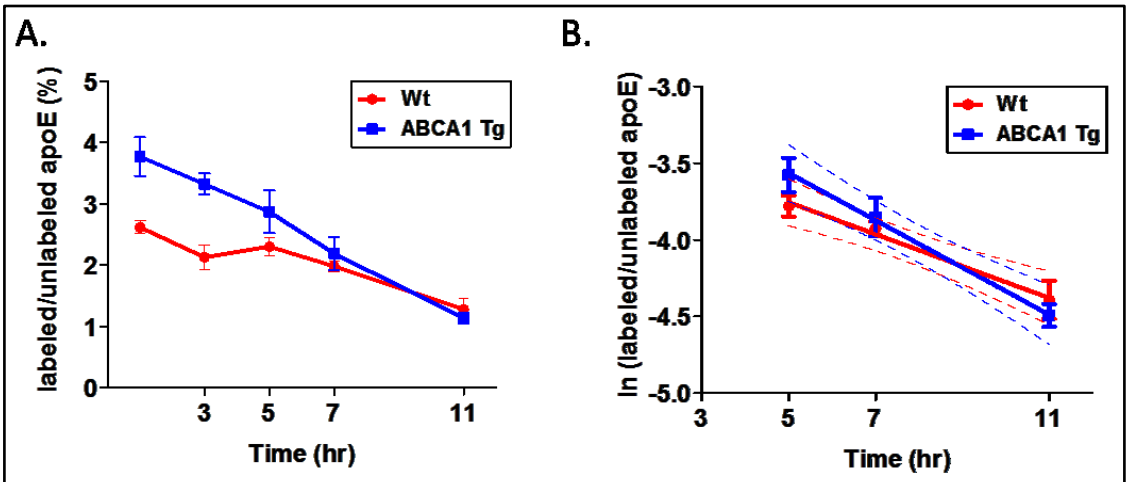

Fig. 4.1. $^{13}C_6$-leucine brain apoE labeling in the presence of ABCA1 overexpression. (A) Cohorts of wildtype and ABCA1 transgenic mice were labeled with $^{13}C_6$-leucine and the brains isolated after predetermined time points. ApoE was then immunoprecipitated from the cortex and the labeled/unlabeled ratios calculated via LC-MS. The labeled/unlabeled ratios were then plotted versus time for each genotype. **(B)** For FCR measurements, the monoexponential slopes of the ln (labeled/unlabeled apoE) curve were measured for ABCA1 Tg and Wt control mice (n=5-6 mice per time point, error bars represent SEM, dotted lines represent 95% confidence band).

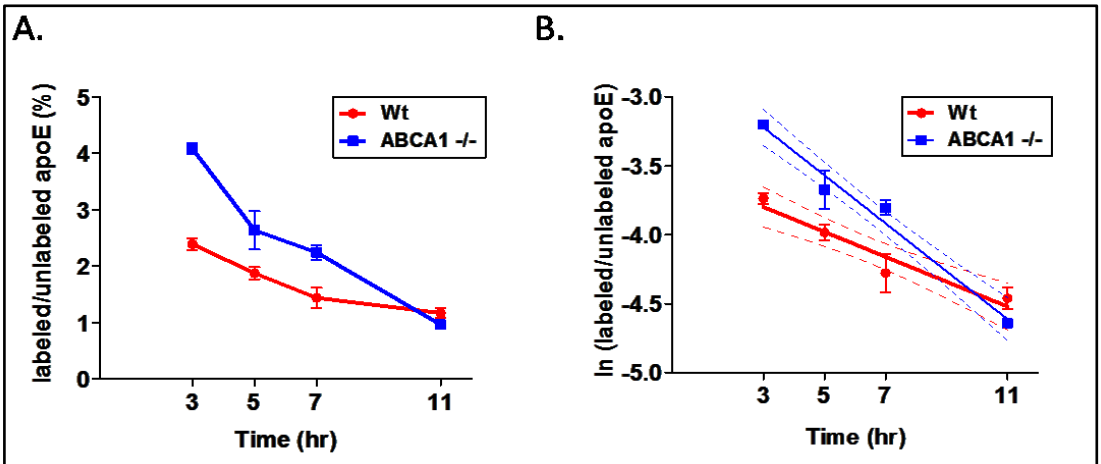

Fig. 4.2. $^{13}C_6$-leucine brain apoE labeling in the setting of ABCA1 deletion. **(A)** Cohorts of wildtype and ABCA1$^{-/-}$ mice were labeled with $^{13}C_6$-leucine and the brains isolated after predetermined time points. The apoE labeled/unlabeled ratios were then calculated and the data plotted as in Fig. 4.1. **(B)** For FCR measurements, the monoexponential slopes were measured for ABCA1$^{-/-}$ mice and Wt control mice as in Fig. 4.1. (n=5-6 mice per time point, error bars represent SEM, dotted lines represent 95% confidence band).

These results demonstrate that the decrease in apoE levels both with ABCA1 deletion and overexpression is due to an increase in the clearance of apoE from the brain.

Table 4.2. Pool Sizes (PS), Fractional Clearance Rates (FCR), Production Rates (PR), and Half-lives for ApoE by Mouse Genotype

Genotype	PS (ng/mg)	FCR (pools/hr)	PR (ng/mg/hr)	Half-life ($t_{1/2}$, hrs)
Wt (ABCA1 Tg control)	135.5±4.8	0.10±0.019	14.08±1.64	6.9
ABCA1 Tg	109.2±3.8	0.15±0.022	16.81±0.96	4.6
P	<0.0001	0.106	0.46	
Wt ($ABCA1^{-/-}$ control)	230.5±12.1	0.09±0.015	20.76±3.64	7.7
$ABCA1^{-/-}$	117.6±8.0	0.17±0.010	20.41±2.13	4.1
P	<0.0001	<0.0001	0.94	

Effect of ABCA1 levels on Aβ clearance rate

To determine whether ABCA1 levels regulate Aβ clearance from the brain, we used SILK analysis to measure the FCR of Aβ in the brains of PDAPP crossed to $ABCA1^{-/-}$ and ABCA1 Tg mice. To limit complications due to incomplete Aβ extraction from tissue with amyloid plaques, all experiments were performed on young animals (3.5 months old) prior to the onset of detectable plaque deposition. For the immunoprecipitation step, we used an antibody to the central domain of Aβ (amino acids 13-28). As a result, the FCR values we obtained for Aβ represent the kinetic parameters for the total amount of Aβ and likely represent the average kinetic rates of all Aβ species

in the brain. Plots of the labeled/unlabeled Aβ values over time along with the monoexponential slopes of these curves for the ABCA1 Tg and ABCA1$^{-/-}$ mice are shown in Figures 4.3A,B and 4.4A,B, respectively. The PS, FCR, and PR and half-life values are given in Table 4.3. The FCR and half-life of Aβ were approximately 0.24 pools/hr and 2.8 to 2.9 hrs, respectively. No statistical differences were observed for these values between the Wt, ABCA1 Tg, and ABCA1$^{-/-}$ genotypes. There were also no differences in the PS or PR between any of the genotypes. Therefore, the amount of ABCA1 in the brain does not appear to regulate Aβ turnover in the mouse brain at an age prior to plaque deposition.

Table 4.3. PS, FCR, PR, and Half-life Values for Aβ by Mouse Genotype

Genotype	PS (pg/mg)	FCR (pools/hr)	PR (pg/mg/hr)	Half-life ($t_{1/2}$, hrs)
Wt (ABCA1 Tg control)	11.23±0.56	0.238±0.016	2.65±0.21	2.91
ABCA1 Tg	11.14±0.46	0.247±0.016	2.77±0.23	2.81
P	0.90	0.69	0.68	
Wt (ABCA1$^{-/-}$ control)	7.67±0.26	0.247±0.023	1.91±0.15	2.81
ABCA1$^{-/-}$	7.87±0.33	0.243±0.016	1.89±0.19	2.85
P	0.64	0.88	0.94	

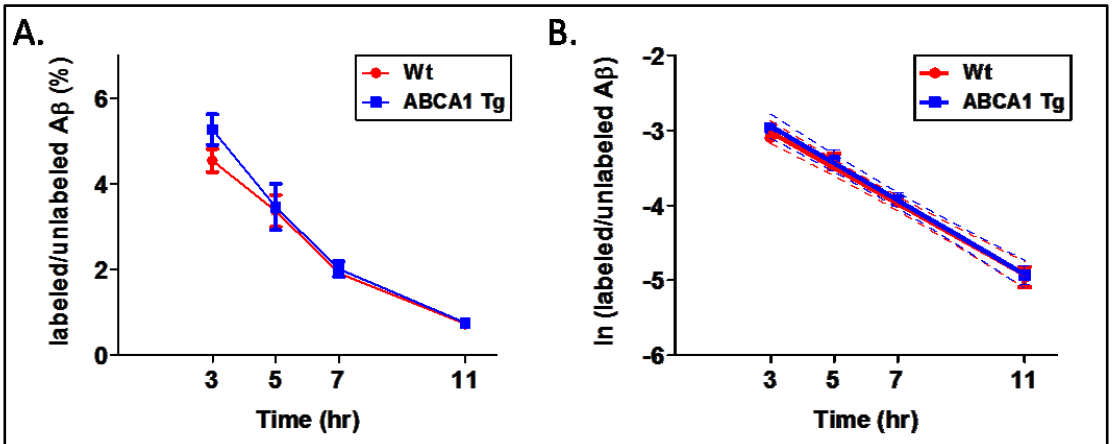

Fig. 4.3. $^{13}C_6$-leucine brain Aβ labeling in the presence of ABCA1 overexpression. (A) Cohorts of wildtype and ABCA1 transgenic mice were labeled with $^{13}C_6$-leucine and the brains isolated after predetermined time points. Total Aβ was immunoprecipitated from the cortex and the labeled/unlabeled ratios were then plotted versus time for each genotype. **(B)** For FCR measurements, the data was plotted as in Figure 4.1B and the monoexponential slopes were calculated for ABCA1 Tg mice and their respective Wt controls (n=5-6 mice per time point, error bars represent SEM, dotted lines represent 95% confidence band).

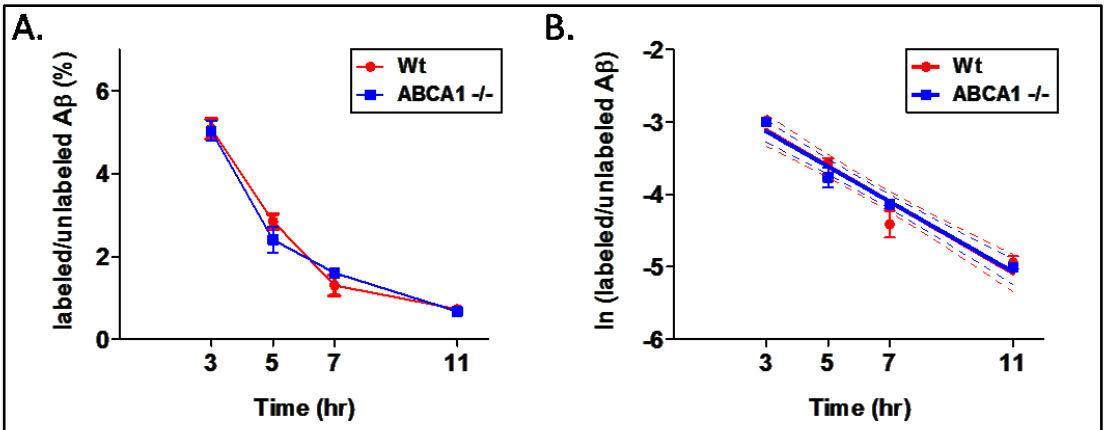

Fig. 4.4. $^{13}C_6$-leucine brain Aβ labeling in the setting of ABCA1 deletion. (A) Cohorts of wildtype and ABCA1$^{-/-}$ mice were labeled with $^{13}C_6$-leucine and the brains isolated after predetermined time points. The Aβ labeled/unlabeled ratios were then calculated and the data plotted as in Fig. 4.3A. **(B)** For FCR measurements, the monoexponential slopes were measured for ABCA1$^{-/-}$ mice and Wt control mice as in Fig. 4.3B. (n=5-6 mice per time point, error bars represent SEM, dotted lines represent 95% confidence band).

Discussion

Previous studies in mice have demonstrated that altering ABCA1 levels in the brain affects both the amount of apoE and the extent of Aβ deposition in the brain. ApoE levels were significantly decreased in the brains of both ABCA1$^{-/-}$ and ABCA1 Tg mice, though to a greater extent in ABCA1$^{-/-}$ mice (Hirsch-Reinshagen et al., 2004; Wahrle et al., 2008; Wahrle et al., 2004). The reason for the decreased apoE levels was hypothesized to be due to the increased catabolism of apoE in both cases. When bred with APP transgenic mice, ABCA1 deficient mice had either similar amounts or increased Aβ accumulation in the brain (Hirsch-Reinshagen et al., 2005; Koldamova et al., 2005a; Wahrle et al., 2005). Conversely, increasing brain ABCA1 levels in APP transgenic mice led to a significant decrease in the extent of Aβ and amyloid deposition in the brain (Wahrle et al., 2008). Because ABCA1 deletion and overexpression both decreased apoE levels but exerted opposing effects on Aβ deposition, it was hypothesized that ABCA1 functions in regulating Aβ deposition via a process other than solely regulating apoE levels. One possibility is that the effect of ABCA1 on the extent of apoE lipidation regulates the ability of apoE to alter either Aβ clearance or fibrillization. In this chapter, we used stable isotope labeling kinetics (SILK) to analyze how deleting or overexpressing ABCA1 alters the kinetic properties of apoE and Aβ in the mouse brain. Both ABCA1 overexpression and deletion increased the fractional clearance rate of apoE from the brain and decreased the total amount of apoE. However, altering ABCA1 levels had no effect on the Aβ fractional clearance rate or Aβ levels in the brain.

The increased FCR of apoE in the ABCA1$^{-/-}$ mice parallels nicely with plasma kinetic studies performed in humans with loss-of-function mutations in ABCA1 (Schaefer et al., 1981; Schaefer et al., 2001). These studies infused radioiodinated apoA-I or apolipoprotein B-100 (apoB-100) into individuals with Tangier's disease and control individuals and measured the disappearance of the labeled apoA-I and apoB-100 over time. The catabolism of apoA-I high density lipoprotein (HDL) and low density lipoprotein apolipoprotein B-100 (LDL B-100) were increased in the plasma of Tangier's disease patients, suggesting decreased stability of poorly-lipidated lipoprotein particles. The mechanism underlying the rapid catabolism of apoA-I in these individuals and the apoE in our mouse studies is unclear, but could be due to abnormalities in either receptor function or degradative enzyme activity caused by changes in the structural characteristics of the lipoprotein particles. It is also possible that the mechanisms underlying the increased apoE catabolism in mice with ABCA1 overexpression and deletion are not the same. The lipidation of apoE significantly alters its propensity to bind to LDLR, with increased lipid levels leading to enhanced binding (Innerarity and Mahley, 1978). As a result, the faster apoE clearance rate in the ABCA1 Tg mice may be due to increased LDLR-mediated clearance of the more highly lipidated apoE-containing lipoprotein particles.

In the experiments described in this chapter, we first used SILK to measure the kinetics of Aβ in the mouse brain. Previous studies have measured Aβ clearance from the brain either using [^{35}S]methionine labeling (Savage et al., 1998), or by measuring the disappearance of Aβ following the pharmacological inhibition of Aβ production

(Abramowski et al., 2008; Barten et al., 2005; Cirrito et al., 2003). The half-life of Aβ clearance in these studies ranged from 30 min to 2 hr. Consistent with these studies, we observed a half-life for Aβ of approximately 2.8-2.9 hrs (Table 4.3). In comparison to other studies, our technique has unique advantages in that it does not require a radioactive tracer and kinetics are determined in the steady-state, which is not possible with the inhibition of Aβ production. Future SILK studies in mice could compare the kinetics of specific species of Aβ (such as Aβ38, Aβ40, and Aβ42) and analyze how Aβ metabolism changes as mice age.

Several studies in cell culture have shown that ABCA1 regulates both the production and clearance of Aβ. Overexpression of ABCA1 decreased the production and secretion of Aβ in both neuronal and non-neuronal cell lines (Kim et al., 2007; Sun et al., 2003). In primary microglia, ABCA1 deletion decreased the intracellular degradation of Aβ (Jiang et al., 2008). Less evidence exists *in vivo* that ABCA1 levels alter the production or clearance of Aβ. No changes in the proteolytic processing of APP were observed in APP transgenic mice crossed to ABCA1$^{-/-}$ or ABCA1 Tg mice (Koldamova et al., 2005a; Wahrle et al., 2008). A study measuring the disappearance of radiolabeled Aβ injected into the brains of ABCA1$^{-/-}$ mice also found no effect on Aβ clearance across the blood-brain barrier (Akanuma et al., 2008). In this chapter, we used SILK analysis to determine the effect of ABCA1 overexpression and deletion on the clearance and production rates of endogenously-produced Aβ. Our results suggest that at a young age prior to the onset of plaque deposition, ABCA1 levels do not alter Aβ clearance or production in the mouse brain. Though we cannot rule out the possibility that changes in

Aβ clearance develop as the mice age, our current data suggests that the effect of ABCA1 on Aβ deposition in the brain may not occur due to altered metabolism of Aβ.

Future studies should analyze other possible mechanisms for how ABCA1 could regulate Aβ levels and deposition in the brain. It is possible that the effect of ABCA1 is caused by altered modulation of differentially lipidated forms of apoE on Aβ aggregation or fibrillogenesis. A previous study has shown that increasing the lipidation of apoE enhances the ability of apoE to bind to Aβ *in vitro* (Tokuda et al., 2000). However, whether or not increased apoE-Aβ binding leads to more or less Aβ deposition *in vivo* is currently unknown. The possibility also exists that ABCA1 modulates Aβ deposition in a manner that is independent of apoE. ABCA1 levels may regulate the extent of intracellular cholesterol levels, which in turn could alter Aβ secretion (Di Paolo and Kim, 2011). ABCA1 could also modulate the function of other proteins involved in brain lipoprotein metabolism, such as apoA-I or apolipoprotein J (apoJ). Therefore, further work is needed to determine the molecular mechanism responsible for the role ABCA1 plays in regulating Aβ amyloidogenesis

Conclusions

In this chapter, we have used stable isotope labeling kinetics (SILK) coupled with mass spectrometry to analyze the effect of ABCA1 levels on the metabolism of apoE and Aβ in the mouse brain. ABCA1 had previously been shown to regulate both the amount of apoE in the brain, along with the extent of Aβ deposition, and represents a potential molecular target for lowering brain amyloid levels in AD patients. The FCR of apoE was

increased 1.9- and 1.5-fold in mice that either lacked or overexpressed ABCA1, respectively. ABCA1 deletion and overexpression also decreased the total amount of apoE protein in the brain. However, ABCA1 had no effect on the FCR or production rate of Aβ, suggesting that ABCA1 does not regulate Aβ metabolism in the brain.

Chapter 5

Preliminary Studies:

Effect of the LDLR-regulatory Protein PCSK9 on Aβ Levels and Deposition

(This work was completed with the assistance of several individuals. Dr. Jungsu Kim, Devika Bagchi, and Floy Stewart performed the staining experiments and plaque analysis. Hong Jiang helped with the brain tissue collection and ELISA experiments.)

Summary

Previously we have shown that increasing LDLR levels in the brains of APP transgenic mice decreases the extent of Aβ deposition and enhances the clearance of Aβ. In chapter 2 of this thesis, we have also demonstrated that increasing LDLR levels enhances the uptake and degradation of Aβ by astrocytes. Therefore, these results suggest that finding pathways that regulate brain LDLR levels will identify potential therapeutic targets for the treatment of Alzheimer's disease. The protein proprotein convertase subtilisin/kexin type 9 (PCSK9) has been shown to play an important role in the degradation of LDLR in cell lines and peripheral tissues. However, the ability of PCSK9 to regulate LDLR levels in the brain has not been studied. In this chapter, we describe preliminary studies that analyzed the effect of PCSK9 on LDLR protein levels in the mouse brain. We also analyzed the effect of PCSK9 deletion on Aβ deposition in the brains of APP transgenic mice. Our preliminary results suggest that PCSK9 does not regulate LDLR levels in the brain, but the level of PCSK9 does alter the extent of Aβ deposition through an unknown mechanism.

Introduction

Increasing the amount of LDLR in the brain decreases the extent of Aβ deposition and enhances Aβ clearance from the brains of APP transgenic mice (Kim et al., 2009b). Based on the experiments in chapter 1 of this thesis, LDLR also promotes the cellular uptake and degradation of soluble Aβ by glial cells. These results suggest that increasing brain LDLR levels represents a potential therapeutic avenue for lowering amyloid load in the Alzheimer's disease (AD) brain. One method to increase LDLR levels would be to inhibit LDLR degradation in the brain. However, the molecular pathways mediating LDLR degradation in the brain are not well-characterized.

PCSK9 is an important regulator of peripheral LDL catabolism via its ability to facilitate LDLR degradation (Horton et al., 2009). In humans, gain-of-function and loss-of-function mutations in PCSK9 have been identified that cause hyper- and hypocholesterolemia, respectively (Abifadel et al., 2003; Cohen et al., 2005). Studies in mice demonstrated that the cause of the cholesterol metabolism abnormalities with altered PCSK9 levels was the ability of PCSK9 to alter LDLR levels. Hepatic overexpression of PCSK9 resulted in hypercholesterolemia and a significant decrease in the amount of LDLR protein (Maxwell and Breslow, 2004; Park et al., 2004), while PCSK9 deletion caused a decrease in plasma cholesterol and increased LDLR protein levels (Rashid et al., 2005). In these experiments, altering PCSK9 levels had no effect on the amount of LDLR mRNA, suggesting that PCSK9 regulates LDLR post-transcriptionally. Subsequent studies in both cell culture and mouse models have demonstrated that PCSK9 is a secreted protein that circulates in the blood, and secreted

PCSK9 is capable of decreasing liver LDLR levels (Benjannet et al., 2004; Lagace et al., 2006; Seidah et al., 2003). At a molecular level, PCSK9 appears to exert its effect on LDLR by directly binding to LDLR on the cell surface and facilitating its trafficking to the lysosomal pathway following endocytosis (Fisher et al., 2007; Lagace et al., 2006; Yamamoto et al., 2011; Zhang et al., 2007). Because of its effects on peripheral cholesterol levels, PCSK9 has gained significant attention as a potential therapeutic target to treat cardiovascular disease (Horton et al., 2009).

The role of PCSK9 in the brain and its effect on brain LDLR levels has not been extensively studied. In the developing mouse brain, PCSK9 deletion has been shown to increase LDLR levels and decrease apoE levels (Rousselet et al., 2011). However, two studies have shown that adult PCSK9$^{-/-}$ mice do not have changes in brain LDLR levels (Liu et al., 2010; Rousselet et al., 2011). Interestingly, PCSK9$^{-/-}$ mice have been shown to have increased levels of mouse Aβ in the brain due to increased levels of the enzyme beta-site APP cleaving enzyme 1 (BACE1) that cleaves the amyloid precursor protein (APP) to produce Aβ (Jonas et al., 2008). In the preliminary data described in this chapter, we have evaluated in our hands the levels of LDLR and apoE in the brains of PCSK9$^{-/-}$ mice. We also crossed the PCSK9$^{-/-}$ mice to an APP transgenic mouse model to evaluate the effect of PCSK9 deletion on Aβ deposition in the brain.

Experimental Procedures

Mouse breeding - APPswe/PSEN1ΔE9 (APP/PS1) transgenic mice were bred with PCSK9$^{-/-}$ mice (purchased from Jackson Labs, Bar Harbor, ME) (Rashid et al., 2005) to

generate mice that were APP/PS1$^{+/-}$PCSK9$^{+/-}$. The APP/PS1$^{+/-}$ PCSK9$^{+/-}$ mice were then bred to PCSK9$^{+/-}$ mice to produce mice of the following genotypes used in the experiments: APP/PS1/PCSK9$^{+/+}$, APP/PS1/PCSK9$^{+/-}$, and APP/PS1/PCSK9$^{-/-}$. All experiments were approved by the animal studies committee of Washington University School of Medicine.

Quantitative analyses of amyloid deposition - Brain hemispheres from 7-month-old mice were placed in 30% sucrose prior to freezing and cutting on a freezing sliding microtome. Serial coronal sections of the brain at 50 μm intervals were collected using the rostral (anterior commissure) to the caudal edge of the hippocampus as landmarks. Sections were stained with biotinylated Aβ (HJ3.4) antibody to detect Aβ in the brain, or X-34 dye to detect fibrillar amyloid. All stained brain sections were scanned using a NanoZoomer slide scanner. The scanned images of sections stained with Aβ antibody were then converted to grayscale and exported using NDP viewer software. These exported images were set at a threshold to highlight plaques and then the cortex and hippocampus were analyzed by the "Analyze Particles" function in the Image J software. The particles identified as plaques by the program were individually inspected to verify whether the particle was a plaque or not. The X-34 stained sections were converted to grayscale and exported using ACDSee Pro 2 software. These exported images were also set at a threshold to highlight fibrillar plaques and quantified in a similar manner to the Aβ antibody stained sections. Three brain sections per mouse, each separated by 300 microns, were used for quantification. The average of the results from three sections was

used to represent plaque load for each mouse. For analysis of Aβ plaque in the cortex, the cortex immediately dorsal to the hippocampus was assessed. All analyses were performed in a blinded manner. Our sample size for the Aβ (HJ3.4) and X-34 staining were as follows: n=7 APP/PS1/PCSK9$^{+/+}$ males, n=8 APP/PS1/PCSK9$^{-/-}$ males, n=6 APP/PS1/PCSK9$^{+/+}$ females, and n=11 APP/PS1/PCSK9$^{-/-}$ females.

ELISA to measure brain apoE and Aβ levels - A sequential tissue extraction was performed on cortical brain hemispheres from 7-month-old mice. The brains were sequentially homogenized with PBS, modified RIPA buffer (Millipore, USA), and 5M Guanidine HCl in the presence of a protease inhibitor mixture (Roche, USA). The levels of Aβ and apoE were measured using sandwich enzyme-linked immunosorbent assays (ELISA). For the Aβ ELISA, HJ2 (Aβ35-40) and HJ7.4 (Aβ37-42) were used as the capture antibodies and HJ5.1-biotin (Aβ13-28) was used as the detection antibody. HJ6.2 and HJ6.3-biotin were used as the capture and detection antibodies, respectively, for the apoE ELISA. Sample sizes for the ELISAs were as follows: 4 APP/PS1/PCSK9$^{+/+}$ males, 2 APP/PS1/PCSK9$^{-/-}$ males, 5 APP/PS1/PCSK9$^{+/+}$ females, and 8 APP/PS1/PCSK9$^{-/-}$ females.

Immunoblot detection of PCSK9 and LDLR levels – Brain tissue was lysed by the addition of RIPA buffer (1% NP-40, 1% sodium deoxycholate, 0.1% SDS, 25 mM Tris-HCl, 150 mM NaCl) followed by sonication (2 rounds of 20-1 sec pulses). The lysates were then spun down at 14,000 rpm for 20 minutes and the supernatant was collected.

Protein concentration was determined by bicinchoninic acid (BCA) protein assay. Equal amounts of protein for each sample were run on 4-12% Bis-Tris XT gels and transferred to polyvinylidene fluoride (PVDF) membranes (0.45 μm pore size). All membranes were then blocked in 5% milk in TBS-T (tris-buffered saline with 0.125% Tween-20). Blots were probed for LDLR (Novus Cat#NB110-57162 and MBL Cat#JM3839-100) and PCSK9 (R&D Systems). Protein signal from the membranes was measured using the Lumigen TMA-6 ECL detection kit (Lumigen, USA).

Statistics - All data are presented as mean ±standard error of the mean (SEM) unless otherwise noted. Statistical significance (*$p<0.05$, **$p<0.01$, ***$p<0.001$) was determined using GraphPad Prism Software using a two-tailed student's t-test.

Results

PCSK9 deletion does not affect LDLR and apoE levels in the brain. In the mouse liver, PCSK9 deletion has previously been shown to cause a significant increase in the level of LDLR (Rashid et al., 2005). To determine whether PCSK9 deletion exerts a similar effect in the brain, we measured LDLR levels by immunoblot in the brains of both $PCSK9^{+/+}$ and $PCSK9^{-/-}$ mice (Fig. 5.1A). In the brain cortex, we observed no differences in the LDLR levels between $PCSK9^{+/+}$ and $PCSK9^{-/-}$ mice. Similar to previous studies, LDLR levels were increased in the livers of $PCSK9^{-/-}$ mice. Somewhat surprisingly, we could not detect any PCSK9 protein in the brain via immunoblot analysis (Fig. 5.1A). Whether PCSK9 protein is present at a level below the sensitivity of this assay or PCSK9

protein is not expressed in the brain cortex is currently unknown. We also measured apoE levels in both the plasma (Fig. 5.1B) and brain cortex (Fig. 5.1C) of the PCSK9$^{+/+}$ and PCSK9$^{-/-}$ mice. In the plasma, apoE levels were significantly decreased in the PCSK9$^{-/-}$ mice, likely due to the increased amount of LDLR. However, PCSK9 deletion had no effect on the amount of apoE present in the brain. Therefore, these results confirm that PCSK9 deletion does not alter LDLR levels in the mouse brain.

PCSK9 deletion decreases Aβ and amyloid deposition in the mouse brain. Despite the fact that the amount of PCSK9 had no effect on LDLR levels in the brain, we decided to analyze the effect of PCSK9 deletion on Aβ deposition in the brain. The possibility still remained that PCSK9 could affect Aβ through an LDLR-independent mechanism, such as through modulation of BACE1 levels has had previously been shown (Jonas et al., 2008). We bred APP/PS1 mice with PCSK9$^{-/-}$ mice to generate APP/PS1/PCSK9$^{+/+}$ and APP/PS1/PCSK9$^{-/-}$ mice. The extent of Aβ deposition was analyzed by both histochemical and biochemical methods. We analyzed male and female mice as separate groups because of previously noted differences between sex in the amount of Aβ deposition (Kim et al., 2009b). Brain sections from 7-month old APP/PS1/PCSK9$^{+/+}$ and APP/PS1/PCSK9$^{-/-}$ mice were immunostained with biotinylated-HJ3.4 antibody (anti-Aβ 1-16) (Fig. 5.2A). Quantitative analyses of anti-Aβ immunostaining demonstrated that the amount of Aβ deposition was significantly decreased in both the cortex (Fig. 5.2B) and hippocampus (Fig. 5.2C) of female mice. The inhibitory effect of PCSK9 deletion on Aβ

deposition was not statistically significant in male mice, though a trend toward decreased Aβ accumulation was observed.

To determine the effect of PCSK9 deletion on fibrillar amyloid deposition, brain sections were stained with X-34 dye (Fig. 5.3A). Similar to the Aβ immunostaining results, female APP/PS1/PCSK9$^{-/-}$ mice had significantly decreased levels of X-34-positive fibrillar plaque load in both the cortex (Fig. 5.3B) and hippocampus (Fig. 5.3C). Male APP/PS1/PCSK9$^{-/-}$ mice had statistically significant decreased levels of X-34-positive fibrillar plaque load in the cortex (Fig. 5.3B), but not the hippocampus (Fig. 5.3C). Biochemical analyses of cortical Aβ levels demonstrated a trend toward a reduction in insoluble Aβ40 levels (Fig. 5.4A) and insoluble Aβ42 levels (Fig. 5.4B) with PCSK9 deletion. However, the decrease was only significant for insoluble Aβ40 levels in male mice. The reason for the discrepancy in the differences between Aβ deposition between genotypes and the lack of a strong difference in the biochemical analysis is unknown. In summary, PCSK9 deletion causes a significant reduction in the extent of Aβ deposition and amyloid load in female APP/PS1/PCSK9$^{-/-}$ mice, and a trend toward a reduction in male APP/PS1/PCSK9$^{-/-}$ mice.

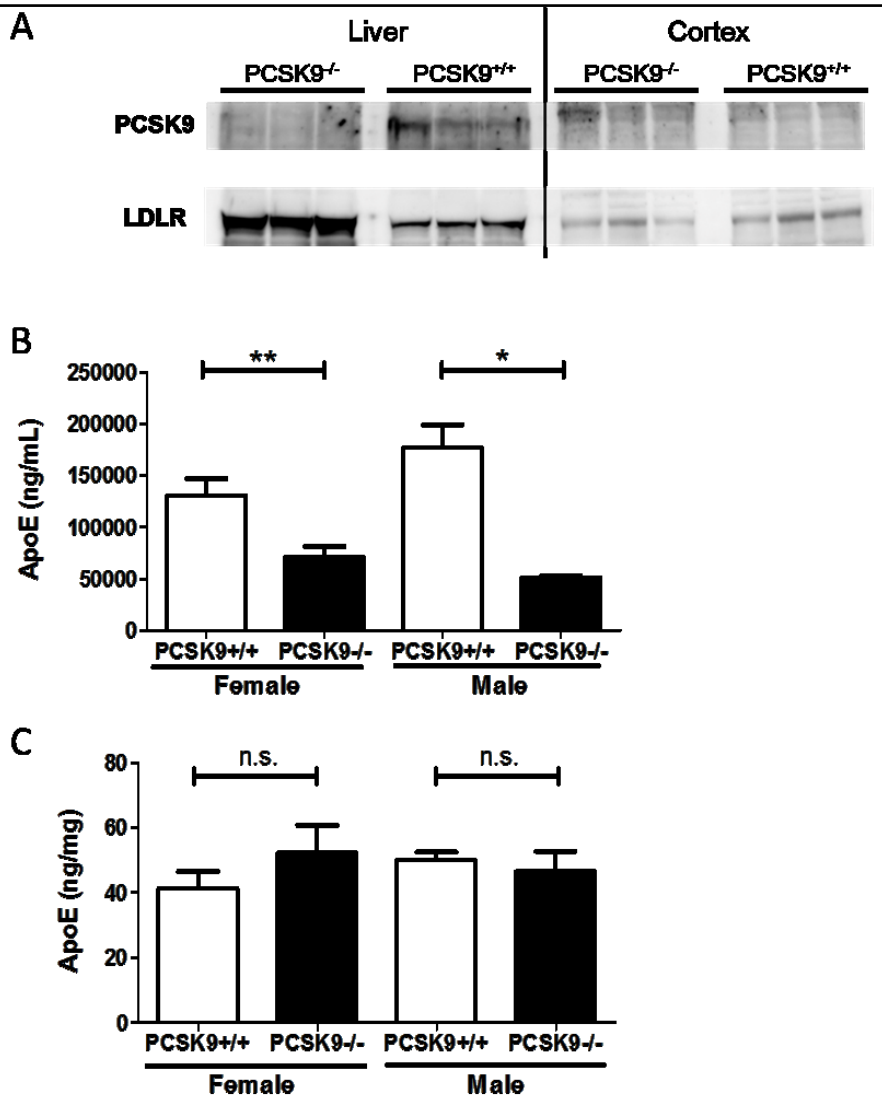

Fig. 5.1. LDLR and apoE levels in the brain and periphery of PCSK9$^{-/-}$ mice. **(A)** PCSK9 and LDLR levels were measured in the liver and brain cortex by immunoblot. The levels of apoE were measured in the **(B)** plasma and **(C)** cortex via ELISA. Mean ± SEM * denotes $p<0.05$, ** denotes $p<0.01$, n.s. not significant

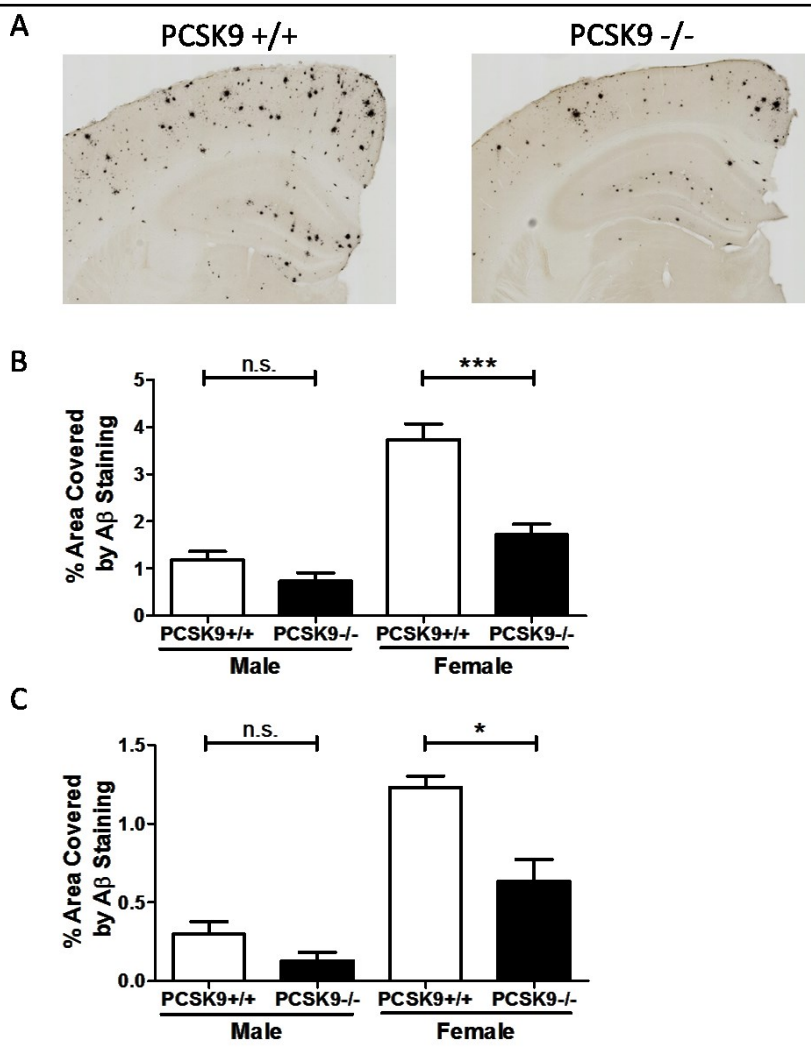

Fig. 5.2. Effect of PCSK9 deletion on Aβ deposition. (**A)** $PCSK9^{+/+}$ and $PCSK9^{+/-}$ brain sections were stained with an anti-Aβ antibody. The % area covered by Aβ staining was quantified for both the (**B)** cortex and **(C)** hippocampus of male and female mice. The representative images shown are from female mice. Mean ± SEM * denotes $p<0.05$, *** denotes $p<0.001$, n.s. not significant

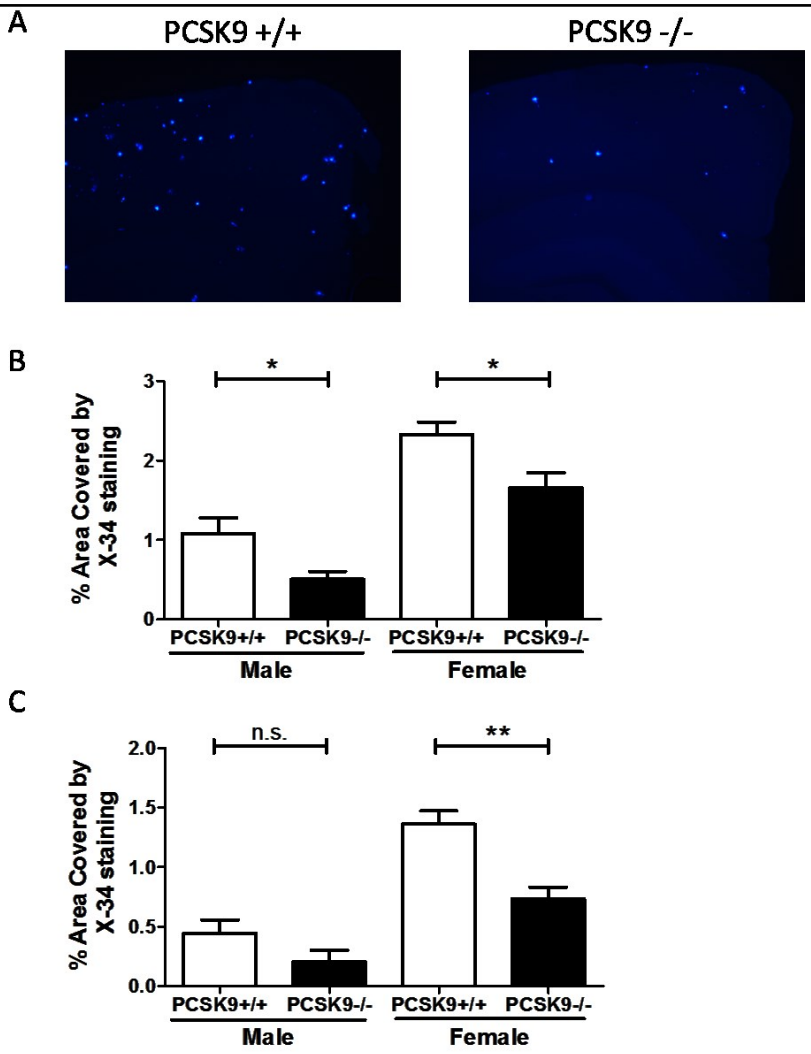

Fig. 5.3. Effect of PCSK9 deletion on amyloid deposition. (**A)** $PCSK9^{+/+}$ and $PCSK9^{+/-}$ brain sections were stained with X-34 to detect amyloid plaques. The % area covered by X-34 staining was quantified for both the (**B)** cortex and **(C)** hippocampus of male and female mice. The representative images shown are from female mice. Mean ± SEM * denotes $p<0.05$, *** denotes $p<0.001$, n.s. not significant

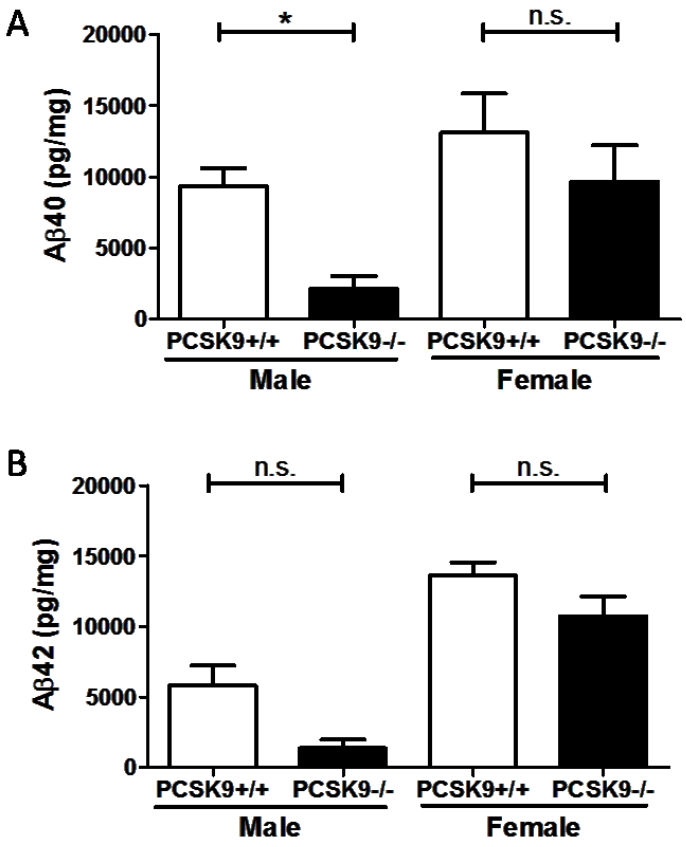

Fig. 5.4. Effect of PCSK9 deletion on Aβ levels in the brain. Insoluble cortex Aβ levels were measured in the guanidine tissue lysate using (**A)** Aβ40 and **(B)** Aβ42 ELISA's. Mean ± SEM * denotes $p<0.05$, n.s. not significant

Discussion and Future Directions

Since the accumulation of Aβ in the brain has been hypothesized to be one of the primary pathogenic events in AD (Hardy and Selkoe, 2002), significant effort has been devoted to understanding the molecular pathways that modulate Aβ clearance from the brain. We have previously demonstrated that increasing the expression of LDLR in the mouse brain significantly decreased the amount of Aβ deposition and amyloid load (Kim et al., 2009b). Therefore, identifying methods of promoting the expression of LDLR or inhibiting the degradation of LDLR in the brain represents a potential means of lowering Aβ levels. PCSK9 is a protein that has been shown to directly promote LDLR degradation, and for this reason has been the focus of attention for developing therapeutics to lower peripheral cholesterol levels (Horton et al., 2009). However, the effect of PCSK9 on LDLR in the brain has not been extensively studied. In this chapter, we analyzed the effect of PCSK9 deletion on brain LDLR and apoE levels. We also crossed PCSK9$^{-/-}$ mice with an APP transgenic mouse model to analyze the effect of PCSK9 levels on Aβ deposition in the brain. We hypothesized that PCSK9$^{-/-}$ mice would have increased LDLR levels, and as a result the amount of Aβ deposition would decrease.

Our preliminary studies suggest that PCSK9 does not regulate LDLR or apoE levels in the mouse brain. While we observed an increase in liver LDLR levels and decrease in plasma apoE levels in PCSK9$^{-/-}$ mice, brain LDLR and apoE levels did not change. These results are similar to the findings published previously by two other groups (Liu et al., 2010; Rousselet et al., 2011). Despite no observed effect on brain LDLR levels, PCSK9 deletion decreased both Aβ deposition and amyloid plaque load in female

mice. The mechanism underlying this observation is currently unclear, but it still may occur through the effect of PCSK9 on LDLR. A previous study has shown that in the ischemic stroke mouse model, PCSK9 levels are upregulated in the dentate gyrus while hippocampal LDLR levels decrease (Rousselet et al., 2011). The decrease in LDLR levels is attenuated in mice that lack PCSK9. A similar effect could be occurring in mice with Aβ deposition, leading to a local increase in PCSK9 and decrease in LDLR levels in the vicinity of Aβ plaques and ultimately resulting in impaired clearance of Aβ. With PCSK9 deletion, the effect of Aβ deposition on LDLR levels may be attenuated. Further experiments could look at the levels of PCSK9 and LDLR in regions surrounding plaque deposition. It is also possible that PCSK9 may effect Aβ deposition in the brain through its effect on peripheral apoE levels. The role of peripheral apoE in central nervous system Aβ clearance has not been thoroughly evaluated. The possibility exists that peripheral apoE can regulate brain Aβ levels and amyloidosis by influencing plasma Aβ clearance. However, this has yet to be tested experimentally. Therefore, further work is needed to determine what role peripheral apoE levels have on CNS Aβ levels and pathology.

PCSK9 could also regulate Aβ deposition through an LDLR-independent mechanism. PCSK9 has been shown to facilitate the degradation of BACE1 in both cell culture and the mouse brain (Jonas et al., 2008). Though we have yet to measure BACE1 levels in the APP/PS1/PCSK9$^{-/-}$ mice, the effect of PCSK9 on decreasing BACE1 levels would predict higher Aβ levels in the PCSK9$^{-/-}$ mouse brain. Since we observed lower levels of Aβ deposition, the BACE1 mechanism likely is not responsible for our results. Another possibility is that PCSK9 regulates the levels of other LDLR family members in

the brain. A previous study has shown that PCSK9 also facilitates the degradation of VLDLR and ApoER2 (Poirier et al., 2008). However, it is not yet known whether either of these receptors modulates Aβ levels in the mouse brain. Finally, it is possible that the effect of PCSK9 on Aβ deposition is due to an effect on an unidentified target of PCSK9. For instance, several recent studies have shown via microarray technology that PCSK9 affects the expression of genes in multiple cellular pathways, including the unfolded protein response, inflammation and stress response, and protein ubiquitination (Lan et al., 2010; Ranheim et al., 2008). Therefore, further studies are necessary in the mouse brain to identify novel targets of PCSK9 that may influence the extent of Aβ degradation in the brain.

Chapter 6

Conclusions and Future Directions

Summary

The initial description and evolution of the amyloid cascade hypothesis as an underlying factor in AD pathogenesis has spurred extensive research to characterize the factors involved in Aβ homeostasis in the brain. In particular, significant effort has been devoted to defining the molecular and systemic pathways that modulate Aβ clearance from the brain. Significant evidence exists from both cellular and animal models that the isoform of apoE and the amount of apoE in the brain influence both the extent of Aβ aggregation and its metabolism (Kim et al., 2009a). Therefore, understanding how apoE levels are modulated in the brain will further elucidate the mechanisms underlying Aβ clearance and identify novel therapeutic targets. Receptors for apoE (such as LDLR) and proteins that influence apoE lipidation status (such as ABCA1) both have been shown to affect Aβ levels and deposition in the brain. In this thesis work, we have analyzed how the modulation of LDLR and ABCA1 levels alters the clearance of apoE and Aβ at a cellular and systemic level.

In chapter two, we demonstrated that the amount of LDLR in astrocytes regulates the extent of Aβ uptake and degradation. We showed that increasing LDLR levels in primary astrocytes increased both the uptake and clearance of Aβ, while deletion of LDLR impaired the uptake of Aβ. Overexpression of LDLR also enhanced the cellular degradation of Aβ and facilitated the vesicular transport of Aβ to lysosomes. The increased Aβ uptake and clearance in the setting of LDLR overexpression occurred even in the absence of apoE, suggesting an apoE-independent effect of LDLR on Aβ. Finally,

we provided evidence that Aβ can directly bind to LDLR, suggesting LDLR-mediated Aβ uptake could occur through an interaction between LDLR and Aβ.

In the third chapter, we described a novel method to measure the kinetics of proteins in the brain using stable isotope labeling coupled with mass spectrometry. In this technique, we pulse labeled various cohorts of mice with $^{13}C_6$-leucine and isolated the brains after pre-determined time points. We then measured the extent of $^{13}C_6$-leucine incorporation in the brain tissue lysate over time using mass spectrometry to measure the ratio of labeled to unlabeled protein. The fractional clearance rate was then calculated by analyzing the time course of disappearance for the labeled protein. We validated this technique by demonstrating that the clearance of apoE is enhanced in the brains of mice overexpressing LDLR. We also applied this technique to measure the clearance of the apoE isoforms from the brains of the human apoE targeted-replacement mice. No significant differences in the fractional clearance rate were measured between the isoforms, though there was a trend for apoE4 being cleared more slowly than apoE2 and apoE3.

In the experiments in chapter 4, we used our stable isotope labeling kinetics technique to analyze the effect of ABCA1 levels on the clearance of apoE and Aβ from the mouse brain. We observed that the fractional clearance rate of apoE was increased 1.9- and 1.5- fold in mice that either lacked or overexpressed ABCA1, respectively. Both ABCA1 deletion and overexpression also decreased the total amount of apoE protein in the brain. To measure the effect of ABCA1 levels on Aβ clearance, we crossed PDAPP transgenic mice with either ABCA1$^{-/-}$ mice or ABCA1 transgenic mice. After labeling the

mice with $^{13}C_6$-leucine, we observed that ABCA1 levels had no effect on the FCR or production rate of Aβ, suggesting that ABCA1 does not regulate Aβ metabolism in the brain.

Finally, in the fifth chapter we describe preliminary studies analyzing the effect of PCSK9 levels on the amount of LDLR and Aβ deposition in the brain. We found that deletion of PCSK9 increased LDLR levels and decreased apoE levels in the periphery, but had no effect on LDLR and apoE levels in the brain. However, we did observe that PCSK9 deletion decreased the amount of Aβ deposition and amyloid load in the mouse brain through a mechanism that has yet to be defined.

Cellular degradation of Aβ *in vivo* and the role of LDLR

Though cells in culture have been shown to endocytose and degrade Aβ, the role of cellular degradation in the clearance of Aβ in the brain remains unclear. Two approaches have been taken to study the potential ability of cells to degrade Aβ *in vivo*. One approach has been to ablate a whole population of cells and analyze the effect on Aβ levels and deposition in the brain. This approach has primarily been used to study the ability of microglia to degrade soluble and fibrillar Aβ. By treating mice that express the thymidine kinase (TK) of herpes simplex virus under the *CD11b* promoter with ganciclovir, it is possible to selectively ablate all microglial cells in the brain. The *CD11b*-TK mice have been crossed with APP transgenic mouse models to analyze the effect of microglia on Aβ deposition (Grathwohl et al., 2009; Simard et al., 2006). Somewhat surprisingly, the results from these studies have suggested that resident

microglia in the brain play little to no role in modulating brain Aβ deposition, as Aβ levels do not change when microglia are absent. Another approach has been to manipulate specific enzymes that function in cellular degradation, such as those in the endolysosomal pathway. For instance, genetic deletion of the lysosomal protein cathepsin B has been shown to increase Aβ levels and worsen plaque pathology while overexpression of cathepsin B reduced plaques (Mueller-Steiner et al., 2006; Sun et al., 2008). However, in these studies it is difficult to attribute the effect of cathepsin B solely to intracellular Aβ degradation because cathepsin B is also secreted into the extracellular environment and is present within amyloid plaques. Therefore, new approaches are needed that solely alter cellular degradation pathways in order to definitively determine whether cellular clearance pathways alter Aβ pathology *in vivo*.

Despite evidence of extensive astrogliosis in the AD brain, the role of astrocytes in the cellular degradation of Aβ and clearance of Aβ deposits *in vivo* is unknown. The likely reason for this is the lack of animal models that have increased or decreased astrocytic function. Similar to microglia, attempts have been made to ablate the astrocyte population *in vivo* using ganciclovir treatment of mice expressing TK under the astrocyte-specific *GFAP* promoter (Bush et al., 1999; Bush et al., 1998). However, since the effect of ganciclovir treatment requires cell division, the loss of astrocytes in this model was minimal and only occurred following tissue injury. Another approach has been to target specific proteins that are upregulated in astrocytes following injury, such as vimentin, glial fibrillary acidic protein (GFAP), and signal transducer and activator of transcription 3 (STAT3). In both a vimentin/GFAP double knockout mouse and a STAT3 astrocyte-

specific knockout mouse (Herrmann et al., 2008; Okada et al., 2006; Pekny et al., 1999), the ability of astrocytes to respond to injury was impaired. However, the effect on brain Aβ levels and deposition when these proteins are deleted in the astrocytes of APP-transgenic mice has yet to be described.

Rather than targeting cellular function as a whole, a more feasible method of analyzing the ability of cells to degrade Aβ *in vivo* would be to target pathways that specifically play a role in Aβ uptake and degradation. Since we have shown in chapter 2 that LDLR functions in the uptake of Aβ by astrocytes in culture, it would be interesting to determine if selectively overexpressing or deleting LDLR in astrocytes plays a role in regulating Aβ levels and deposition in the brain. LDLR could be selectively overexpressed in astrocytes in the mouse brain using either a transgene or virus with a *GFAP* promoter. Selective deletion of LDLR could be achieved in mice by crossing mice expressing the Cre recombinase under a *GFAP* promoter to mice expressing a floxed construct of LDLR. In both cases, it would be ideal to manipulate LDLR levels in apoE$^{-/-}$ mice to avoid the confounding effect of changes in apoE levels. If astrocyte-specific alteration of LDLR levels in the setting of apoE deletion alters Aβ deposition or clearance, it would strongly suggest that LDLR facilitates the cellular degradation of Aβ *in vivo*.

Role of LDLR in other modes of Aβ clearance

Though we have hypothesized that LDLR affects Aβ levels in the brain by facilitating its cellular degradation, LDLR may also function in other pathways of Aβ

clearance. LDLR may facilitate the transport of Aβ across the blood-brain-barrier (BBB), as has been shown for LRP1 (Deane et al., 2004; Shibata et al., 2000). This could be assessed both *in vitro* and in the mouse brain. The ability of LDLR to facilitate Aβ endocytosis and clearance by brain endothelial cells could be assessed by measuring the uptake and degradation of Aβ by mouse brain capillary preparations isolated from LDLR transgenic and knock-out brains. LDLR-mediated clearance across the BBB could also be assessed in LDLR transgenic and knockout mice brains by measuring the transcytosis of a labeled form of Aβ from the brain to the blood, as has been done before for I^{125}-labeled Aβ (Shibata et al., 2000). It is important to emphasize that astrocytes are one of the main cell types that make up the BBB, and as such, they could play a role in both the cellular degradation of Aβ and its clearance across the BBB.

It is also possible that LDLR regulates Aβ deposition in the brain by facilitating Aβ clearance in the periphery. Several studies have suggested that brain Aβ levels are altered by regulating the amount of Aβ-binding proteins in the plasma, which act as an Aβ sink (DeMattos et al., 2001a; Matsuoka et al., 2003; Sagare et al., 2007). However, the ability of peripheral proteins to function as Aβ sinks remains controversial. Peripherally injected Aβ-binding proteins may enter the brain (Yamada et al., 2009), and as such it is not easy to determine whether differences in brain Aβ levels are due to altered stability of Aβ due to binding to the injected protein, or actual differences in Aβ clearance. Despite these issues, the possibility remains that a dynamic equilibrium exists between plasma and brain Aβ levels, and through regulating peripheral Aβ levels the amount of Aβ clearance in the brain may be altered. In terms of LDLR, this hypothesis

could be tested by crossing mice that overexpress LDLR selectively in the liver (Pathak et al., 1990) with APP transgenic mice. In these mice, LDLR should only regulate Aβ clearance from the plasma. If brain Aβ levels and plaque loads are decreased with liver-specific LDLR overexpression, it would suggest that peripheral LDLR or its effect on plasma apoE levels could regulate brain Aβ deposition.

Effect of apoE on LDLR:Aβ interaction

Another major question that remains to be addressed is to what extent apoE modulates Aβ binding to apoE receptors, and how this modulation affects Aβ uptake into cells. Though our experiments in chapter 2 demonstrate that LDLR regulates soluble Aβ uptake and clearance in an apoE-independent manner, apoE may still have a role in the receptor-mediated uptake of Aβ. For instance, apoE has been shown to directly interact with the Aβ peptide in culture and in the brain (LaDu et al., 1994; Namba et al., 1991; Strittmatter et al., 1993b; Tokuda et al., 2000; Wisniewski et al., 1993). Whether soluble Aβ bound to apoE is endocytosed to a greater or lesser extent than free Aβ by apoE receptors remains unknown. For instance, if the clearance of Aβ through an apoE/Aβ complex is more efficient than the pathways involved in the clearance of unbound Aβ, apoE will promote Aβ clearance. Further studies are needed in culture to determine the rates of Aβ clearance when it is unbound and bound to apoE, and how each of the apoE receptors influences Aβ clearance in these different states.

Since Aβ has been shown to bind to both LDLR and LRP1, it is also possible that apoE could compete with free Aβ for binding to these receptors. A previous study has

shown that Aβ competes with apoE-containing VLDL particles for receptor-mediated endocytosis in human skin fibroblasts (Winkler et al., 1999). However, the specific receptors involved in this competition were not defined. If this competition occurred *in vivo*, more apoE in the brain would likely impair the clearance of Aβ via LDLR and LRP1 and lead to accumulation of Aβ in the brain. Results from the genetic manipulation of apoE in mice support this possibility, as increased amounts of apoE led to increased levels of Aβ deposition in the brain (Bales et al., 1999; Bales et al., 1997; Kim et al., 2011). In the future, competition experiments between apoE and Aβ for binding to both LDLR and LRP1 could be performed in both cell-free conditions and in the setting of a cellular membrane. By demonstrating that apoE impairs the ability of Aβ to co-immunoprecipitate with LDLR or LRP1, this would suggest that apoE impairs the ability of Aβ to bind to these receptors. It would also be interesting to determine whether increasing levels of apoE abrogates the effect of LDLR overexpression on Aβ uptake and clearance by primary astrocytes.

If apoE does compete with Aβ for binding to LDLR or LRP1, it would be illuminating to determine if there is an isoform-dependent difference in the ability of apoE to compete with Aβ. ApoE has been shown to bind to LDLR in an isoform-specific manner, with apoE2 having a much weaker binding than apoE3 and apoE4 (Weisgraber et al., 1982). As a result, apoE2 would theoretically be a much weaker competitor for Aβ binding to LDLR than apoE3 and apoE4, and consequently impair LDLR-mediated Aβ uptake to a much lesser extent than apoE3 and apoE4. This could in part explain the lower Aβ deposition in the brains of APP-transgenic mice that express human apoE2

versus apoE3 and apoE4 (Bales et al., 2009; Fagan et al., 2002), and in humans with the apoE2 allele (Morris et al., 2010). The amount of LDLR could also be important in determining whether apoE and Aβ compete for binding. For instance, when LDLR is sufficiently expressed there may be little competition of apoE and Aβ for binding to LDLR. However, when LDLR levels decrease the level of competition may increase and apoE may impair Aβ uptake. Interestingly, a recent study has shown that the amount of LDLR in the brain decreases with age in rats (Segatto et al., 2011). Therefore, if a similar phenomenon occurs in mice or humans, one hypothesis may be that the decrease in LDLR levels with age leads to greater competition between apoE and Aβ for binding to LDLR and impaired clearance of Aβ. Future studies should look at the levels of LDLR in the mouse and human brain at different ages.

LDLR, Idol, and LXR treatment

Two proteins that have been shown to play an important role in regulating the degradation of LDLR are PCSK9 and the inducible degrader of LDLR (Idol). Our preliminary data presented in chapter 5 suggest that PCSK9 does not regulate LDLR levels in the brain. The function of Idol in the brain has yet to be defined. Idol is an E3 ubiquitin ligase that is activated by the sterol-sensitive liver X receptors (LXRs) and ubiquitinates LDLR in order to target it for degradation (Scotti et al., 2011; Zelcer et al., 2009). Idol levels are upregulated following LXR activation, which leads to a decrease in LDLR levels (Zelcer et al., 2009). In cells that lack Idol, LDLR levels are significantly increased and the ability of LXR ligands to decrease LDLR levels is diminished (Scotti et

al., 2011). Inhibition of the Idol pathway therefore represents an attractive therapeutic target for increasing LDLR levels.

Future experiments should address whether Idol can regulate LDLR levels in the brain. Mice could first be treated with LXR agonists to determine if LDLR is down regulated, and Idol levels in the brain could be assessed. Viral-mediated expression of Idol in the brain could then be used to determine if increasing Idol levels in the brain decreases LDLR. If Idol does regulate brain LDLR levels, its function in the mouse brain could be deleted by making a knock-out mouse or decreased by knocking-down the *IDOL* gene via viral-delivered shRNA. Assuming LDLR levels increase with Idol deletion, the $Idol^{-/-}$ mice could be crossed with APP transgenic mice to analyze the effect of Idol deletion on Aβ levels and deposition in the mouse brain. One would hypothesize that Idol deletion would decrease Aβ plaque load due to the LDLR upregulation.

Since ABCA1 and apoE are transcriptionally upregulated by LXR (Beaven and Tontonoz, 2006), synthetic LXR ligands have attracted attention for their potential use as AD therapeutics. Animal studies have shown that treatment with various synthetic LXR agonists decreases Aβ and plaque levels. In young APP transgenic mice that do not yet exhibit Aβ deposition, treatment with the LXR agonist TO901317 led to a decrease in the levels of Aβ40 (Koldamova et al., 2005b) and Aβ42 (Koldamova et al., 2005b; Riddell et al., 2007). Treatment of APP transgenic mice with the LXR agonist GW3965 for 4 months at an age in which plaque deposition has occurred led to a significant decrease in plaque numbers along with Aβ40 and Aβ42 levels (Jiang et al., 2008). Since LXR upregulation also decreases LDLR levels via the Idol pathway, this effect may lessen the

ability of LXR agonists to decrease Aβ levels. Therefore, a valuable follow-up to these studies would be to treat APP mice that lack Idol and see if the effects of LXR agonists on Aβ pathology are enhanced.

ApoE levels and the effect on Aβ pathology

The issue of whether more or less apoE is beneficial in decreasing brain Aβ levels remains an important issue, since targeting apoE levels is an attractive therapeutic approach for treating AD. Results from the genetic manipulation of apoE levels in mice suggested that increasing apoE levels leads to more Aβ deposition in the brain (Bales et al., 1999; Bales et al., 1997; Holtzman et al., 2000b; Kim et al., 2011). However, treatment of mice with drugs that increase apoE levels, such as LXR agonists and the retinoid X receptor (RXR) agonist bexarotene, decreased Aβ levels and amyloid deposition in the brain (Cramer et al., 2012; Jiang et al., 2008). The reason for this discrepancy is unclear. The genetic studies have the caveat that apoE levels are different from birth, which could have other effects that modulate brain Aβ levels (such as altered membrane cholesterol content). In the pharmacologic upregulation of apoE, it is difficult to solely attribute the effect of the drugs to their effect of apoE levels due to multiple targets. Future experiments could more definitively demonstrate whether apoE levels are beneficial for decreasing Aβ levels by decreasing apoE levels in adult mice. ApoE2, apoE3, or apoE4 targeted-replacement mice could be altered such that the apoE locus is flanked by lox sites. These mice could then be crossed to inducible Cre mice and APP transgenic mice, and the levels of apoE could be decreased in adult mice both prior to and

after the onset of plaque deposition. ApoE levels in APP transgenic mice could also be decreased using RNA interference or increased via viral transduction. In either case, the changes in Aβ levels and deposition after decreasing apoE levels in these models would definitively demonstrate whether less apoE is beneficial for Aβ pathology and a target for future therapies.

Finally, the mechanism by which the amount of human apoE affects Aβ deposition remains to be determined. Solid evidence exists that the human apoE isoforms differentially modulate Aβ clearance from the brain (Castellano et al., 2011; Deane et al., 2008). However, whether altering human apoE levels in the brain affects Aβ clearance has not directly been tested. Our SILK technique could be applied to address this issue in the mouse brain. Aβ clearance rates could be measured in both homozygous and hemizygous human apoE targeted-replacement mice crossed to an APP transgenic mouse line. Regardless of the results from this experiment, it is important to emphasize that apoE levels may also affect Aβ deposition by directly altering the propensity for Aβ to aggregate and form fibrillar structures.

Concluding Remarks

The work presented in this thesis adds to the growing body of knowledge demonstrating that proteins that influence apoE levels and function in the brain play an important role in the pathogenesis of AD. We show for the first time that LDLR modulates the cellular metabolism of Aβ by glial cells. We also provided evidence that LDLR can directly interact with Aβ, a finding that could potentially be exploited for the

design of therapeutics that target Aβ clearance in the brain. We have also described a stable isotope labeling method that can be used to measure the turnover of proteins in the mouse brain. We used this technique to analyze the kinetics of both mouse and human apoE in the mouse brain for the first time, and demonstrated that both LDLR and ABCA1 levels alter apoE clearance. We also demonstrated that the levels of the protein ABCA1 do not regulate the clearance of Aβ from the mouse brain. This technique will be of value for future studies attempting to elucidate the mechanisms underlying the pathogenesis of both AD and other neurodegenerative disease, and also for characterizing the efficiency of therapeutics that target protein turnover in the brain.

References

Abifadel, M., Varret, M., Rabes, J.P., Allard, D., Ouguerram, K., Devillers, M., Cruaud, C., Benjannet, S., Wickham, L., Erlich, D.*, et al.* (2003). Mutations in PCSK9 cause autosomal dominant hypercholesterolemia. Nat Genet *34*, 154-156.

Abramowski, D., Wiederhold, K.H., Furrer, U., Jaton, A.L., Neuenschwander, A., Runser, M.J., Danner, S., Reichwald, J., Ammaturo, D., Staab, D.*, et al.* (2008). Dynamics of Abeta turnover and deposition in different beta-amyloid precursor protein transgenic mouse models following gamma-secretase inhibition. J Pharmacol Exp Ther *327*, 411-424.

Aebersold, R., and Mann, M. (2003). Mass spectrometry-based proteomics. Nature *422*, 198-207.

Akanuma, S., Ohtsuki, S., Doi, Y., Tachikawa, M., Ito, S., Hori, S., Asashima, T., Hashimoto, T., Yamada, K., Ueda, K.*, et al.* (2008). ATP-binding cassette transporter A1 (ABCA1) deficiency does not attenuate the brain-to-blood efflux transport of human amyloid-beta peptide (1-40) at the blood-brain barrier. Neurochem Int *52*, 956-961.

Balch, W.E., Morimoto, R.I., Dillin, A., and Kelly, J.W. (2008). Adapting proteostasis for disease intervention. Science *319*, 916-919.

Bales, K.R., Liu, F., Wu, S., Lin, S., Koger, D., DeLong, C., Hansen, J.C., Sullivan, P.M., and Paul, S.M. (2009). Human APOE isoform-dependent effects on brain beta-amyloid levels in PDAPP transgenic mice. J Neurosci *29*, 6771-6779.

Bales, K.R., Verina, T., Cummins, D.J., Du, Y., Dodel, R.C., Saura, J., Fishman, C.E., DeLong, C.A., Piccardo, P., Petegnief, V.*, et al.* (1999). Apolipoprotein E is essential for amyloid deposition in the APP(V717F) transgenic mouse model of Alzheimer's disease. Proc Natl Acad Sci U S A *96*, 15233-15238.

Bales, K.R., Verina, T., Dodel, R.C., Du, Y., Altstiel, L., Bender, M., Hyslop, P., Johnstone, E.M., Little, S.P., Cummins, D.J.*, et al.* (1997). Lack of apolipoprotein E dramatically reduces amyloid beta-peptide deposition. Nat Genet *17*, 263-264.

Bamberger, M.E., Harris, M.E., McDonald, D.R., Husemann, J., and Landreth, G.E. (2003). A cell surface receptor complex for fibrillar beta-amyloid mediates microglial activation. J Neurosci *23*, 2665-2674.

Barten, D.M., Guss, V.L., Corsa, J.A., Loo, A., Hansel, S.B., Zheng, M., Munoz, B., Srinivasan, K., Wang, B., Robertson, B.J.*, et al.* (2005). Dynamics of {beta}-amyloid reductions in brain, cerebrospinal fluid, and plasma of {beta}-amyloid

precursor protein transgenic mice treated with a {gamma}-secretase inhibitor. J Pharmacol Exp Ther *312*, 635-643.

Bateman, R.J., Munsell, L.Y., Chen, X., Holtzman, D.M., and Yarasheski, K.E. (2007). Stable isotope labeling tandem mass spectrometry (SILT) to quantify protein production and clearance rates. J Am Soc Mass Spectrom *18*, 997-1006.

Bateman, R.J., Munsell, L.Y., Morris, J.C., Swarm, R., Yarasheski, K.E., and Holtzman, D.M. (2006). Human amyloid-beta synthesis and clearance rates as measured in cerebrospinal fluid in vivo. Nat Med *12*, 856-861.

Bateman, R.J., Siemers, E.R., Mawuenyega, K.G., Wen, G., Browning, K.R., Sigurdson, W.C., Yarasheski, K.E., Friedrich, S.W., Demattos, R.B., May, P.C.*, et al.* (2009). A gamma-secretase inhibitor decreases amyloid-beta production in the central nervous system. Ann Neurol *66*, 48-54.

Beaven, S.W., and Tontonoz, P. (2006). Nuclear receptors in lipid metabolism: targeting the heart of dyslipidemia. Annu Rev Med *57*, 313-329.

Beffert, U., Aumont, N., Dea, D., Lussier-Cacan, S., Davignon, J., and Poirier, J. (1998). Beta-amyloid peptides increase the binding and internalization of apolipoprotein E to hippocampal neurons. J Neurochem *70*, 1458-1466.

Beffert, U., Aumont, N., Dea, D., Lussier-Cacan, S., Davignon, J., and Poirier, J. (1999a). Apolipoprotein E isoform-specific reduction of extracellular amyloid in neuronal cultures. Brain Res Mol Brain Res *68*, 181-185.

Beffert, U., Cohn, J.S., Petit-Turcotte, C., Tremblay, M., Aumont, N., Ramassamy, C., Davignon, J., and Poirier, J. (1999b). Apolipoprotein E and beta-amyloid levels in the hippocampus and frontal cortex of Alzheimer's disease subjects are disease-related and apolipoprotein E genotype dependent. Brain Res *843*, 87-94.

Bekris, L.M., Millard, S.P., Galloway, N.M., Vuletic, S., Albers, J.J., Li, G., Galasko, D.R., DeCarli, C., Farlow, M.R., Clark, C.M.*, et al.* (2008). Multiple SNPs within and surrounding the apolipoprotein E gene influence cerebrospinal fluid apolipoprotein E protein levels. J Alzheimers Dis *13*, 255-266.

Bell, R.D., Sagare, A.P., Friedman, A.E., Bedi, G.S., Holtzman, D.M., Deane, R., and Zlokovic, B.V. (2007). Transport pathways for clearance of human Alzheimer's amyloid beta-peptide and apolipoproteins E and J in the mouse central nervous system. J Cereb Blood Flow Metab *27*, 909-918.

Benjannet, S., Rhainds, D., Essalmani, R., Mayne, J., Wickham, L., Jin, W., Asselin, M.C., Hamelin, J., Varret, M., Allard, D.*, et al.* (2004). NARC-1/PCSK9 and its

natural mutants: zymogen cleavage and effects on the low density lipoprotein (LDL) receptor and LDL cholesterol. J Biol Chem *279*, 48865-48875.

Bertram, L., McQueen, M.B., Mullin, K., Blacker, D., and Tanzi, R.E. (2007). Systematic meta-analyses of Alzheimer disease genetic association studies: the AlzGene database. Nat Genet *39*, 17-23.

Bertrand, P., Poirier, J., Oda, T., Finch, C.E., and Pasinetti, G.M. (1995). Association of apolipoprotein E genotype with brain levels of apolipoprotein E and apolipoprotein J (clusterin) in Alzheimer disease. Brain Res Mol Brain Res *33*, 174-178.

Blacklow, S.C. (2007). Versatility in ligand recognition by LDL receptor family proteins: advances and frontiers. Curr Opin Struct Biol *17*, 419-426.

Bodzioch, M., Orso, E., Klucken, J., Langmann, T., Bottcher, A., Diederich, W., Drobnik, W., Barlage, S., Buchler, C., Porsch-Ozcurumez, M.*, et al.* (1999). The gene encoding ATP-binding cassette transporter 1 is mutated in Tangier disease. Nat Genet *22*, 347-351.

Bolmont, T., Haiss, F., Eicke, D., Radde, R., Mathis, C.A., Klunk, W.E., Kohsaka, S., Jucker, M., and Calhoun, M.E. (2008). Dynamics of the microglial/amyloid interaction indicate a role in plaque maintenance. J Neurosci *28*, 4283-4292.

Brewer, H.B., Jr., Remaley, A.T., Neufeld, E.B., Basso, F., and Joyce, C. (2004). Regulation of plasma high-density lipoprotein levels by the ABCA1 transporter and the emerging role of high-density lipoprotein in the treatment of cardiovascular disease. Arterioscler Thromb Vasc Biol *24*, 1755-1760.

Brooks-Wilson, A., Marcil, M., Clee, S.M., Zhang, L.H., Roomp, K., van Dam, M., Yu, L., Brewer, C., Collins, J.A., Molhuizen, H.O.*, et al.* (1999). Mutations in ABC1 in Tangier disease and familial high-density lipoprotein deficiency. Nat Genet *22*, 336-345.

Brown, M.S., and Goldstein, J.L. (1986). A receptor-mediated pathway for cholesterol homeostasis. Science *232*, 34-47.

Burgess, B.L., Parkinson, P.F., Racke, M.M., Hirsch-Reinshagen, V., Fan, J., Wong, C., Stukas, S., Theroux, L., Chan, J.Y., Donkin, J.*, et al.* (2008). ABCG1 influences the brain cholesterol biosynthetic pathway but does not affect amyloid precursor protein or apolipoprotein E metabolism in vivo. J Lipid Res *49*, 1254-1267.

Bush, T.G., Puvanachandra, N., Horner, C.H., Polito, A., Ostenfeld, T., Svendsen, C.N., Mucke, L., Johnson, M.H., and Sofroniew, M.V. (1999). Leukocyte infiltration,

neuronal degeneration, and neurite outgrowth after ablation of scar-forming, reactive astrocytes in adult transgenic mice. Neuron *23*, 297-308.

Bush, T.G., Savidge, T.C., Freeman, T.C., Cox, H.J., Campbell, E.A., Mucke, L., Johnson, M.H., and Sofroniew, M.V. (1998). Fulminant jejuno-ileitis following ablation of enteric glia in adult transgenic mice. Cell *93*, 189-201.

Cao, D., Fukuchi, K., Wan, H., Kim, H., and Li, L. (2006). Lack of LDL receptor aggravates learning deficits and amyloid deposits in Alzheimer transgenic mice. Neurobiol Aging *27*, 1632-1643.

Castano, E.M., Prelli, F., Wisniewski, T., Golabek, A., Kumar, R.A., Soto, C., and Frangione, B. (1995). Fibrillogenesis in Alzheimer's disease of amyloid beta peptides and apolipoprotein E. Biochem J *306 (Pt 2)*, 599-604.

Castellano, J.M., Kim, J., Stewart, F.R., Jiang, H., Demattos, R.B., Patterson, B.W., Fagan, A.M., Morris, J.C., Mawuenyega, K.G., Cruchaga, C.*, et al.* (2011). Human apoE Isoforms Differentially Regulate Brain Amyloid-{beta} Peptide Clearance. Sci Transl Med *3*, 89ra57.

Chung, H., Brazil, M.I., Soe, T.T., and Maxfield, F.R. (1999). Uptake, degradation, and release of fibrillar and soluble forms of Alzheimer's amyloid beta-peptide by microglial cells. J Biol Chem *274*, 32301-32308.

Cirrito, J.R., Kang, J.E., Lee, J., Stewart, F.R., Verges, D.K., Silverio, L.M., Bu, G., Mennerick, S., and Holtzman, D.M. (2008). Endocytosis is required for synaptic activity-dependent release of amyloid-beta in vivo. Neuron *58*, 42-51.

Cirrito, J.R., May, P.C., O'Dell, M.A., Taylor, J.W., Parsadanian, M., Cramer, J.W., Audia, J.E., Nissen, J.S., Bales, K.R., Paul, S.M.*, et al.* (2003). In vivo assessment of brain interstitial fluid with microdialysis reveals plaque-associated changes in amyloid-beta metabolism and half-life. J Neurosci *23*, 8844-8853.

Cohen, J., Pertsemlidis, A., Kotowski, I.K., Graham, R., Garcia, C.K., and Hobbs, H.H. (2005). Low LDL cholesterol in individuals of African descent resulting from frequent nonsense mutations in PCSK9. Nat Genet *37*, 161-165.

Cole, G.M., and Ard, M.D. (2000). Influence of lipoproteins on microglial degradation of Alzheimer's amyloid beta-protein. Microsc Res Tech *50*, 316-324.

Corder, E.H., Saunders, A.M., Risch, N.J., Strittmatter, W.J., Schmechel, D.E., Gaskell, P.C., Jr., Rimmler, J.B., Locke, P.A., Conneally, P.M., Schmader, K.E.*, et al.* (1994). Protective effect of apolipoprotein E type 2 allele for late onset Alzheimer disease. Nat Genet *7*, 180-184.

Corder, E.H., Saunders, A.M., Strittmatter, W.J., Schmechel, D.E., Gaskell, P.C., Small, G.W., Roses, A.D., Haines, J.L., and Pericak-Vance, M.A. (1993). Gene dose of apolipoprotein E type 4 allele and the risk of Alzheimer's disease in late onset families. Science *261*, 921-923.

Cramer, P.E., Cirrito, J.R., Wesson, D.W., Lee, C.Y., Karlo, J.C., Zinn, A.E., Casali, B.T., Restivo, J.L., Goebel, W.D., James, M.J., *et al.* (2012). ApoE-Directed Therapeutics Rapidly Clear beta-Amyloid and Reverse Deficits in AD Mouse Models. Science *335*, 1503-1506.

De Strooper, B. (2010). Proteases and proteolysis in Alzheimer disease: a multifactorial view on the disease process. Physiol Rev *90*, 465-494.

Deane, R., Sagare, A., Hamm, K., Parisi, M., Lane, S., Finn, M.B., Holtzman, D.M., and Zlokovic, B.V. (2008). ApoE isoform-specific disruption of amyloid beta peptide clearance from mouse brain. J Clin Invest *118*, 4002-4013.

Deane, R., Wu, Z., Sagare, A., Davis, J., Du Yan, S., Hamm, K., Xu, F., Parisi, M., LaRue, B., Hu, H.W., *et al.* (2004). LRP/amyloid beta-peptide interaction mediates differential brain efflux of Abeta isoforms. Neuron *43*, 333-344.

DeMattos, R.B., Bales, K.R., Cummins, D.J., Dodart, J.C., Paul, S.M., and Holtzman, D.M. (2001a). Peripheral anti-A beta antibody alters CNS and plasma A beta clearance and decreases brain A beta burden in a mouse model of Alzheimer's disease. Proc Natl Acad Sci U S A *98*, 8850-8855.

DeMattos, R.B., Brendza, R.P., Heuser, J.E., Kierson, M., Cirrito, J.R., Fryer, J., Sullivan, P.M., Fagan, A.M., Han, X., and Holtzman, D.M. (2001b). Purification and characterization of astrocyte-secreted apolipoprotein E and J-containing lipoproteins from wild-type and human apoE transgenic mice. Neurochem Int *39*, 415-425.

DeMattos, R.B., Cirrito, J.R., Parsadanian, M., May, P.C., O'Dell, M.A., Taylor, J.W., Harmony, J.A., Aronow, B.J., Bales, K.R., Paul, S.M., *et al.* (2004). ApoE and clusterin cooperatively suppress Abeta levels and deposition: evidence that ApoE regulates extracellular Abeta metabolism in vivo. Neuron *41*, 193-202.

Demeester, N., Castro, G., Desrumaux, C., De Geitere, C., Fruchart, J.C., Santens, P., Mulleners, E., Engelborghs, S., De Deyn, P.P., Vandekerckhove, J., *et al.* (2000). Characterization and functional studies of lipoproteins, lipid transfer proteins, and lecithin:cholesterol acyltransferase in CSF of normal individuals and patients with Alzheimer's disease. J Lipid Res *41*, 963-974.

Di Paolo, G., and Kim, T.W. (2011). Linking lipids to Alzheimer's disease: cholesterol and beyond. Nat Rev Neurosci *12*, 284-296.

DiFiglia, M., Sapp, E., Chase, K.O., Davies, S.W., Bates, G.P., Vonsattel, J.P., and Aronin, N. (1997). Aggregation of huntingtin in neuronal intranuclear inclusions and dystrophic neurites in brain. Science *277*, 1990-1993.

Doherty, M.K., and Beynon, R.J. (2006). Protein turnover on the scale of the proteome. Expert Rev Proteomics *3*, 97-110.

Doherty, M.K., Hammond, D.E., Clague, M.J., Gaskell, S.J., and Beynon, R.J. (2009). Turnover of the human proteome: determination of protein intracellular stability by dynamic SILAC. J Proteome Res *8*, 104-112.

Doherty, M.K., Whitehead, C., McCormack, H., Gaskell, S.J., and Beynon, R.J. (2005). Proteome dynamics in complex organisms: using stable isotopes to monitor individual protein turnover rates. Proteomics *5*, 522-533.

Dunn, K.W., and Maxfield, F.R. (1992). Delivery of ligands from sorting endosomes to late endosomes occurs by maturation of sorting endosomes. J Cell Biol *117*, 301-310.

Elder, G.A., Cho, J.Y., English, D.F., Franciosi, S., Schmeidler, J., Sosa, M.A., Gasperi, R.D., Fisher, E.A., Mathews, P.M., Haroutunian, V.*, et al.* (2007). Elevated plasma cholesterol does not affect brain Abeta in mice lacking the low-density lipoprotein receptor. J Neurochem *102*, 1220-1231.

Elshourbagy, N.A., Liao, W.S., Mahley, R.W., and Taylor, J.M. (1985). Apolipoprotein E mRNA is abundant in the brain and adrenals, as well as in the liver, and is present in other peripheral tissues of rats and marmosets. Proc Natl Acad Sci U S A *82*, 203-207.

Evans, K.C., Berger, E.P., Cho, C.G., Weisgraber, K.H., and Lansbury, P.T., Jr. (1995). Apolipoprotein E is a kinetic but not a thermodynamic inhibitor of amyloid formation: implications for the pathogenesis and treatment of Alzheimer disease. Proc Natl Acad Sci U S A *92*, 763-767.

Fagan, A.M., Holtzman, D.M., Munson, G., Mathur, T., Schneider, D., Chang, L.K., Getz, G.S., Reardon, C.A., Lukens, J., Shah, J.A.*, et al.* (1999). Unique lipoproteins secreted by primary astrocytes from wild type, apoE (-/-), and human apoE transgenic mice. J Biol Chem *274*, 30001-30007.

Fagan, A.M., Watson, M., Parsadanian, M., Bales, K.R., Paul, S.M., and Holtzman, D.M. (2002). Human and murine ApoE markedly alters A beta metabolism before and

after plaque formation in a mouse model of Alzheimer's disease. Neurobiol Dis *9*, 305-318.

Fisher, T.S., Lo Surdo, P., Pandit, S., Mattu, M., Santoro, J.C., Wisniewski, D., Cummings, R.T., Calzetta, A., Cubbon, R.M., Fischer, P.A.*, et al.* (2007). Effects of pH and low density lipoprotein (LDL) on PCSK9-dependent LDL receptor regulation. J Biol Chem *282*, 20502-20512.

Fryer, J.D., Demattos, R.B., McCormick, L.M., O'Dell, M.A., Spinner, M.L., Bales, K.R., Paul, S.M., Sullivan, P.M., Parsadanian, M., Bu, G.*, et al.* (2005a). The low density lipoprotein receptor regulates the level of central nervous system human and murine apolipoprotein E but does not modify amyloid plaque pathology in PDAPP mice. J Biol Chem *280*, 25754-25759.

Fryer, J.D., Simmons, K., Parsadanian, M., Bales, K.R., Paul, S.M., Sullivan, P.M., and Holtzman, D.M. (2005b). Human apolipoprotein E4 alters the amyloid-beta 40:42 ratio and promotes the formation of cerebral amyloid angiopathy in an amyloid precursor protein transgenic model. J Neurosci *25*, 2803-2810.

Fuentealba, R.A., Liu, Q., Zhang, J., Kanekiyo, T., Hu, X., Lee, J.M., LaDu, M.J., and Bu, G. (2010). Low-density lipoprotein receptor-related protein 1 (LRP1) mediates neuronal Abeta42 uptake and lysosomal trafficking. PLoS One *5*, e11884.

Fukumoto, H., Ingelsson, M., Garevik, N., Wahlund, L.O., Nukina, N., Yaguchi, Y., Shibata, M., Hyman, B.T., Rebeck, G.W., and Irizarry, M.C. (2003). APOE epsilon 3/ epsilon 4 heterozygotes have an elevated proportion of apolipoprotein E4 in cerebrospinal fluid relative to plasma, independent of Alzheimer's disease diagnosis. Exp Neurol *183*, 249-253.

Funato, H., Yoshimura, M., Yamazaki, T., Saido, T.C., Ito, Y., Yokofujita, J., Okeda, R., and Ihara, Y. (1998). Astrocytes containing amyloid beta-protein (Abeta)-positive granules are associated with Abeta40-positive diffuse plaques in the aged human brain. Am J Pathol *152*, 983-992.

Garlick, P.J., McNurlan, M.A., Essen, P., and Wernerman, J. (1994). Measurement of tissue protein synthesis rates in vivo: a critical analysis of contrasting methods. Am J Physiol *266*, E287-297.

Ghiso, J., Shayo, M., Calero, M., Ng, D., Tomidokoro, Y., Gandy, S., Rostagno, A., and Frangione, B. (2004). Systemic catabolism of Alzheimer's Abeta40 and Abeta42. J Biol Chem *279*, 45897-45908.

Goedert, M. (2001). Alpha-synuclein and neurodegenerative diseases. Nat Rev Neurosci *2*, 492-501.

Goldstein, J.L., Brown, M.S., Anderson, R.G., Russell, D.W., and Schneider, W.J. (1985). Receptor-mediated endocytosis: concepts emerging from the LDL receptor system. Annu Rev Cell Biol *1*, 1-39.

Grathwohl, S.A., Kalin, R.E., Bolmont, T., Prokop, S., Winkelmann, G., Kaeser, S.A., Odenthal, J., Radde, R., Eldh, T., Gandy, S.*, et al.* (2009). Formation and maintenance of Alzheimer's disease beta-amyloid plaques in the absence of microglia. Nat Neurosci *12*, 1361-1363.

Grehan, S., Tse, E., and Taylor, J.M. (2001). Two distal downstream enhancers direct expression of the human apolipoprotein E gene to astrocytes in the brain. J Neurosci *21*, 812-822.

Hardy, J. (2006). A hundred years of Alzheimer's disease research. Neuron *52*, 3-13.

Hardy, J., and Selkoe, D.J. (2002). The amyloid hypothesis of Alzheimer's disease: progress and problems on the road to therapeutics. Science *297*, 353-356.

Harr, S.D., Uint, L., Hollister, R., Hyman, B.T., and Mendez, A.J. (1996). Brain expression of apolipoproteins E, J, and A-I in Alzheimer's disease. J Neurochem *66*, 2429-2435.

Herrmann, J.E., Imura, T., Song, B., Qi, J., Ao, Y., Nguyen, T.K., Korsak, R.A., Takeda, K., Akira, S., and Sofroniew, M.V. (2008). STAT3 is a critical regulator of astrogliosis and scar formation after spinal cord injury. J Neurosci *28*, 7231-7243.

Herz, J., and Bock, H.H. (2002). Lipoprotein receptors in the nervous system. Annu Rev Biochem *71*, 405-434.

Hickman, S.E., Allison, E.K., and El Khoury, J. (2008). Microglial dysfunction and defective beta-amyloid clearance pathways in aging Alzheimer's disease mice. J Neurosci *28*, 8354-8360.

Hirsch-Reinshagen, V., Donkin, J., Stukas, S., Chan, J., Wilkinson, A., Fan, J., Parks, J.S., Kuivenhoven, J.A., Lutjohann, D., Pritchard, H.*, et al.* (2009). LCAT synthesized by primary astrocytes esterifies cholesterol on glia-derived lipoproteins. J Lipid Res *50*, 885-893.

Hirsch-Reinshagen, V., Maia, L.F., Burgess, B.L., Blain, J.F., Naus, K.E., McIsaac, S.A., Parkinson, P.F., Chan, J.Y., Tansley, G.H., Hayden, M.R.*, et al.* (2005). The absence of ABCA1 decreases soluble ApoE levels but does not diminish amyloid

deposition in two murine models of Alzheimer disease. J Biol Chem *280*, 43243-43256.

Hirsch-Reinshagen, V., and Wellington, C.L. (2007). Cholesterol metabolism, apolipoprotein E, adenosine triphosphate-binding cassette transporters, and Alzheimer's disease. Curr Opin Lipidol *18*, 325-332.

Hirsch-Reinshagen, V., Zhou, S., Burgess, B.L., Bernier, L., McIsaac, S.A., Chan, J.Y., Tansley, G.H., Cohn, J.S., Hayden, M.R., and Wellington, C.L. (2004). Deficiency of ABCA1 impairs apolipoprotein E metabolism in brain. J Biol Chem *279*, 41197-41207.

Holtzman, D.M., Bales, K.R., Tenkova, T., Fagan, A.M., Parsadanian, M., Sartorius, L.J., Mackey, B., Olney, J., McKeel, D., Wozniak, D.*, et al.* (2000a). Apolipoprotein E isoform-dependent amyloid deposition and neuritic degeneration in a mouse model of Alzheimer's disease. Proc Natl Acad Sci U S A *97*, 2892-2897.

Holtzman, D.M., Bales, K.R., Wu, S., Bhat, P., Parsadanian, M., Fagan, A.M., Chang, L.K., Sun, Y., and Paul, S.M. (1999). Expression of human apolipoprotein E reduces amyloid-beta deposition in a mouse model of Alzheimer's disease. J Clin Invest *103*, R15-R21.

Holtzman, D.M., Fagan, A.M., Mackey, B., Tenkova, T., Sartorius, L., Paul, S.M., Bales, K., Ashe, K.H., Irizarry, M.C., and Hyman, B.T. (2000b). Apolipoprotein E facilitates neuritic and cerebrovascular plaque formation in an Alzheimer's disease model. Ann Neurol *47*, 739-747.

Holtzman, D.M., Morris, J.C., and Goate, A.M. (2011). Alzheimer's disease: the challenge of the second century. Sci Transl Med *3*, 77sr71.

Horton, J.D., Cohen, J.C., and Hobbs, H.H. (2009). PCSK9: a convertase that coordinates LDL catabolism. J Lipid Res *50 Suppl*, S172-177.

Hu, X., Crick, S.L., Bu, G., Frieden, C., Pappu, R.V., and Lee, J.M. (2009). Amyloid seeds formed by cellular uptake, concentration, and aggregation of the amyloid-beta peptide. Proc Natl Acad Sci U S A *106*, 20324-20329.

Imoberdorf, R., Garlick, P.J., McNurlan, M.A., Casella, G.A., Peheim, E., Turgay, M., Bartsch, P., and Ballmer, P.E. (2001). Enhanced synthesis of albumin and fibrinogen at high altitude. J Appl Physiol *90*, 528-537.

Innerarity, T.L., and Mahley, R.W. (1978). Enhanced binding by cultured human fibroblasts of apo-E-containing lipoproteins as compared with low density lipoproteins. Biochemistry *17*, 1440-1447.

Itagaki, S., McGeer, P.L., Akiyama, H., Zhu, S., and Selkoe, D. (1989). Relationship of microglia and astrocytes to amyloid deposits of Alzheimer disease. J Neuroimmunol *24*, 173-182.

Iwata, N., Tsubuki, S., Takaki, Y., Shirotani, K., Lu, B., Gerard, N.P., Gerard, C., Hama, E., Lee, H.J., and Saido, T.C. (2001). Metabolic regulation of brain Abeta by neprilysin. Science *292*, 1550-1552.

Jarrett, J.T., Berger, E.P., and Lansbury, P.T., Jr. (1993). The carboxy terminus of the beta amyloid protein is critical for the seeding of amyloid formation: implications for the pathogenesis of Alzheimer's disease. Biochemistry *32*, 4693-4697.

Jiang, Q., Lee, C.Y., Mandrekar, S., Wilkinson, B., Cramer, P., Zelcer, N., Mann, K., Lamb, B., Willson, T.M., Collins, J.L.*, et al.* (2008). ApoE promotes the proteolytic degradation of Abeta. Neuron *58*, 681-693.

Jonas, A. (1998). Regulation of lecithin cholesterol acyltransferase activity. Prog Lipid Res *37*, 209-234.

Jonas, M.C., Costantini, C., and Puglielli, L. (2008). PCSK9 is required for the disposal of non-acetylated intermediates of the nascent membrane protein BACE1. EMBO Rep *9*, 916-922.

Kanekiyo, T., and Bu, G. (2009). Receptor-associated protein interacts with amyloid-beta peptide and promotes its cellular uptake. J Biol Chem *284*, 33352-33359.

Kanekiyo, T., Zhang, J., Liu, Q., Liu, C.C., Zhang, L., and Bu, G. (2011). Heparan sulphate proteoglycan and the low-density lipoprotein receptor-related protein 1 constitute major pathways for neuronal amyloid-beta uptake. J Neurosci *31*, 1644-1651.

Kantarci, K., Lowe, V., Przybelski, S.A., Weigand, S.D., Senjem, M.L., Ivnik, R.J., Preboske, G.M., Roberts, R., Geda, Y.E., Boeve, B.F.*, et al.* (2012). APOE modifies the association between Abeta load and cognition in cognitively normal older adults. Neurology *78*, 232-240.

Katsouri, L., and Georgopoulos, S. (2011). Lack of LDL receptor enhances amyloid deposition and decreases glial response in an Alzheimer's disease mouse model. PLoS One *6*, e21880.

Kennedy, M.A., Barrera, G.C., Nakamura, K., Baldan, A., Tarr, P., Fishbein, M.C., Frank, J., Francone, O.L., and Edwards, P.A. (2005). ABCG1 has a critical role in mediating cholesterol efflux to HDL and preventing cellular lipid accumulation. Cell Metab *1*, 121-131.

Kim, J., Basak, J.M., and Holtzman, D.M. (2009a). The role of apolipoprotein E in Alzheimer's disease. Neuron *63*, 287-303.

Kim, J., Castellano, J.M., Jiang, H., Basak, J.M., Parsadanian, M., Pham, V., Mason, S.M., Paul, S.M., and Holtzman, D.M. (2009b). Overexpression of low-density lipoprotein receptor in the brain markedly inhibits amyloid deposition and increases extracellular A beta clearance. Neuron *64*, 632-644.

Kim, J., Jiang, H., Park, S., Eltorai, A.E., Stewart, F.R., Yoon, H., Basak, J.M., Finn, M.B., and Holtzman, D.M. (2011). Haploinsufficiency of human APOE reduces amyloid deposition in a mouse model of amyloid-beta amyloidosis. J Neurosci *31*, 18007-18012.

Kim, W.S., Rahmanto, A.S., Kamili, A., Rye, K.A., Guillemin, G.J., Gelissen, I.C., Jessup, W., Hill, A.F., and Garner, B. (2007). Role of ABCG1 and ABCA1 in regulation of neuronal cholesterol efflux to apolipoprotein E discs and suppression of amyloid-beta peptide generation. J Biol Chem *282*, 2851-2861.

Koistinaho, M., Lin, S., Wu, X., Esterman, M., Koger, D., Hanson, J., Higgs, R., Liu, F., Malkani, S., Bales, K.R.*, et al.* (2004). Apolipoprotein E promotes astrocyte colocalization and degradation of deposited amyloid-beta peptides. Nat Med *10*, 719-726.

Koldamova, R., Staufenbiel, M., and Lefterov, I. (2005a). Lack of ABCA1 considerably decreases brain ApoE level and increases amyloid deposition in APP23 mice. J Biol Chem *280*, 43224-43235.

Koldamova, R.P., Lefterov, I.M., Staufenbiel, M., Wolfe, D., Huang, S., Glorioso, J.C., Walter, M., Roth, M.G., and Lazo, J.S. (2005b). The liver X receptor ligand T0901317 decreases amyloid beta production in vitro and in a mouse model of Alzheimer's disease. J Biol Chem *280*, 4079-4088.

Koo, E.H., and Squazzo, S.L. (1994). Evidence that production and release of amyloid beta-protein involves the endocytic pathway. J Biol Chem *269*, 17386-17389.

Korwek, K.M., Trotter, J.H., Ladu, M.J., Sullivan, P.M., and Weeber, E.J. (2009). ApoE isoform-dependent changes in hippocampal synaptic function. Mol Neurodegener *4*, 21.

Krimbou, L., Denis, M., Haidar, B., Carrier, M., Marcil, M., and Genest, J., Jr. (2004). Molecular interactions between apoE and ABCA1: impact on apoE lipidation. J Lipid Res *45*, 839-848.

LaDu, M.J., Falduto, M.T., Manelli, A.M., Reardon, C.A., Getz, G.S., and Frail, D.E. (1994). Isoform-specific binding of apolipoprotein E to beta-amyloid. J Biol Chem *269*, 23403-23406.

LaFerla, F.M., Green, K.N., and Oddo, S. (2007). Intracellular amyloid-beta in Alzheimer's disease. Nat Rev Neurosci *8*, 499-509.

Lagace, T.A., Curtis, D.E., Garuti, R., McNutt, M.C., Park, S.W., Prather, H.B., Anderson, N.N., Ho, Y.K., Hammer, R.E., and Horton, J.D. (2006). Secreted PCSK9 decreases the number of LDL receptors in hepatocytes and in livers of parabiotic mice. J Clin Invest *116*, 2995-3005.

Lan, H., Pang, L., Smith, M.M., Levitan, D., Ding, W., Liu, L., Shan, L., Shah, V.V., Laverty, M., Arreaza, G.*, et al.* (2010). Proprotein convertase subtilisin/kexin type 9 (PCSK9) affects gene expression pathways beyond cholesterol metabolism in liver cells. J Cell Physiol *224*, 273-281.

Lawn, R.M., Wade, D.P., Garvin, M.R., Wang, X., Schwartz, K., Porter, J.G., Seilhamer, J.J., Vaughan, A.M., and Oram, J.F. (1999). The Tangier disease gene product ABC1 controls the cellular apolipoprotein-mediated lipid removal pathway. J Clin Invest *104*, R25-31.

Lee, C.Y., and Landreth, G.E. (2010). The role of microglia in amyloid clearance from the AD brain. J Neural Transm *117*, 949-960.

Lee, C.Y., Tse, W., Smith, J.D., and Landreth, G.E. (2012). Apolipoprotein E Promotes beta-Amyloid Trafficking and Degradation by Modulating Microglial Cholesterol Levels. J Biol Chem *287*, 2032-2044.

Lehtimaki, T., Pirttila, T., Mehta, P.D., Wisniewski, H.M., Frey, H., and Nikkari, T. (1995). Apolipoprotein E (apoE) polymorphism and its influence on ApoE concentrations in the cerebrospinal fluid in Finnish patients with Alzheimer's disease. Hum Genet *95*, 39-42.

Li, M., Husic, N., Lin, Y., Christensen, H., Malik, I., McIver, S., Daniels, C.M., Harris, D.A., Kotzbauer, P.T., Goldberg, M.P.*, et al.* (2010). Optimal promoter usage for lentiviral vector-mediated transduction of cultured central nervous system cells. J Neurosci Methods *189*, 56-64.

Liu, M., Wu, G., Baysarowich, J., Kavana, M., Addona, G.H., Bierilo, K.K., Mudgett, J.S., Pavlovic, G., Sitlani, A., Renger, J.J.*, et al.* (2010). PCSK9 is not involved in the degradation of LDL receptors and BACE1 in the adult mouse brain. J Lipid Res *51*, 2611-2618.

Liu, Q., Zerbinatti, C.V., Zhang, J., Hoe, H.S., Wang, B., Cole, S.L., Herz, J., Muglia, L., and Bu, G. (2007). Amyloid precursor protein regulates brain apolipoprotein E and cholesterol metabolism through lipoprotein receptor LRP1. Neuron *56*, 66-78.

Ma, J., Yee, A., Brewer, H.B., Jr., Das, S., and Potter, H. (1994). Amyloid-associated proteins alpha 1-antichymotrypsin and apolipoprotein E promote assembly of Alzheimer beta-protein into filaments. Nature *372*, 92-94.

Mahley, R.W. (1988). Apolipoprotein E: cholesterol transport protein with expanding role in cell biology. Science *240*, 622-630.

Mahley, R.W., Huang, Y., and Weisgraber, K.H. (2006). Putting cholesterol in its place: apoE and reverse cholesterol transport. J Clin Invest *116*, 1226-1229.

Mandelkow, E.M., and Mandelkow, E. (1998). Tau in Alzheimer's disease. Trends Cell Biol *8*, 425-427.

Mandrekar, S., Jiang, Q., Lee, C.Y., Koenigsknecht-Talboo, J., Holtzman, D.M., and Landreth, G.E. (2009). Microglia mediate the clearance of soluble Abeta through fluid phase macropinocytosis. J Neurosci *29*, 4252-4262.

Mandybur, T.I., and Chuirazzi, C.C. (1990). Astrocytes and the plaques of Alzheimer's disease. Neurology *40*, 635-639.

Mann, K.M., Thorngate, F.E., Katoh-Fukui, Y., Hamanaka, H., Williams, D.L., Fujita, S., and Lamb, B.T. (2004). Independent effects of APOE on cholesterol metabolism and brain Abeta levels in an Alzheimer disease mouse model. Hum Mol Genet *13*, 1959-1968.

Masters, C.L., Simms, G., Weinman, N.A., Multhaup, G., McDonald, B.L., and Beyreuther, K. (1985). Amyloid plaque core protein in Alzheimer disease and Down syndrome. Proc Natl Acad Sci U S A *82*, 4245-4249.

Matsuoka, Y., Saito, M., LaFrancois, J., Gaynor, K., Olm, V., Wang, L., Casey, E., Lu, Y., Shiratori, C., Lemere, C., *et al.* (2003). Novel therapeutic approach for the treatment of Alzheimer's disease by peripheral administration of agents with an affinity to beta-amyloid. J Neurosci *23*, 29-33.

Mauch, D.H., Nagler, K., Schumacher, S., Goritz, C., Muller, E.C., Otto, A., and Pfrieger, F.W. (2001). CNS synaptogenesis promoted by glia-derived cholesterol. Science *294*, 1354-1357.

Mawuenyega, K.G., Sigurdson, W., Ovod, V., Munsell, L., Kasten, T., Morris, J.C., Yarasheski, K.E., and Bateman, R.J. (2010). Decreased clearance of CNS beta-amyloid in Alzheimer's disease. Science *330*, 1774.

Maxwell, K.N., and Breslow, J.L. (2004). Adenoviral-mediated expression of Pcsk9 in mice results in a low-density lipoprotein receptor knockout phenotype. Proc Natl Acad Sci U S A *101*, 7100-7105.

Melchor, J.P., Pawlak, R., and Strickland, S. (2003). The tissue plasminogen activator-plasminogen proteolytic cascade accelerates amyloid-beta (Abeta) degradation and inhibits Abeta-induced neurodegeneration. J Neurosci *23*, 8867-8871.

Morikawa, M., Fryer, J.D., Sullivan, P.M., Christopher, E.A., Wahrle, S.E., DeMattos, R.B., O'Dell, M.A., Fagan, A.M., Lashuel, H.A., Walz, T.*, et al.* (2005). Production and characterization of astrocyte-derived human apolipoprotein E isoforms from immortalized astrocytes and their interactions with amyloid-beta. Neurobiol Dis *19*, 66-76.

Morris, J.C., Roe, C.M., Xiong, C., Fagan, A.M., Goate, A.M., Holtzman, D.M., and Mintun, M.A. (2010). APOE predicts amyloid-beta but not tau Alzheimer pathology in cognitively normal aging. Ann Neurol *67*, 122-131.

Mueller-Steiner, S., Zhou, Y., Arai, H., Roberson, E.D., Sun, B., Chen, J., Wang, X., Yu, G., Esposito, L., Mucke, L.*, et al.* (2006). Antiamyloidogenic and neuroprotective functions of cathepsin B: implications for Alzheimer's disease. Neuron *51*, 703-714.

Nagele, R.G., D'Andrea, M.R., Lee, H., Venkataraman, V., and Wang, H.Y. (2003). Astrocytes accumulate A beta 42 and give rise to astrocytic amyloid plaques in Alzheimer disease brains. Brain Res *971*, 197-209.

Namba, Y., Tomonaga, M., Kawasaki, H., Otomo, E., and Ikeda, K. (1991). Apolipoprotein E immunoreactivity in cerebral amyloid deposits and neurofibrillary tangles in Alzheimer's disease and kuru plaque amyloid in Creutzfeldt-Jakob disease. Brain Res *541*, 163-166.

Nielsen, H.M., Veerhuis, R., Holmqvist, B., and Janciauskiene, S. (2009). Binding and uptake of A beta1-42 by primary human astrocytes in vitro. Glia *57*, 978-988.

Okada, S., Nakamura, M., Katoh, H., Miyao, T., Shimazaki, T., Ishii, K., Yamane, J., Yoshimura, A., Iwamoto, Y., Toyama, Y.*, et al.* (2006). Conditional ablation of Stat3 or Socs3 discloses a dual role for reactive astrocytes after spinal cord injury. Nat Med *12*, 829-834.

Ong, S.E., Blagoev, B., Kratchmarova, I., Kristensen, D.B., Steen, H., Pandey, A., and Mann, M. (2002). Stable isotope labeling by amino acids in cell culture, SILAC, as a simple and accurate approach to expression proteomics. Mol Cell Proteomics *1*, 376-386.

Ong, S.E., and Mann, M. (2005). Mass spectrometry-based proteomics turns quantitative. Nat Chem Biol *1*, 252-262.

Paresce, D.M., Chung, H., and Maxfield, F.R. (1997). Slow degradation of aggregates of the Alzheimer's disease amyloid beta-protein by microglial cells. J Biol Chem *272*, 29390-29397.

Paresce, D.M., Ghosh, R.N., and Maxfield, F.R. (1996). Microglial cells internalize aggregates of the Alzheimer's disease amyloid beta-protein via a scavenger receptor. Neuron *17*, 553-565.

Park, S.W., Moon, Y.A., and Horton, J.D. (2004). Post-transcriptional regulation of low density lipoprotein receptor protein by proprotein convertase subtilisin/kexin type 9a in mouse liver. J Biol Chem *279*, 50630-50638.

Pathak, R.K., Yokode, M., Hammer, R.E., Hofmann, S.L., Brown, M.S., Goldstein, J.L., and Anderson, R.G. (1990). Tissue-specific sorting of the human LDL receptor in polarized epithelia of transgenic mice. J Cell Biol *111*, 347-359.

Patterson, B.W., Carraro, F., and Wolfe, R.R. (1993). Measurement of 15N enrichment in multiple amino acids and urea in a single analysis by gas chromatography/mass spectrometry. Biol Mass Spectrom *22*, 518-523.

Patterson, B.W., Mittendorfer, B., Elias, N., Satyanarayana, R., and Klein, S. (2002). Use of stable isotopically labeled tracers to measure very low density lipoprotein-triglyceride turnover. J Lipid Res *43*, 223-233.

Pekny, M., Johansson, C.B., Eliasson, C., Stakeberg, J., Wallen, A., Perlmann, T., Lendahl, U., Betsholtz, C., Berthold, C.H., and Frisen, J. (1999). Abnormal reaction to central nervous system injury in mice lacking glial fibrillary acidic protein and vimentin. J Cell Biol *145*, 503-514.

Pfrieger, F.W., and Ungerer, N. (2011). Cholesterol metabolism in neurons and astrocytes. Prog Lipid Res *50*, 357-371.

Pike, C.J., Cummings, B.J., and Cotman, C.W. (1995). Early association of reactive astrocytes with senile plaques in Alzheimer's disease. Exp Neurol *132*, 172-179.

Pitas, R.E., Boyles, J.K., Lee, S.H., Hui, D., and Weisgraber, K.H. (1987). Lipoproteins and their receptors in the central nervous system. Characterization of the lipoproteins in cerebrospinal fluid and identification of apolipoprotein B,E(LDL) receptors in the brain. J Biol Chem *262*, 14352-14360.

Pluta, R., Barcikowska, M., Misicka, A., Lipkowski, A.W., Spisacka, S., and Januszewski, S. (1999). Ischemic rats as a model in the study of the neurobiological role of human beta-amyloid peptide. Time-dependent disappearing diffuse amyloid plaques in brain. Neuroreport *10*, 3615-3619.

Poirier, S., Mayer, G., Benjannet, S., Bergeron, E., Marcinkiewicz, J., Nassoury, N., Mayer, H., Nimpf, J., Prat, A., and Seidah, N.G. (2008). The proprotein convertase PCSK9 induces the degradation of low density lipoprotein receptor (LDLR) and its closest family members VLDLR and ApoER2. J Biol Chem *283*, 2363-2372.

Pratt, J.M., Petty, J., Riba-Garcia, I., Robertson, D.H., Gaskell, S.J., Oliver, S.G., and Beynon, R.J. (2002). Dynamics of protein turnover, a missing dimension in proteomics. Mol Cell Proteomics *1*, 579-591.

Price, J.C., Guan, S., Burlingame, A., Prusiner, S.B., and Ghaemmaghami, S. (2010). Analysis of proteome dynamics in the mouse brain. Proc Natl Acad Sci U S A *107*, 14508-14513.

Qiu, W.Q., Walsh, D.M., Ye, Z., Vekrellis, K., Zhang, J., Podlisny, M.B., Rosner, M.R., Safavi, A., Hersh, L.B., and Selkoe, D.J. (1998). Insulin-degrading enzyme regulates extracellular levels of amyloid beta-protein by degradation. J Biol Chem *273*, 32730-32738.

Ramaswamy, G., Xu, Q., Huang, Y., and Weisgraber, K.H. (2005). Effect of domain interaction on apolipoprotein E levels in mouse brain. J Neurosci *25*, 10658-10663.

Ranheim, T., Mattingsdal, M., Lindvall, J.M., Holla, O.L., Berge, K.E., Kulseth, M.A., and Leren, T.P. (2008). Genome-wide expression analysis of cells expressing gain of function mutant D374Y-PCSK9. J Cell Physiol *217*, 459-467.

Rapp, A., Gmeiner, B., and Huttinger, M. (2006). Implication of apoE isoforms in cholesterol metabolism by primary rat hippocampal neurons and astrocytes. Biochimie *88*, 473-483.

Rashid, S., Curtis, D.E., Garuti, R., Anderson, N.N., Bashmakov, Y., Ho, Y.K., Hammer, R.E., Moon, Y.A., and Horton, J.D. (2005). Decreased plasma cholesterol and

hypersensitivity to statins in mice lacking Pcsk9. Proc Natl Acad Sci U S A *102*, 5374-5379.

Rebeck, G.W., Reiter, J.S., Strickland, D.K., and Hyman, B.T. (1993). Apolipoprotein E in sporadic Alzheimer's disease: allelic variation and receptor interactions. Neuron *11*, 575-580.

Reed-Geaghan, E.G., Savage, J.C., Hise, A.G., and Landreth, G.E. (2009). CD14 and toll-like receptors 2 and 4 are required for fibrillar A{beta}-stimulated microglial activation. J Neurosci *29*, 11982-11992.

Reiman, E.M., Chen, K., Liu, X., Bandy, D., Yu, M., Lee, W., Ayutyanont, N., Keppler, J., Reeder, S.A., Langbaum, J.B.*, et al.* (2009). Fibrillar amyloid-beta burden in cognitively normal people at 3 levels of genetic risk for Alzheimer's disease. Proc Natl Acad Sci U S A *106*, 6820-6825.

Riddell, D.R., Zhou, H., Atchison, K., Warwick, H.K., Atkinson, P.J., Jefferson, J., Xu, L., Aschmies, S., Kirksey, Y., Hu, Y.*, et al.* (2008). Impact of apolipoprotein E (ApoE) polymorphism on brain ApoE levels. J Neurosci *28*, 11445-11453.

Riddell, D.R., Zhou, H., Comery, T.A., Kouranova, E., Lo, C.F., Warwick, H.K., Ring, R.H., Kirksey, Y., Aschmies, S., Xu, J.*, et al.* (2007). The LXR agonist TO901317 selectively lowers hippocampal Abeta42 and improves memory in the Tg2576 mouse model of Alzheimer's disease. Mol Cell Neurosci *34*, 621-628.

Roses, A.D. (1996). Apolipoprotein E alleles as risk factors in Alzheimer's disease. Annu Rev Med *47*, 387-400.

Rousselet, E., Marcinkiewicz, J., Kriz, J., Zhou, A., Hatten, M.E., Prat, A., and Seidah, N.G. (2011). PCSK9 reduces the protein levels of the LDL receptor in mouse brain during development and after ischemic stroke. J Lipid Res *52*, 1383-1391.

Rovelet-Lecrux, A., Hannequin, D., Raux, G., Le Meur, N., Laquerriere, A., Vital, A., Dumanchin, C., Feuillette, S., Brice, A., Vercelletto, M.*, et al.* (2006). APP locus duplication causes autosomal dominant early-onset Alzheimer disease with cerebral amyloid angiopathy. Nat Genet *38*, 24-26.

Rust, S., Rosier, M., Funke, H., Real, J., Amoura, Z., Piette, J.C., Deleuze, J.F., Brewer, H.B., Duverger, N., Denefle, P.*, et al.* (1999). Tangier disease is caused by mutations in the gene encoding ATP-binding cassette transporter 1. Nat Genet *22*, 352-355.

Saavedra, L., Mohamed, A., Ma, V., Kar, S., and de Chaves, E.P. (2007). Internalization of beta-amyloid peptide by primary neurons in the absence of apolipoprotein E. J Biol Chem *282*, 35722-35732.

Sagare, A., Deane, R., Bell, R.D., Johnson, B., Hamm, K., Pendu, R., Marky, A., Lenting, P.J., Wu, Z., Zarcone, T.*, et al.* (2007). Clearance of amyloid-beta by circulating lipoprotein receptors. Nat Med *13*, 1029-1031.

Savage, M.J., Trusko, S.P., Howland, D.S., Pinsker, L.R., Mistretta, S., Reaume, A.G., Greenberg, B.D., Siman, R., and Scott, R.W. (1998). Turnover of amyloid beta-protein in mouse brain and acute reduction of its level by phorbol ester. J Neurosci *18*, 1743-1752.

Schaefer, E.J., Anderson, D.W., Zech, L.A., Lindgren, F.T., Bronzert, T.B., Rubalcaba, E.A., and Brewer, H.B., Jr. (1981). Metabolism of high density lipoprotein subfractions and constituents in Tangier disease following the infusion of high density lipoproteins. J Lipid Res *22*, 217-228.

Schaefer, E.J., Blum, C.B., Levy, R.I., Jenkins, L.L., Alaupovic, P., Foster, D.M., and Brewer, H.B., Jr. (1978). Metabolism of high-density lipoprotein apolipoproteins in Tangier disease. N Engl J Med *299*, 905-910.

Schaefer, E.J., Brousseau, M.E., Diffenderfer, M.R., Cohn, J.S., Welty, F.K., O'Connor, J., Jr., Dolnikowski, G.G., Wang, J., Hegele, R.A., and Jones, P.J. (2001). Cholesterol and apolipoprotein B metabolism in Tangier disease. Atherosclerosis *159*, 231-236.

Schmechel, D.E., Saunders, A.M., Strittmatter, W.J., Crain, B.J., Hulette, C.M., Joo, S.H., Pericak-Vance, M.A., Goldgaber, D., and Roses, A.D. (1993). Increased amyloid beta-peptide deposition in cerebral cortex as a consequence of apolipoprotein E genotype in late-onset Alzheimer disease. Proc Natl Acad Sci U S A *90*, 9649-9653.

Schwanhausser, B., Gossen, M., Dittmar, G., and Selbach, M. (2009). Global analysis of cellular protein translation by pulsed SILAC. Proteomics *9*, 205-209.

Scotti, E., Hong, C., Yoshinaga, Y., Tu, Y., Hu, Y., Zelcer, N., Boyadjian, R., de Jong, P.J., Young, S.G., Fong, L.G.*, et al.* (2011). Targeted disruption of the idol gene alters cellular regulation of the low-density lipoprotein receptor by sterols and liver x receptor agonists. Mol Cell Biol *31*, 1885-1893.

Segatto, M., Trapani, L., Marino, M., and Pallottini, V. (2011). Age- and sex-related differences in extra-hepatic low-density lipoprotein receptor. J Cell Physiol *226*, 2610-2616.

Seidah, N.G., Benjannet, S., Wickham, L., Marcinkiewicz, J., Jasmin, S.B., Stifani, S., Basak, A., Prat, A., and Chretien, M. (2003). The secretory proprotein convertase neural apoptosis-regulated convertase 1 (NARC-1): liver regeneration and neuronal differentiation. Proc Natl Acad Sci U S A *100*, 928-933.

Selkoe, D.J. (2001). Clearing the brain's amyloid cobwebs. Neuron *32*, 177-180.

Shaffer, L.M., Dority, M.D., Gupta-Bansal, R., Frederickson, R.C., Younkin, S.G., and Brunden, K.R. (1995). Amyloid beta protein (A beta) removal by neuroglial cells in culture. Neurobiol Aging *16*, 737-745.

Shibata, M., Yamada, S., Kumar, S.R., Calero, M., Bading, J., Frangione, B., Holtzman, D.M., Miller, C.A., Strickland, D.K., Ghiso, J.*, et al.* (2000). Clearance of Alzheimer's amyloid-beta(1-40) peptide from brain by LDL receptor-related protein-1 at the blood-brain barrier. J Clin Invest *106*, 1489-1499.

Simard, A.R., Soulet, D., Gowing, G., Julien, J.P., and Rivest, S. (2006). Bone marrow-derived microglia play a critical role in restricting senile plaque formation in Alzheimer's disease. Neuron *49*, 489-502.

Smith, E.E., and Greenberg, S.M. (2009). Beta-amyloid, blood vessels, and brain function. Stroke *40*, 2601-2606.

Smith, Q.R., Momma, S., Aoyagi, M., and Rapoport, S.I. (1987). Kinetics of neutral amino acid transport across the blood-brain barrier. J Neurochem *49*, 1651-1658.

Strittmatter, W.J., Saunders, A.M., Goedert, M., Weisgraber, K.H., Dong, L.M., Jakes, R., Huang, D.Y., Pericak-Vance, M., Schmechel, D., and Roses, A.D. (1994). Isoform-specific interactions of apolipoprotein E with microtubule-associated protein tau: implications for Alzheimer disease. Proc Natl Acad Sci U S A *91*, 11183-11186.

Strittmatter, W.J., Saunders, A.M., Schmechel, D., Pericak-Vance, M., Enghild, J., Salvesen, G.S., and Roses, A.D. (1993a). Apolipoprotein E: high-avidity binding to beta-amyloid and increased frequency of type 4 allele in late-onset familial Alzheimer disease. Proc Natl Acad Sci U S A *90*, 1977-1981.

Strittmatter, W.J., Weisgraber, K.H., Huang, D.Y., Dong, L.M., Salvesen, G.S., Pericak-Vance, M., Schmechel, D., Saunders, A.M., Goldgaber, D., and Roses, A.D. (1993b). Binding of human apolipoprotein E to synthetic amyloid beta peptide: isoform-specific effects and implications for late-onset Alzheimer disease. Proc Natl Acad Sci U S A *90*, 8098-8102.

Sullivan, P.M., Mace, B.E., Maeda, N., and Schmechel, D.E. (2004). Marked regional differences of brain human apolipoprotein E expression in targeted replacement mice. Neuroscience *124*, 725-733.

Sullivan, P.M., Mezdour, H., Aratani, Y., Knouff, C., Najib, J., Reddick, R.L., Quarfordt, S.H., and Maeda, N. (1997). Targeted replacement of the mouse apolipoprotein E gene with the common human APOE3 allele enhances diet-induced hypercholesterolemia and atherosclerosis. J Biol Chem *272*, 17972-17980.

Sun, B., Zhou, Y., Halabisky, B., Lo, I., Cho, S.H., Mueller-Steiner, S., Devidze, N., Wang, X., Grubb, A., and Gan, L. (2008). Cystatin C-cathepsin B axis regulates amyloid beta levels and associated neuronal deficits in an animal model of Alzheimer's disease. Neuron *60*, 247-257.

Sun, Y., Yao, J., Kim, T.W., and Tall, A.R. (2003). Expression of liver X receptor target genes decreases cellular amyloid beta peptide secretion. J Biol Chem *278*, 27688-27694.

Tachikawa, M., Watanabe, M., Hori, S., Fukaya, M., Ohtsuki, S., Asashima, T., and Terasaki, T. (2005). Distinct spatio-temporal expression of ABCA and ABCG transporters in the developing and adult mouse brain. J Neurochem *95*, 294-304.

Tanzi, R.E., and Bertram, L. (2005). Twenty years of the Alzheimer's disease amyloid hypothesis: a genetic perspective. Cell *120*, 545-555.

Tanzi, R.E., Moir, R.D., and Wagner, S.L. (2004). Clearance of Alzheimer's Abeta peptide: the many roads to perdition. Neuron *43*, 605-608.

Thal, D.R., Hartig, W., and Schober, R. (1999). Diffuse plaques in the molecular layer show intracellular A beta(8-17)-immunoreactive deposits in subpial astrocytes. Clin Neuropathol *18*, 226-231.

Thal, D.R., Schultz, C., Dehghani, F., Yamaguchi, H., Braak, H., and Braak, E. (2000). Amyloid beta-protein (Abeta)-containing astrocytes are located preferentially near N-terminal-truncated Abeta deposits in the human entorhinal cortex. Acta Neuropathol *100*, 608-617.

Tiraboschi, P., Hansen, L.A., Masliah, E., Alford, M., Thal, L.J., and Corey-Bloom, J. (2004). Impact of APOE genotype on neuropathologic and neurochemical markers of Alzheimer disease. Neurology *62*, 1977-1983.

Tokuda, T., Calero, M., Matsubara, E., Vidal, R., Kumar, A., Permanne, B., Zlokovic, B., Smith, J.D., Ladu, M.J., Rostagno, A.*, et al.* (2000). Lipidation of apolipoprotein

E influences its isoform-specific interaction with Alzheimer's amyloid beta peptides. Biochem J *348 Pt 2*, 359-365.

Trojanowski, J.Q., and Dickson, D. (2001). Update on the neuropathological diagnosis of frontotemporal dementias. J Neuropathol Exp Neurol *60*, 1123-1126.

Vaughan, A.M., and Oram, J.F. (2006). ABCA1 and ABCG1 or ABCG4 act sequentially to remove cellular cholesterol and generate cholesterol-rich HDL. J Lipid Res *47*, 2433-2443.

Verghese, P.B., Castellano, J.M., and Holtzman, D.M. (2011). Apolipoprotein E in Alzheimer's disease and other neurological disorders. Lancet Neurol *10*, 241-252.

Vitek, M.P., Brown, C.M., and Colton, C.A. (2009). APOE genotype-specific differences in the innate immune response. Neurobiol Aging *30*, 1350-1360.

Wahrle, S.E., Jiang, H., Parsadanian, M., Hartman, R.E., Bales, K.R., Paul, S.M., and Holtzman, D.M. (2005). Deletion of Abca1 increases Abeta deposition in the PDAPP transgenic mouse model of Alzheimer disease. J Biol Chem *280*, 43236-43242.

Wahrle, S.E., Jiang, H., Parsadanian, M., Kim, J., Li, A., Knoten, A., Jain, S., Hirsch-Reinshagen, V., Wellington, C.L., Bales, K.R.*, et al.* (2008). Overexpression of ABCA1 reduces amyloid deposition in the PDAPP mouse model of Alzheimer disease. J Clin Invest *118*, 671-682.

Wahrle, S.E., Jiang, H., Parsadanian, M., Legleiter, J., Han, X., Fryer, J.D., Kowalewski, T., and Holtzman, D.M. (2004). ABCA1 is required for normal central nervous system ApoE levels and for lipidation of astrocyte-secreted apoE. J Biol Chem *279*, 40987-40993.

Wahrle, S.E., Shah, A.R., Fagan, A.M., Smemo, S., Kauwe, J.S., Grupe, A., Hinrichs, A., Mayo, K., Jiang, H., Thal, L.J.*, et al.* (2007). Apolipoprotein E levels in cerebrospinal fluid and the effects of ABCA1 polymorphisms. Mol Neurodegener *2*, 7.

Wang, X., Collins, H.L., Ranalletta, M., Fuki, I.V., Billheimer, J.T., Rothblat, G.H., Tall, A.R., and Rader, D.J. (2007). Macrophage ABCA1 and ABCG1, but not SR-BI, promote macrophage reverse cholesterol transport in vivo. J Clin Invest *117*, 2216-2224.

Warden, C.H., Langner, C.A., Gordon, J.I., Taylor, B.A., McLean, J.W., and Lusis, A.J. (1989). Tissue-specific expression, developmental regulation, and chromosomal

mapping of the lecithin: cholesterol acyltransferase gene. Evidence for expression in brain and testes as well as liver. J Biol Chem *264*, 21573-21581.

Weisgraber, K.H., Innerarity, T.L., and Mahley, R.W. (1982). Abnormal lipoprotein receptor-binding activity of the human E apoprotein due to cysteine-arginine interchange at a single site. J Biol Chem *257*, 2518-2521.

Weller, R.O., Subash, M., Preston, S.D., Mazanti, I., and Carare, R.O. (2008). Perivascular drainage of amyloid-beta peptides from the brain and its failure in cerebral amyloid angiopathy and Alzheimer's disease. Brain Pathol *18*, 253-266.

Wellington, C.L., Walker, E.K., Suarez, A., Kwok, A., Bissada, N., Singaraja, R., Yang, Y.Z., Zhang, L.H., James, E., Wilson, J.E.*, et al.* (2002). ABCA1 mRNA and protein distribution patterns predict multiple different roles and levels of regulation. Lab Invest *82*, 273-283.

Winkler, K., Scharnagl, H., Tisljar, U., Hoschutzky, H., Friedrich, I., Hoffmann, M.M., Huttinger, M., Wieland, H., and Marz, W. (1999). Competition of Abeta amyloid peptide and apolipoprotein E for receptor-mediated endocytosis. J Lipid Res *40*, 447-455.

Wisniewski, T., Castano, E.M., Golabek, A., Vogel, T., and Frangione, B. (1994). Acceleration of Alzheimer's fibril formation by apolipoprotein E in vitro. Am J Pathol *145*, 1030-1035.

Wisniewski, T., and Frangione, B. (1992). Apolipoprotein E: a pathological chaperone protein in patients with cerebral and systemic amyloid. Neurosci Lett *135*, 235-238.

Wisniewski, T., Golabek, A., Matsubara, E., Ghiso, J., and Frangione, B. (1993). Apolipoprotein E: binding to soluble Alzheimer's beta-amyloid. Biochem Biophys Res Commun *192*, 359-365.

Wolfe, R.R., and Chinkes, D.L. (2005). Isotope tracers in metabolic research : principles and practice of kinetic analysis, 2nd edn (Hoboken, N.J., Wiley-Liss).

Wood, S.J., Chan, W., and Wetzel, R. (1996). Seeding of A beta fibril formation is inhibited by all three isotypes of apolipoprotein E. Biochemistry *35*, 12623-12628.

Wyss-Coray, T. (2006). Inflammation in Alzheimer disease: driving force, bystander or beneficial response? Nat Med *12*, 1005-1015.

Wyss-Coray, T., Loike, J.D., Brionne, T.C., Lu, E., Anankov, R., Yan, F., Silverstein, S.C., and Husemann, J. (2003). Adult mouse astrocytes degrade amyloid-beta in vitro and in situ. Nat Med *9*, 453-457.

Yamada, K., Hashimoto, T., Yabuki, C., Nagae, Y., Tachikawa, M., Strickland, D.K., Liu, Q., Bu, G., Basak, J.M., Holtzman, D.M.*, et al.* (2008). The low density lipoprotein receptor-related protein 1 mediates uptake of amyloid beta peptides in an in vitro model of the blood-brain barrier cells. J Biol Chem *283*, 34554-34562.

Yamada, K., Yabuki, C., Seubert, P., Schenk, D., Hori, Y., Ohtsuki, S., Terasaki, T., Hashimoto, T., and Iwatsubo, T. (2009). Abeta immunotherapy: intracerebral sequestration of Abeta by an anti-Abeta monoclonal antibody 266 with high affinity to soluble Abeta. J Neurosci *29*, 11393-11398.

Yamamoto, T., Lu, C., and Ryan, R.O. (2011). A two-step binding model of PCSK9 interaction with the low density lipoprotein receptor. J Biol Chem *286*, 5464-5470.

Yamauchi, K., Tozuka, M., Hidaka, H., Nakabayashi, T., Sugano, M., and Katsuyama, T. (2002). Isoform-specific effect of apolipoprotein E on endocytosis of beta-amyloid in cultures of neuroblastoma cells. Ann Clin Lab Sci *32*, 65-74.

Yamauchi, K., Tozuka, M., Hidaka, H., Nakabayashi, T., Sugano, M., Kondo, Y., Nakagawara, A., and Katsuyama, T. (2000). Effect of apolipoprotein AII on the interaction of apolipoprotein E with beta-amyloid: some apo(E-AII) complexes inhibit the internalization of beta-amyloid in cultures of neuroblastoma cells. J Neurosci Res *62*, 608-614.

Yang, D.S., Small, D.H., Seydel, U., Smith, J.D., Hallmayer, J., Gandy, S.E., and Martins, R.N. (1999). Apolipoprotein E promotes the binding and uptake of beta-amyloid into Chinese hamster ovary cells in an isoform-specific manner. Neuroscience *90*, 1217-1226.

Yin, K.J., Cirrito, J.R., Yan, P., Hu, X., Xiao, Q., Pan, X., Bateman, R., Song, H., Hsu, F.F., Turk, J.*, et al.* (2006). Matrix metalloproteinases expressed by astrocytes mediate extracellular amyloid-beta peptide catabolism. J Neurosci *26*, 10939-10948.

Zannis, V.I., Breslow, J.L., Utermann, G., Mahley, R.W., Weisgraber, K.H., Havel, R.J., Goldstein, J.L., Brown, M.S., Schonfeld, G., Hazzard, W.R.*, et al.* (1982). Proposed nomenclature of apoE isoproteins, apoE genotypes, and phenotypes. J Lipid Res *23*, 911-914.

Zelcer, N., Hong, C., Boyadjian, R., and Tontonoz, P. (2009). LXR regulates cholesterol uptake through Idol-dependent ubiquitination of the LDL receptor. Science *325*, 100-104.

Zerbinatti, C.V., Wahrle, S.E., Kim, H., Cam, J.A., Bales, K., Paul, S.M., Holtzman, D.M., and Bu, G. (2006). Apolipoprotein E and low density lipoprotein receptor-related protein facilitate intraneuronal Abeta42 accumulation in amyloid model mice. J Biol Chem *281*, 36180-36186.

Zhang, D.W., Lagace, T.A., Garuti, R., Zhao, Z., McDonald, M., Horton, J.D., Cohen, J.C., and Hobbs, H.H. (2007). Binding of proprotein convertase subtilisin/kexin type 9 to epidermal growth factor-like repeat A of low density lipoprotein receptor decreases receptor recycling and increases degradation. J Biol Chem *282*, 18602-18612.

Zhang, X.J., Chinkes, D.L., and Wolfe, R.R. (2002). Measurement of muscle protein fractional synthesis and breakdown rates from a pulse tracer injection. Am J Physiol Endocrinol Metab *283*, E753-764.

Zlokovic, B.V. (2008). The blood-brain barrier in health and chronic neurodegenerative disorders. Neuron *57*, 178-201.